Intelligent Control of Connected Autonomous Vehicles in Mixed Autonomy Environments

Mingyang Chen

A dissertation submitted in partial fulfillment

of the requirements for the degree of

Doctor of Philosophy

of

University College London.

Department of Electrical and Electronic Engineering

University College London

June 6, 2025

I, Mingyang Chen, confirm that the work presented in this thesis is my own. Where information has been derived from other sources, I confirm that this has been indicated in the work.

Nomenclature

Abbreviation

ACC	Adaptive Cruise Control
CACC	Cooperative Adaptive Cruise Control
CAV	Connected and Autonomous Vehicle
CBF	Control Barrier Function
CC	Central Coordinator
ComZ	Communication Zone
CZ	Control Zone
DRL	Deep Reinforcement Learning
DQN	Deep Q Network
EV	Electric Vehicle
IC	Intersection Controller
IDM	Intelligent Driver Model
HDV	Human-Driven Vehicle
HJE	Hamilton-Jacobi Equation
HIL	Human-in-the-Loop
MPC	Model Predictive Control
MZ	Merging Zone
NN	Neural Network
RL	Reinforcement Learning
RSU	Roadside Unit
SPAT	Signal Phase and Timing
V2X	Vehicle to Everything

Notation

$a^q_{l,i,j}$	Vehicle acceleration
$D^q_{l,j}$, $\lambda^q_{l,i,j}$	Lengths of a platoon and a vehicle
$\mathscr{J}$, $\mathscr{V}$, $\mathscr{P}$	Sets of road lanes, vehicles and platoons
$\mathscr{L}(\bar{\mathscr{L}})$	Set of platoon numbers (queue included)
l^{q*}_j	Optimal number of platoons to cross in qth phase and jth lane
L_{ComZ}, L_{CZ}	Lengths of communication, and control zones
L_{MZ}	Length of merging zone
$p^q_{l,i,j}$	Vehicle position
$\mathscr{S}^q$	Information set of the qth signal phase
$s^q_{l,i,j}$	Vehicle headway distance
s_0	Standstill spacing between vehicles
$T_{n^q_j}$	Discharging time required for the queue in qth phase and jth lane
T_0	Safe time headway
T^q, T^{q*}	SPAT duration of qth signal phase and its optimal value
t^q	Start time of the qth signal phase
$\tilde{t}_{l,j}$, $\bar{t}_{l,j}$	Platoon ComZ and CZ entering time
$t^{wait}_{l,j}$	Platoon waiting time at the intersection
$t^q_{f,l,j}$	Target crossing time of lth platoon in the jth lane
$u^q_{l,j}$, $\tau^q_{l,j}$	CAV control input and time-lag
$v^q_{l,i,j}$	Vehicle velocity
v^{q*}_j, s^{q*}_j	Target driving speed and headway distance in the CZ
ϕ_i, θ_i	The steering angle and the heading angle of the i th vehicle
$\mathscr{C}_i$	The ith coalition
$\mathbf{u}_i$, $\mathbf{x}_i$	The control input and state of the ith coalition

$\Phi^q_{l,i,j}$, $\phi^q_{l,i,j}$	Vehicle fuel consumption and its rate of change
$\mathbb{R}$, $\mathbb{R}_{\geq 0}$	Real numbers and none-negative real numbers
$\mathbb{N}$, $\mathbb{N}_{\geq 0}$	Nature numbers and none-negative nature numbers
t	Independent time variable
$\mid a \mid$	The absolute value of the number $a \in \mathbb{R}$
$\mid\mid x \mid\mid_2$	The Euclidian norm of the vector $x \in \mathbb{R}^n$
$\mid\mid x \mid\mid_\infty$	The infinity norm of the vector $x \in \mathbb{R}^n$
∞	Infinity
$\in$	$X \in Y$ indicates that X takes value from the set Y
$\forall$	For all
$\oplus$	The Minkowski sum of sets $\mathbb{W} \oplus \mathbb{V} = \{x+y \mid x \in \mathbb{W}, y \in \mathbb{V}\}$

Subscripts and superscripts

i, j, l, q	Index of vehicles, intersection road lanes, platoons and signal phase
$\hat{}$	Estimate
*	Optimum or steady state

Abstract

In recent years, the advent of connected and autonomous vehicles (CAVs) that feature advanced sensing, communication, and control capabilities has gained increasing attention and market interest. However, mixed traffic from human-driven vehicles (HDV) and CAVs will dominate road traffic in the foreseeable future, while complicated interactions between different types of vehicles with various driving behaviors can affect traffic efficiency and safety. To address such concerns, this thesis focuses on the control of CAVs in mixed-traffic environments.

The first part of this thesis is dedicated to investigating the trade-off between intersection throughput and the energy efficiency of all vehicles on the road by co-optimizing signal phase and time (SPAT) and CAV trajectories. Instead of using further alternative signal phases to promote CAV-led platoons, the platoon formation is enforced by trajectory optimization and lane-changing is not allowed in this part. However, lane-changing maneuvers are inevitable and thus the interactions between CAVs and HDVs need further study. In the second part of this thesis, a game-based optimal lane change control framework for the CAV is proposed. The lane-changing involves one CAV and one HDV is comprehensively studied where their interaction is considered by a Stackelberg game, which yields an unconstrained optimal control solution by the Hamilton–Jacobi equation (HJE). Moreover, a theoretical proof is provided to show that the unconstrained optimal strategy is an asymptotically stable equilibrium, and with a suitable design of the weight matrices, safety can be guaranteed. The final part of this thesis extends to multi-vehicle lane-changing scenarios. A game-based coalition structure is proposed to group all the vehicles based on their position and lane-changing intention. To enhance robustness against

human uncertainty, data-enabled predictive control is applied to the CAVs. Human-in-the-loop (HIL) experiments are conducted to show the real-time performance of the proposed method.

Impact Statement

Urban road transportation is facing a growing challenge as the number of vehicles continues to escalate, resulting in significant traffic congestion, elevated energy consumption levels, and an increased likelihood of accidents [1, 2]. The advent of CAVs presents a potential solution to these issues by offering a more responsive, cooperative, and efficient mode of transportation compared to traditional vehicles, thereby addressing the aforementioned concerns and promoting a more fluid flow of traffic [3,4]. However, there exists a transition period for road vehicles from current HDVs to CAVs [5]. In reality, the uncertainty of human drivers can disrupt the mixed-traffic system. Therefore, the study of mixed driving environments is more complicated and challenging than the study of fully connected autonomous driving environments [6, 7]. CAVs not only need to provide safe and efficient performance in cluttered environments but also need to interact with other uncertain traffic participants [8]. Thus this thesis focuses on the coordination and control of CAVs in mixed-autonomy environments. In particular, the robustness against human uncertainties, heterogeneity of CAVs, and real-time performance are comprehensively studied. Moreover, the HIL experiments are also conducted to validate the practical applicability.

Acknowledgements

This thesis is conducted at the Department of Electronic and Electrical Engineering, University College London (UCL). Pursuing the Doctor of Philosophy (Ph.D.) has been an arduous and memorable journey. I must appreciate the support and help from my supervisor, my family, and my friends. Thanks to everyone's help, I was able to successfully complete this thesis.

Firstly, I would like to express my sincerest gratitude to my supervisor Dr. Boli Chen. A teacher, imparting knowledge and dispelling doubts. It is precisely because of his generous teachings that my understanding of academia has deepened and my character has been tempered. It is his earnest teachings that have enabled me to break free from prejudices, broaden my horizons, and achieve innovative results. It is precisely because of his words and deeds that I have discovered that our academic work is not just talking on paper. On the contrary, these works can promote social development and benefit all mankind. If it weren't for my supervisor Dr. Boli Chen, my academic world would be like an eternal darkness. At the same time, I would like to thank our school for providing me with a valuable platform. As is well known, UCL has a long history and profound heritage; its academic achievements are remarkable, and its reputation is renowned throughout the world. The resources provided by the school have cleared the thorns on my academic path. The humanized care of the school has allowed me to continue my scientific research during the epidemic, without stopping for a day.

Secondly, I would like to express my gratitude to my co-authors who made brilliant contributions and provided generous help to my academic research. Those talented and outstanding co-authors including Prof. Guodong Yin, Prof. Yougang

Bian, Prof. Weizhuang Chao, Prof. Jingjing Jiang, and Prof. Simos A Evangelou, whose valuable guidance and experience make me benefit a lot. In particular, other brilliant and excellent co-authors including Dr. Bingbing Li, Dr. Hao Sun, Dr. Sunan Zhang, Dr.Xiaoyang Wang, Dr. Ziniu Hu, and Dr.Shuang Li also support me unconditionally and help me with publications. Meanwhile, I am also thankful to my colleagues, including Dr. Yifeng Mao, Dr. Shaowei Yuan, Dr. Sheng Yu, Dr. Yixun Wen, Dr. Yan Chen, Dr. Yinxiang Lin, Dr. Ruixuan Zhao.

Finally, I must express my deepest gratitude to my parents. They always encourage me during difficult times. They support me unconditionally and provide many valuable suggestions so that I can overcome challenges. Their accompany makes this tough journey less difficult. I'm really grateful for these encouragements and support.

Contents

List of Figures

List of Tables

Chapter 1

Introduction

1.1 Background

With the development of technology and the acceleration of urbanization worldwide, the number of cars is increasing day by day, and it is expected to exceed 1 billion by 2024, which may bring severe congestion as illustrated by Fig. 1.1, increased fuel consumption, and ballooned traffic accidents. It is reported that in 2019, atmospheric CO_2 concentrations were at the peak in the past 2 million years, and concentrations of CH_4 and N_2O were higher at the peak in the past 800,000 years [9]. Moreover, more than 25 thousand people were killed or seriously injured in the U.K. in the last year [10]. Many efforts have been made to mitigate these issues. Net-zero smart cities are designed to reduce greenhouse gas emissions. It is reported that decarbonizing transportation accounts for about 16% of global greenhouse gas emissions. With the emerging 5G technology, the intelligent transportation system is capable of low-latency communication, and real-time traffic monitoring. This cooperative infrastructure can improve safety and overall traffic efficiency. As a crucial part of the smart city, CAV with enhanced electrification and digitization also has the potential to address these mentioned issues [11].

The first research on CAV technology can date back to the 1990s [12]. With the continuous advancement of technologies [13, 14], CAVs at different levels and functions have developed rapidly, and the market share of L1-L3 CAV is increasing [15]. It is predicted that the global penetration rate of CAVs will increase from

Figure 1.1: Complex mixed-traffic environments with high uncertainty and high scalability.

10% in 2018 to 70% in 2027. Equipped with advanced sensing and communication units, CAVs can acquire multi-modal dynamic traffic information, which can greatly improve road safety and driving comfort. For example, CAVs can reduce unnecessary vehicle stops and avoid hard acceleration based on information from the surrounding vehicles. Furthermore, in intelligent transportation systems, where there is sufficient communication infrastructure (i.e. roadside units (RSUs), central coordinator (CC)), CAVs can make full use of the real-time on-road traffic information such as SPAT plans via vehicle-to-vehicle (V2V), and vehicle-to-infrastructure (V2I) communications to alleviate traffic congestion and meanwhile improve individual driving comfort. Fig. 1.2 gives a sketch of the intersection in the future smart city. Although there is no doubt that with higher penetration of CAVs, road transportation can be made more flexible, cooperative control of a large number of CAVs needs further investigation.

When it comes to fuel consumption and greenhouse gas emissions, transportation electrification is unanimously recognized as a solution to alleviate environmental pollution, as it utilizes clean energy instead of fossil fuels. According to the U.K. road-map [16], electric vehicles have higher thermal efficiency and can avoid the emission of pollutants, and there is an exponential growth in vehicle electrification, from under 0.01% in 2010 to over 8.6% of global car shares in 2021. Thus, electric vehicles shall dominate the road by 2050. Another report [17] can also val-

Figure 1.2: A sketch of the smart city in the future.

idate this trend, as the percentage of electric vehicles worldwide will rise from 3% in 2020 to 15% in 2025 and then surge to 32% and 58% in 2030 and 2040, respectively. Despite the huge progress in vehicle electrification, additional efforts are needed. If net-zero emissions can be achieved in the 2050s, oil share will drop to over 10% in the transportation area. In addition to electrification, other renewable energy, such as hydrogen, also need to be explored [10].

However, the current trend of intelligent automobile development is not going smoothly. There are still technical difficulties that have not yet been overcome in fully autonomous driving that are applicable to various scenarios. The large-scale market substitution of CAVs will be slow. It can be seen that the mixed traffic where HDVs and CAVs coexist will be the mainstream of road traffic in the foreseeable future [18, 19]. In complex traffic environments mixed with HDVs and CAVs, the complicated interactions between different types of vehicles may offset the positive impact CAVs have brought to traffic efficiency and safety. For example, the variability and unpredictability of human drivers can make CAV control significantly more challenging. As a result, the mixed traffic scenario has recently received more

attention. In civil engineering, research focuses on the dynamic road design, including dedicated CAV zones and flexible lane markings. In telecommunications engineering, improving the reliability and quality of vehicle-to-everything (V2X) communication has become a key area of study. In addition, determining legal accountability in accidents involving CAVs also receives much research attention. Despite the breadth of research across these disciplines, this thesis specifically focuses on the control strategies for CAVs operating in mixed urban traffic.

1.2 Challenges and Contributions

Reviewing the research on the control of CAVs in mixed-traffic environments [20–31], although certain theoretical achievements and engineering practices have been made, there are still some shortcomings, and more advanced control approaches are required to address these challenges.

1.2.1 Research Challenges

Urgent challenges to be solved in the control of CAVs in mixed-traffic environments are summarized as follows:

- **Scalability.** As there are a large number of on-road vehicles, it is challenging to formulate a comprehensive model that can guarantee global optimality and meanwhile maintaining an affordable computation burden. Furthermore, ensuring the robustness and real-time applicability of the proposed algorithms to deal with the time-varying nature.

- **Human-machine interaction.** HDVs are inevitable in mixed-traffic scenarios, which often make the mixed-traffic environment evolve into a complicated state. Firstly, the lack of communication between HDVs and CAVs [32, 33]. Secondly, HDVs may have behavioral characteristics such as fluctuations. Thus, modeling the interactions between CAVs and HDVs in a more realistic way is a challenge [34, 35].

- **Environmental impacts.** To pursue environmental and sustainability goals, control of CAVs should emphasize more on fuel consumption reduction.

However, traffic efficiency and driving comfort are also important objectives in urban scenarios. It is a challenge to find the balance between fuel consumption, and traffic efficiency. To be specific, this may lead to multi-objective optimization, which is hard to solve. Moreover, the energy consumption modeling will bring additional nonlinearity and complexity [36–38].

- **AI-based approaches** The Learning-based method is a promising solution in traffic control, however, there are still some concerns. During the training procedure, although reward functions are designed for safety-critical control, no hard constraint on safety is activated, such as collision avoidance, speed limits, etc. Thus, how to guarantee the safety of these methods is the key challenge [39–41]. In addition, how to deal with the compatibility of data in different scenarios is also a tough issue [42].

- **Network privacy and security.** Although connectivity and cloud computing may facilitate traffic control in mixed-traffic environments, privacy and cyber-security concerns arise. It is challenging to protect data privacy and maintain cyber-security during communications and coordination [43, 44].

Among all these challenges, this thesis focuses on the design of HDV-in-the-loop CAV and traffic control strategies for urban environments, with particular attention to algorithm scalability and energy efficiency. Urban intersections inevitably involve a large number of vehicles, making the development of a computationally efficient traffic coordination framework essential for improving overall traffic performance. Traffic congestion may incur increased fuel consumption and greenhouse gas emissions, which have negative environmental impacts. Multi-objective optimization can be utilized to deal with these different factors, but how to balance these factors effectively needs further study. To investigate CAV-HDV interactions, this thesis focuses on lane-changing behavior, which is a fundamental and frequent maneuver in urban traffic. Understanding lane-changing is crucial, as it forms the basis for analyzing more complex maneuvers such as overtaking, turning, and navigating roundabouts.

1.2.2 Aims and Contributions

Considering the above-mentioned research challenges, the objectives to be achieved in this thesis are listed in Fig. 1.3. To be specific, an urban road system architec-

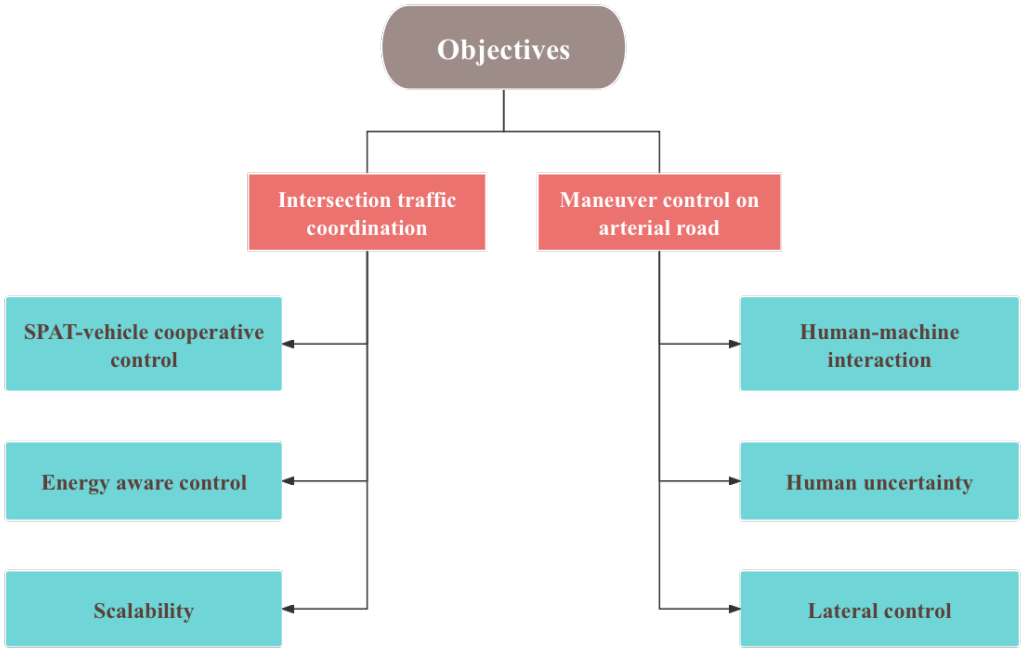

Figure 1.3: Objectives to be achieved in this thesis.

ture 1.4 in reference to [45] is formulated. As can be seen in Fig. 1.4, the layout consists of a lane-changing zone and a car-following zone. In the lane-changing zone, vehicles can conduct lane-changing and overtaking maneuvers, which are prohibited in the car-following zone. The reason for designing such a layout is that this thesis focuses on signal-vehicle cooperative control and scenarios where vehicles can change lanes. In particular, lane-changing and overtaking maneuvers can be carefully studied in the lane-changing zone and then the signal-vehicle cooperative control can be further investigated in the car-following zone. RSUs collect the vehicles' information and forward it to CAVs and coordinators. The coordinators are responsible for control of traffic signals and CAVs. Based on this layout, the research goals of the proposed CAV control in mixed-traffic environments can be summarized into the following aspects:

- Design effective intersection traffic optimization model blending SPAT and

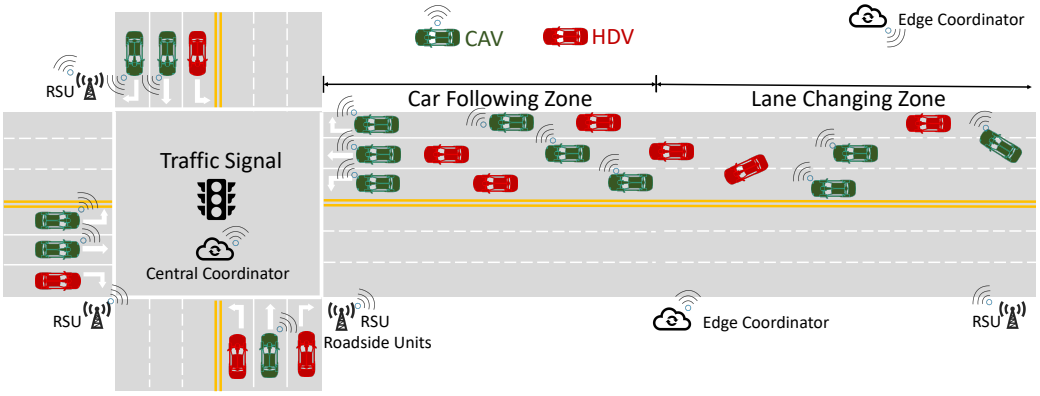

Figure 1.4: The urban road system architecture with mixed autonomy vehicles. RSUs can gather vehicle information, while coordinators are responsible for manipulating SPAT and controlling CAVs.

vehicle trajectory control. This model should improve overall intersection traffic performance while being computationally efficient.

- Develop a novel structure to effectively model the interactions between HDVs and CAVs, which can benefit the safety-guaranteed lane-changing control in mixed-traffic environments.

- Combine the model-based method and data-driven method in designing lane-changing control in mixed-traffic environments. This combination should be theoretically provable while remaining flexible in dealing with uncertainties brought by humans and HDVs.

- Design and conduct experiments to evaluate the real-time performance of the traffic control methods, especially in mixed traffic scenarios

To solve the above-mentioned goals, novel algorithms are proposed, and contributions are listed as follows:

1. This thesis proposes a two-layer signal-vehicle coupled optimal control strategy in mixed-traffic environments, which is formulated as two cascaded optimization problems by a notion of mixed platoons. In particular, the upper layer is designed to minimize the total waiting time of all vehicles in the intersection, while the lower layer is formulated to minimize the aggregated

vehicle energy consumption by adequately exploiting the signal plan, number of crossing vehicles, and target crossing speed obtained in the upper layer. Extensive simulation results are provided to examine the performance of the proposed framework and to reveal the impact of this algorithm at different CAV penetration rates, traffic demands, and electric vehicle ratios.

2. A game-theoretic trajectory planning scheme for CAV in response to the movement of an HDV in the target lane is proposed. The interaction between the two vehicles is modeled as a Stackelberg game, allowing both vehicles to change lanes. An optimal control strategy is developed for CAV derived from the Hamilton–Jacobi equation. These strategies are shown to constitute equilibrium points, and their stability is analyzed. By constructing a zeroing control barrier function, we demonstrate that the designed equilibrium strategy ensures the collision avoidance set remains forward invariant with an appropriate choice of weight matrices for the CAV cost function. Finally, numerical simulations validate the effectiveness of the proposed method.

3. A two-layer learning-and-game-based coalitional decision-making and control strategy for multi-vehicle lane-changing is proposed. In particular, a game-based coalition formation is proposed in the upper layer, which could facilitate lane-changing and improve computation efficiency compared with global optimal control. In the lower layer, a Stackelberg game-based framework is utilized to model the interaction between CAVs and HDVs. To enhance robustness against human uncertainty, a data-enabled predictive control is applied to CAVs. Extensive simulations are conducted based on data representing different driving behaviors, whose results demonstrate the effectiveness of this proposed framework in various lane-changing scenarios involving HDVs with different aggressiveness.

4. The HIL experiments are conducted in order to verify the practical applicability of the proposed methods in different scenarios. The effect of electric vehicles on energy efficiency is also examined by comparison with conven-

tional vehicles.

1.3 Thesis Outline

The remainder of this thesis is structured as follows. In Chapter 2, comprehensive works on related topics have been carefully reviewed. In Chapter 3, some general mathematical formulations and preliminary concepts are introduced. In Chapter 4, the mixed platoon-based hierarchical control framework entailing the mixed platoon model, traffic SPAT optimization, and speed trajectory optimization is proposed. The benefit of this method is shown by comparisons with various traditional strategies, where the impact of factors such as traffic density, flow distribution, and penetration rates, are investigated. In Chapter 5, the interaction of both vehicles is considered by a Stackelberg game, which yields an unconstrained optimal control solution. Then a theoretical proof is provided to show such a strategy is an asymptotically stable equilibrium, and with a suitable design of the weight matrices, safety can be guaranteed. In Chapter 6, a two-layer coalitional decision-making and control strategy for multi-vehicle lane-changing in mixed autonomy is proposed. A game-based coalition control is utilized to promote lane-changing behaviors, while the data-enabled predictive control is applied to enhance robustness against human uncertainty. The effectiveness of the proposed method is validated by comprehensive simulations and HIL experiments. Finally, Chapter 7 draws the conclusions and discusses further works.

1.4 Publication List

Journal Papers:

1. **Chen, M.**, Li, B., Bian, Y., Zhuang, W., Simos A E., Pan, X., and Chen, B, Intersection Signal-Vehicle Coupled Coordination with Mixed Autonomy Vehicles. *IEEE Transactions on Transportation Electrification*, PP:1-1, 04 2024

2. Hu, B., Zhang, S., Feng, Y., Li, B., Sun, H., **Chen, M.**, Zhuang, W. and Zhang, Y., A Knowledge-guided Reinforcement Learning Method for

Lateral Path Tracking. *Engineering Applications of Artificial Intelligence*, 139:109588 01 2025

3. **Chen, M.**, Li, B., Zhang, S., Zhang, H., Zhuang, W., Yin, G., and Chen, B, A Game-Theoretical Framework for Safe Decision Making and Control of Mixed Autonomy Vehicles. *IEEE Transactions on Intelligent Transportation Systems.*

4. Sun, H., Li, S., Li, B., **Chen, M.**, Zhang, S., Zhuang, W., Yin, G. and Chen, B., Spatial-Temporal Transformer-based Ecological Car-Following Strategy for Connected Electric Vehicles in Dynamic Environment. *Energy*

Conference Papers:

1. **Chen, M.**, Jiang, J., and Chen, B, 2024. A Game-based Optimal and Safe Lane Change Control of Autonomous Vehicles in Mixed Traffic Scenario. *2024 IEEE 8th International Conference on Control Technology and Applications (CCTA)*. **(Outstanding Student Paper Award)**

2. Li, B., Zhuang, W., Zhang, S.,**Chen, M.**, Yin, G., and Chen, B, 2024. Integrated Battery Lifetime and Energy Efficiency Driving Strategy for Electric Vehicles in Urban Environments. In *2024 IEEE 8th International Conference on Control Technology and Applications (CCTA)*.

Chapter 2

Related Works and Fundamental Concepts

In this chapter, relevant works on related topics will be comprehensively reviewed. To begin with, research on intersection traffic coordination in fully CAV environments is carefully reviewed. This is to demonstrate how CAV technology alleviates urban traffic issues. Then, the survey is extended to traffic coordination in mixed-traffic environments, which is the key problem to be solved in this thesis. The two key elements of intersection traffic coordination, SPAT, and CAV trajectory planning, are reviewed separately. However, SPAT and trajectory planning are mutually coupled, thus the papers on the co-optimization of SPAT and trajectory planning are carefully reviewed. Only focusing on traffic coordination is not enough, as details such as collision avoidance or maneuver control of individual vehicles are always neglected. Therefore, maneuver control of CAVs conducted on arterial roads in mixed-traffic environments is reviewed. To be specific, model-based methods and learning-based methods are studied separately.

2.1 Intersection Traffic Coordination in Fully CAV Environments

Traffic congestion and pollution problems are exacerbated as the number of vehicles continues to increase. However, advanced technologies such as vehicle-to-infrastructure (V2I), vehicle-to-vehicle (V2V) communication, and L3 self-driving

have emerged recently and show great potential in dealing with traffic congestion and fuel consumption [46], and thus facilitate the development of SPAT control. With the controllability of CAVs and collected historical and real-time traffic data such as positions and velocities, trajectory planning of CAVs can be conducted to improve traffic flow distribution and further enhance overall traffic efficiency. Thus traffic control with CAVs has become a popular research topic.

Traditional SPAT control has been well studied including the time slotted-based method [47] and enumerate method [48, 49]. With the engagement of CAVs, their trajectory data is utilized to predict the movement of traffic flow and further optimize SPAT [50, 51]. In addition, considering the connectivity and controllability of CAVs, the concept of signal-free intersection control is formulated [52, 53]. Under such a concept, the CAVs can drive across the intersection without collisions through effective communication and coordination. Among these works, the rule-based method is the most common [54–56]. Although such a method can guarantee the safety of the intersection, global optimality can not be ensured. Due to this, optimization-based methods are developed, where factors such as fuel consumption, traffic delay, safety concerns, and waiting time are considered [57–63]. However, the challenge is that the computation burden of such methods are very high, especially with high traffic demand [64, 65].

Trajectory planning of CAVs can reduce fuel emissions and improve traffic efficiency. The earliest research begins with the car-following models, such as Newell's car-following model [66], Gipps model [67], and Intelligent Driver Model (IDM) [68]. Eco-driving which intends to improve energy efficiency by optimizing trajectory profiles is proposed and carefully studied in [36–38, 69]. To be specific, by providing suggested velocity profiles and velocity limits to CAVs, fuel consumption, vehicle stops and waiting time can be reduced. Feedback control and MPC are applied [70–72], where velocities and positions are formulated as the state variables and acceleration strategies are formulated as the control variables [73, 74]. The computation burden is a noticeable challenge for such an optimization-based control method. To ease the computation burden that comes from the number of ve-

hicles, a promising solution is to form platoons and only control those vehicles that lead platoons [75,76]. The research on trajectory planning of CAVs to benefit traffic can be dated back to 1970s [77]. These studies aimed to find out how much traffic congestion could be alleviated if the vehicle trajectory was controlled by a central coordinator [78–80], where dynamic traffic flow is considered. However, such methods cannot reflect a practical understanding of on-road vehicle flow. Thus, trajectory planning of CAVs is incorporated with the Cell Transmission Model (CTM) to make the analysis more realistic [81]. The CTM divides the roadway into small segments (cells) and updates traffic conditions over time, which can model the complex traffic network in a simple way.

However, the signal and vehicle velocity are mutually coupled. Individual traffic signals or vehicle control is not sufficient to ensure traffic efficiency at a road intersection. A joint control framework of SPAT and vehicle trajectories is proposed in [82, 83]. A two-stage optimization problem with SPAT optimization at the first stage and vehicle trajectory planning at the second stage where no turning movements were considered is formulated in [83]. Dynamic programming is utilized to optimize SPAT. In [82], a unified framework of vehicle trajectories and SPAT optimization is proposed and solved by mixed integer linear programming. The cooperative control of SPAT and vehicle trajectories is also investigated [31, 84–86]. In particular, [86] proposes a cooperative control method that integrates adaptive cruise control and SPAT. The vehicle trajectory planning is divided into an accelerating segment and a cruising segment. SPAT is determined based on planned vehicle trajectories, which guarantee vehicles arrive at the stop line during a green signal phase. In addition, SPAT is further optimized by an enumeration-based method to minimize traveling time and maximize green phase duration in [85].

However, in the foreseeable future, mixed traffic with HDVs and CAVs will be prevalent. While traffic control methods under a fully CAV environment can be a solid foundation for traffic control, there are still some challenges in mixed-traffic environments. These challenges include the uncontrollability of HDVs, as well as ineffective communications with HDVs. In addition, the high uncertainty

and various driving behaviors of humans make it hard to guarantee traffic safety, which is the most crucial part of traffic control. To overcome the above-mentioned challenges, new control methods are needed.

2.2 Intersection Traffic Coordination in Mixed-Traffic Environments

2.2.1 Signal Control and Trajectory Planning in Mixed-Traffic Environments

Traffic signal control in mixed-traffic environments has been well-studied and mainly based on vehicle trajectory data or the integration of vehicle trajectory and infrastructure-based detector data. Infrastructure-based detector data are often used as supplementary data, which can provide traffic flow parameters such as traffic volumes and queue lengths to enhance the accuracy of traffic condition estimation [50, 87]. Optimization-based methods [88–91] and learning-based methods [92–99] are the primary methodologies when conducting SPAT control in mixed traffic environments. In [50], both macroscopic traffic data and detector data are used to estimate the arrival time of traffic flows. A two-level optimization problem is formed. In the upper layer, a ring barrier structure is utilized for SPAT optimization, where barrier durations are optimized by dynamic programming to minimize queue lengths and traffic delay. In the lower layer, SPAT sequences and durations were optimized by enumeration for the given barrier derived from the upper layer. [87] proposes a real-time feedback control method for SPAT based on vehicle cumulative travel time. Kalman filter-based stochastic estimation method was utilized to estimate the vehicle's cumulative travel time, and the SPAT was selected to allow vehicles with the largest cumulative travel time to pass the intersection. Moreover, the intersection capacity is also improved while the vehicle delay is reduced in [100–103]. As for the learning-based method, [97] uses a transformed version of the deep Q network (DQN) model to improve the training efficiency. The number of vehicles in each road segment is used as the input of the network, while the total

waiting time of vehicles is set as the reward function. Although the research on this topic is dominant, microscopic CAV trajectory data are not fully used, as they can reflect the states of individual vehicles instead of overall traffic flow.

The Eco-driving in the mixed traffic environment optimizes CAV trajectories based on SPAT and traffic flows to reduce fuel consumption at intersections [104–113]. For example, [104] utilized MPC to optimize the accelerations of CAVs for reduced fuel consumption according to the SPAT and states of the preceding vehicles, which are assumed to be known or can be collected by on-board sensors of CAVs. The queuing effect is also studied when traffic demand is high [105]. However, Eco-driving may incur increased travel time. Therefore, factors other than fuel consumption are considered in the objective function of trajectory planning, such as vehicle delay [107,108], driving smoothness [112], and safety concerns [107]. In addition, lane changing is further considered in [108], where a two-layer optimization framework jointly optimizes the lateral moving strategies and the longitudinal acceleration strategies for CAVs in mixed-traffic environments is proposed. The parallel Monte Carlo tree search algorithm is designed to find an efficient lane-changing strategy. The above studies only focus on the benefits of target CAVs and mixed platoons, without considering the impact on the overall traffic flow. In [6], an optimal control model is formulated with terminal cost concerning the final states of CAVs at the stop bar (e.g., velocity and time of arrival), which is designed to improve intersection traffic efficiency, and with operating cost concerning the fuel consumption of each CAV. Different from [6], where the passing velocity of CAV is maximized, [114] finds out a higher passing velocity does not ensure a higher traffic efficiency at intersections. The concept of "$1+N$" mixed platoon is proposed and the passing velocity of the mixed platoon is designed such that the number of vehicles passing the intersection can be maximized. Besides model-based methods, the learning-based method is also comprehensively investigated for trajectory planning in mixed-traffic environments [111, 112]. In [112] a reinforcement learning (RL)-based trajectory prediction method is formulated. The velocity of a leading CAV is optimized to reduce the jerking phenomenon, which can offset

the oscillation wave caused by stopping during the red signal phase. CAV states (i.e., positions and velocities), SPAT, relative velocity, and distance with the preceding vehicles are the network inputs. The collision avoidance, desired velocity, and arrival time are considered in the reward function. Despite comprehensive research conducted on mixed traffic, the interaction between vehicle trajectory planning and SPAT is not fully discussed. The cooperative control of SPAT and trajectory planning in a unified framework should be further studied in mixed-traffic environments.

2.2.2 Signal and Vehicle-Coupled Coordination in Mixed-Traffic Environments

Analytical optimization models are commonly used to jointly optimize SPAT and CAV trajectories at intersections in mixed-traffic environments [20–31, 115–117]. Some of these works use an integrated optimization framework to jointly control signal timing and vehicle trajectory, such as [20–22]. For instance, in [22], multi-objective mixed-integer non-linear programming is established to optimize signal timing and vehicle trajectories. This aims to reduce stops at the traffic light and overall delays. Lagrangian relaxation is applied to decompose the original problem into separated lane-level submodels for reduced complexity.

Although the unified framework of SPAT and CAV trajectory planning has the potential to reach the global optimum, the computational burden remains high for such joint optimization schemes due to the scale of the problem [118, 119]. In this context, the hierarchical control/optimization architecture emerges as a promising solution, where, in most cases, SPAT is optimized in the first place, followed by the vehicle trajectory control such as velocity profiles and passing sequences subject to the SPAT plans formed in the upper layer [23], [24]. More specifically, in [23], the signal phase duration is optimized to minimize total delay in the upper layer based on the fundamental diagram model of mixed traffic flow, which embeds CAV penetration rate and stable space headway. Next, the intersection arrival time of all CAVs is determined by finding their individual speed profiles using empirical rules(i.e. a CAV will follow the IDM car-following model if it arrives at the stop line after the planned arrival time). In [25], a joint traffic signal and vehicle speed

rolling-horizon optimization method is introduced. It uses CAV data to optimize SPAT and then offers speed recommendations to each vehicle to reduce the total stops. This takes into account the possible response delay of the HDVs.

The computational burden remains heavy if each CAV is regarded as the individual control unit. An alternative is to form mixed platoons where only the trajectories of platoon-leading CAVs are co-optimized with SPAT at intersections [120, 121]. Platoon-following vehicles are assumed to follow a specific car-following model such as IDM. Recently, [26] proposed a new scheduling method by introducing an additional "white signal phase", during which connected vehicles are forced to keep up with the vehicle immediately ahead to pass the intersection as a platoon. The optimization problem is formulated as a mixed-integer non-linear program linearized and incorporated into a receding horizon framework to tackle the complexities. [27] further investigate the influences of various driving aggressiveness of CAVs on the safety performance of the intersection, which is operated by the additional white signal phase. The robustness of these methods should be further investigated when considering the interactions with HDVs. In addition to model-based methods, promising results have been shown using data-driven and learning-based methods [79, 122] in the context of vehicle and traffic efficiency. In particular, a two-stage framework that sequentially optimizes SPAT and CAV trajectories is formulated in [79]. This framework aims to improve traffic efficiency and reduce total delay, which consists of estimation, planning, and optimization. Long short-term memory networks are utilized in this work to learn traffic patterns and driving behaviors according to CAV information. Then the states of HDVs can be predicted. Deep reinforcement learning (DRL) is applied to optimize SPAT durations with the inputs being the number of arriving vehicles and velocities. Based on the optimized SPAT, the velocities of CAVs will be adjusted for the maximum use of green phase duration. Differently, a joint optimization of SPAT and CAV trajectory is proposed in [122, 123]. The problem is solved using RL to improve traffic safety and efficiency. To be specific, a signal-vehicle control architecture integrating adaptive SPAT control and velocity advisories is proposed in [122]. This method utilizes

the Soft-Actor Critic RL framework to improve real-time traffic safety. The rear-end conflict rate is estimated based on real-time collected traffic parameters such as SPAT. Then the traffic parameters and conflict rate are utilized as inputs to the control system, which aims to minimize the total conflicts and extend the current signal phase accordingly. However, the performance of this learning-based method is largely affected by the quality of training data [42].

Traffic signal control enhances the overall traffic efficiency by optimizing intersection SPAT, while CAV trajectory planning improves the benefits of mixed platoons by optimizing velocity trajectories and acceleration strategies given the specific SPAT information. Although there is no doubt that co-optimization of CAV trajectory planning and SPAT can achieve a better performance than optimization of either one, there exist research gaps in existing co-optimization methods: 1) Investigating more efficient solving methodology to guarantee real-time applicability, while maintaining relatively good performance. 2) The interactive relationship between SPAT and CAV trajectory planning needs further investigation. 3) Study the trade-off between traffic efficiency and vehicle energy consumption.

2.3 Maneuver Control of CAVs on Arterial Roads in Mixed-Traffic Environments

In most research on the cooperative control of SPAT and trajectory planning of CAVs in mixed-traffic environments, HDVs are assumed to follow a specific car-following model such as IDM, and the complicated interactions between HDVs and CAVs are also ignored. However human drivers often make mixed-traffic environments more complex [124, 125]: human driving behaviors fluctuate randomly; illegal driving such as illegal speeding and lane-changing; defecting driving such as slow reactions. In addition, the car-following or lane-changing behaviors of human drivers may change sharply due to their limited observation of the surrounding environments and other uncertainties [126–128]. To comprehensively study this interaction and mutual influences between HDVs and CAVs, safety-oriented lane-changing strategies for CAVs are a good entry point and receive much research

attention.

2.3.1 Model-based Maneuver Control of CAVs

In general, lane-changing control can be classified into model-based and learning-based approaches. The model-based described in this thesis refers to a series of algorithmic knowledge based on mathematical/physical models, empirical knowledge of rules, and domain knowledge for specific applications [129–132]. In can be further divided into rule-based approaches [133], artificial potential fields [134], sampling method [135], optimization-based methods [41, 136–139], PID-based methods [140, 141], Fuzzy logic control [142, 143], etc.

However, rule-based methods can only deal with simple scenarios. When it comes to complex systems, these methods are no longer effective. As the computing power of the controller increases, optimization-based approaches have become the interest of the present research. Among all the optimization-based approaches, Pure Pursuit [144], Linear Quadratic Regulator, and MPC [145, 146] are the most commonly adopted methods. Numerical optimization-based trajectory planners are formulated in [139], which can generate trajectories with continually changing surroundings. In [134, 137], MPC is utilized to generate safe trajectories for CAVs. In addition, with the implementation of MPC, real-time performance can also be ensured. Optimization-based methods have a complete theoretical support system and have natural advantages in analyzing algorithm stability, optimality, and convergence. In addition, the optimization-based model has better interpretability. However in real-world applications, the parameters of optimization-based methods are difficult to tune, the detailed vehicle dynamic mechanism is not yet completely clear, and the cost of knowledge acquisition is high. Meanwhile, existing optimization-based methods are difficult to support the continuous learning and evolution of control behavior. Furthermore, the interaction with surrounding HDVs is often ignored or simply viewed as an obstacle. However, this ignored interaction between CAVs and HDVs is crucial for CAV decision-making and trajectory planning [147–149].

Game theory methods are very promising for dealing with conflict behavior

and cooperation between players, which recently turned out to be an efficient way to model the interaction between CAVs and HDVs [33, 150]. In this context, a differential game theoretical framework is applied in [151] to model the interaction between multi-agents. The differential game is a game that is played in a dynamic environment [152]. Moreover, the iterative linear-quadratic regulator was used, where repeated approximations converge reliably and can be implemented in real time [153, 154]. In [155], the mixed strategy Nash equilibrium theory, together with the intention prediction method, was used to formulate the trajectory planning framework. This combination improves both the driving comfort and the safety of vehicles at uncontrolled intersections.

Another effective game-theoretical framework to model the interaction between HDVs and CAVs is the Stackelberg game because the two players involved in lane-changing can directly observe each other's strategies and intentions, allowing them to minimize their game costs accordingly [32, 156, 157]. Based on this premise, both players adjust their strategies, forming a dynamic game problem. In [158], a game-based model predictive controller is designed to address the mandatory lane change problem in mixed traffic environments. It generates appropriate speed trajectories for CAVs to arrive at a desired longitudinal position and conduct the lane change maneuver optimally. In [159], a merging control for CAVs at ramp intersections considers the interaction between following vehicles in the main lane and merging vehicles. The predicted trajectories of the following vehicles are used to maintain safe longitudinal distances during lane changes. However, the simplicity of the driver model may lead to inaccurate estimations of surrounding positions and future actions. Moreover, these researches ignore the interactions between different CAVs (i.e. CAVs intend to change lanes), and safety cannot be ensured when the surrounding HDVs take a sudden break or acceleration [160].

In [161, 162], mandatory lane-changing strategies for CAVs are designed by considering the cooperation between different CAVs. [163] further investigates the cooperation between CAVs in the merging zone. In [164], a game-based decision-making model allows lane changes at intersections, accounting for the level of co-

operation among vehicles in adjacent lanes, rendering the problem more realistic. In [165, 166], DRL is integrated with the game theoretical framework to deal with the decision-making of CAVs. Scenarios of multilane merging and non-signalized roundabouts are considered in [34, 35], where a game-based Stackelberg method is proposed for the decision-making and trajectory planning of CAV. Moreover, personalized objective functions of each vehicle and system traffic efficiency are taken into account, demonstrating the application of game-based lane change and formulating methodologies to better model the interaction between CAVs and HDVs in mixed traffic.

2.3.2 Learning-based Maneuver Control of CAVs

The learning-based approach focuses on machine learning algorithms that have emerged widely in recent years, such as deep learning and RL [41, 136, 167–170]. Traditionally, learning-based approaches can be segmented into three broad categories, including supervised learning, unsupervised learning, and RL. For lane-changing control specifically, most of these learning-based approaches are either supervised learning (such as Behavior cloning) which extracts a policy based on the demonstrated inputs and outputs [171], or RL which is an area concerned with how controllers take actions in an environment in order to maximize the cumulative rewards by trial-and-error [172–174]. Data-driven methods realized by machine learning have the characteristics of no need for accurate modeling, continuous learning, evolution from data, strong algorithm versatility, etc. And it is supported by tools such as massive open-source models and algorithm libraries. A deep neural network-based decision-making strategy is formulated in [136], which is flexible and can be used in real traffic scenarios. However, such methods often have difficulties in the analysis of theoretical characteristics, and their typical "black box" characteristics also bring problems such as poor generalization and high reliance on high-quality big data [39] or high-fidelity simulation model [40]. A small change in the neural network can cause serious traffic accidents [41]. An alternative is to make use of RL. In [175], a stochastic Markov Decision Process (MDP) is used to model the CAV's interaction with the environment, and then based on the re-

ward function of MDP, RL is applied. However, the learning efficiency of RL needs to be improved. In other words, learning-based methods, whose performance is largely influenced by the quality and quantity of data, still have a long way to go. The data-driven model predictive control method, which is based on the measurable data [43, 44], can overcome the above-mentioned shortcomings. In particular, the data-enabled predictive control method proposed in [44, 176] can achieve safe and optimal control for unknown systems under state measurements. Such methods can avoid identifying a parametric system model and, instead, directly learn the behavior of the system based on Willems' fundamental lemma [177]. Existing work shows that data-enabled predictive control can achieve comparable performance with respect to MPC with precise knowledge of nonlinear and stochastic systems [178, 179].

However, there are still several limitations of the existing works on the lane-changing control of CAVs in mixed-traffic environments: 1) Game-based methods may incur a heavy computation burden and are not applicable when the number of vehicles is large. 2) How to deal with human uncertainty and enhance robustness. 3) CAVs are treated equally. In fact, CAVs have their own driving intentions and are not willing to sacrifice their own driving comfort or efficiency to facilitate other CAVs.

2.4 Summary

This chapter reviews the state-of-the-art research on intelligent control of CAVs. Particular attention is given to studies on intersection traffic coordination and maneuver control on arterial roads. While extensive work has been done in this area, several important limitations remain: 1) High computational demands of existing methods when applied to large-scale traffic with many vehicles. 2) Insufficient exploration of the trade-off between traffic efficiency and vehicle energy consumption. 3) Lack of realistic and safe models for capturing the interactions between HDVs and CAVs, along with limited theoretical analysis of such models. 4) Limited experimental validation of the real-time performance of control strategies in mixed-

traffic environments. This thesis aims to address these gaps by developing scalable, energy-aware, and experimentally validated control strategies for CAVs operating alongside HDVs in urban traffic.

Chapter 3

Preliminary

3.1 Introduction

Following the urban traffic coordination framework in Fig. 1.4, the thesis can be divided into two separate control problems, including the signal-vehicle coupled cooperative control and the lane-changing control. This involves solving some fundamental control problems (i.e., trajectory planning), which include different techniques, such as optimal control-based methods and MPC-based methods. Some general mathematical formulations and preliminary concepts are introduced in this chapter to bridge the general concepts introduced in Chapter 2 and the specific problems considered in the later chapters.

3.2 General Mathematical Formulations and Preliminary Concepts

Trajectory planning and control of CAVs is a critical component in urban traffic. In the signal-vehicle coupled coordination problem, CAVs need to navigate from a starting position to pass the intersection without collision. In particular, this thesis relies on optimization-based methods to formulate trajectory planning as a mathematical optimization problem, aiming to find the best trajectory according to designed cost functions (e.g., shortest trajectory, minimum energy, comfort) while satisfying constraints (e.g., collision avoidance). The problem formulation can be

given as follows:

$$\begin{aligned} \min_{u} \quad & J(x,u) \\ \textbf{s.t.} \quad & g(x,u) \leq 0, \\ & \dot{x} = f(x,u) \end{aligned} \tag{3.1}$$

where $J(x,u)$ is the cost function, which may consider energy consumption (Chapter 4, Chapter 6), comfort (Chapter 6), or deviation from a reference trajectory (Chapter 4, Chapter 5, Chapter 6). x denotes the vehicle states, u is the control input, and $g(x,u)$ stands for inequality constraints. In the context of vehicle trajectory planning, the inequalities may include speed limits, acceleration limits, collision avoidance, road boundaries (Chapter 6), etc. $f(x,u)$ denotes the vehicle motion model. Depending on different scenarios, different motion models are required. For example, in the car-following (Chapter 4) or high-level traffic coordination problems (Chapter 6), the double integrator model can be utilized to characterize the evolution of the vehicle states. While in scenarios where there is lane-changing or overtaking (Chapter 5, Chapter 6), a bicycle model is often required to model the lateral movements of the vehicle.

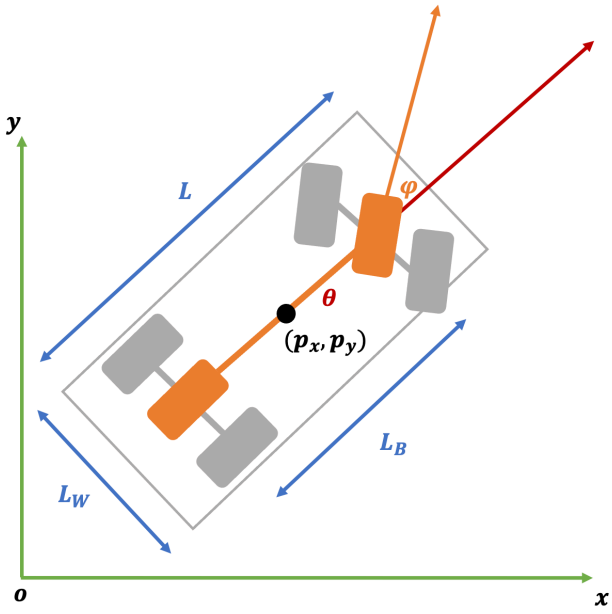

Figure 3.1: Illustration of the bicycle model. With L, L_W, and L_B being the length, width, and wheelbase of the vehicle.

More specifically, the double integrator model is a fundamental second-order

dynamic model, which treats the vehicle as a point mass with position and velocity states, where vehicle acceleration is the control input. The formulation can be given as follows:

$$\begin{cases} \dot{p} = v, \\ \dot{v} = a, \end{cases} \tag{3.2}$$

where $p \in \mathbb{R}$ denotes the vehicle longitudinal positions, v denotes the velocity, and a denotes the acceleration. However, the double integrator model cannot reflect the lateral movement of a vehicle in a realistic way. On the other hand, the bicycle models are often utilized to model the lateral movements of a vehicle. The bicycle model is a kinematic representation of a car-like vehicle, which is more realistic than the double integrator model. The bicycle model utilized in this thesis is illustrated in Fig. 3.1, with the formulation given as follows:

$$\begin{cases} \dot{p_x} = v\cos(\theta), \\ \dot{p_y} = v\sin(\theta), \\ \dot{\theta} = \frac{v}{L_B}\tan(\phi), \\ \dot{v} = a, \end{cases} \tag{3.3}$$

where θ and ϕ are the heading angle and steering angle, respectively. $p_x \in \mathbb{R}$, $p_y \in \mathbb{R}$ are the longitudinal and lateral positions, respectively.

The cost function $J(x,u)$ in traffic trajectory planning often follows a quadratic form. When the vehicle motion model is linear, an unconstrained problem can be formulated as follows:

$$\begin{aligned} \min_{u} \quad & J(x,u) = \int \|x\|_Q^2 + \|u\|_R^2 \, dt \\ \textbf{s.t.} \quad & \dot{x} = Ax + Bu \\ & x(0) = x_0 \end{aligned} \tag{3.4}$$

where Q and R are the positive definite weighting matrices for the state and control input, respectively. $x(0)$ is the initial state of the vehicle. A and B are matrices to characterize the vehicle motion model. A common approach to solving this problem

is by the optimal feedback law:

$$u = -Kx \tag{3.5}$$

where K is the constant gain matrix and is computed via the Algebraic Riccati Equation, which is given as follows:

$$\begin{aligned} &A^T P + PA - PBR^{-1}B^\top P + Q = 0 \\ &K = R^{-1}B^\top P \end{aligned} \tag{3.6}$$

This controller is known as the linear quadratic regulator (LQR), which can find the optimal control for CAVs and ensure stability, however, there are some limitations. In practice, the vehicle motion model is time-varying and nonlinear, which greatly influences the performance of the LQR. In addition, as the constraints are not included in LQR, the collision avoidance of different vehicles is not guaranteed.

Different from LQR, where the control input is determined without feedback from the system's output, MPC uses predictive models to anticipate changes and adjust control input proactively. To be specific, MPC solves finite-horizon optimal control problems iteratively based on real-time measurements while implementing only the first control action. This approach is particularly useful in constrained, multivariable systems like CAVs in urban traffic environments. For the sake of further discussion, the system is specified in discrete time. The mathematical formulation of MPC at each time step k is given as follows:

$$\begin{aligned} \min_{u(k)} \quad & J(x(k),u(k)) = \textstyle\sum_{j=0}^{N-1} l(x(j|k),u(j|k)) + V_f(x(N|k)) \\ \textbf{s.t.} \quad & \text{for } j = 0,1,2,\ldots,N-1, k \in \mathbb{N} \\ & x(j+1|k) = f(x(j|k),u(j|k)) \\ & x(j|k) \in \mathbb{X} \\ & u(j|k) \in \mathbb{U} \\ & x(N|k) \in \mathbb{X}_f \\ & x(0|k) = x_k \end{aligned}$$

where N is the control horizon. $l(x(j|k),u(j|k))$ denotes the stage cost. $V_f(x(N|k))$

denotes the terminal cost, which is designed to ensure stability for MPC. $\mathbb{X}$ and $\mathbb{U}$ denote the constraint set for the state and control input, respectively. $\mathbb{X}_f$ is the terminal set and x_k is the current state. Compared with the full horizon optimal control method, MPC is more flexible for constrained, nonlinear urban traffic systems and is more adaptive to sudden changes on roads.

This real-time optimization capability of MPC is particularly valuable for implementing adaptive cruise control (ACC) in car-following zones of Fig. 1.4, where vehicles must continuously adjust to dynamic traffic conditions while ensuring collision avoidance. The scheme of ACC can be seen in Fig. 3.2, and a typical formulation is given as follows:

$$\begin{aligned} \min_{u} \quad & \textstyle\sum_{k=0}^{N-1} \left\|x(k)-x_{ref}\right\|_Q^2 + \|u(k)\|_R^2 + \|x(N)\|_W^2 \\ \textbf{s.t.} \quad & x(k+1) = f(x(k),u(k)), k \in \mathbb{N} \\ & x(k) \in \mathbb{X} \\ & u(k) \in \mathbb{U} \\ & d(k) \geq d_{safe} \\ & x(k) = x_k \end{aligned} \tag{3.7}$$

where $x(k) = [d(k), v(k)]^\top$, $d(k)$ denotes the distance to the preceding vehicle. x_{ref} includes the desired velocity and the following distance. $d(k) \geq d_{safe}$ is to avoid collision. Under such a control method, CAV automatically adjusts its speed to maintain a predefined speed and keep a safe following distance.

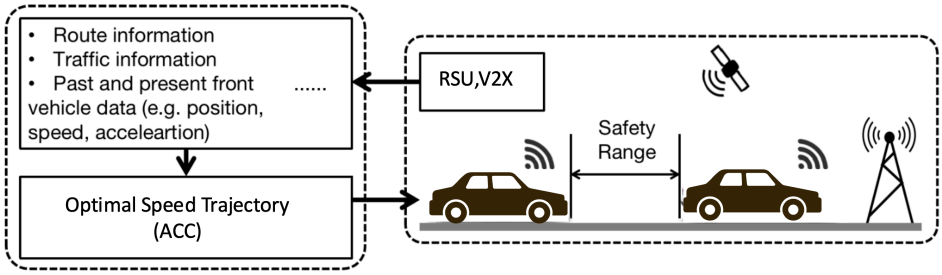

Figure 3.2: The scheme of ACC.

In mixed traffic environments, however, HDVs are not controllable, and car-

following models are utilized to describe how HDVs adjust their speed based on the vehicle ahead. Among different car-following models, this thesis adopts the intelligent driver model (IDM) to realistically simulate human-like acceleration and braking behavior, which is given as follows:

$$a = a_{\max}\left(1 - \left(\frac{v}{v_d}\right)^{\delta} - \left(\frac{s_d(v,\Delta v)}{s}\right)^2\right) \tag{3.8}$$

where $a_{\max}$ is the maximum vehicle acceleration, δ is the acceleration exponent. s denotes the actual gap to the preceding vehicle. Δv is the velocity difference between the preceding vehicle and the HDV (the velocity of the preceding vehicle minus the velocity of the HDV). v_d is the desired constant following velocity of the HDV. s_d is the desired distance headway of a human driver, which is given as follows:

$$s_d = s_0 + vT - \frac{v\Delta v}{2\sqrt{a_{\max}a_b}} \tag{3.9}$$

with s_0 the standstill spacing between consecutive vehicles, a_b the comfortable deceleration of each HDV, and T the safe time headway. HDVs could smoothly adjust their speed in response to both the gap to the preceding vehicle s and the velocity difference Δv based on IDM. By dynamically balancing the pursuit of a desired speed v_d with the maintenance of a safe following distance, IDM generates more realistic and human-like driving behavior compared to rigid constant-time-gap models. Additionally, IDM inherently accounts for driver comfort by constraining jerk, resulting in naturalistic acceleration and deceleration profiles that mimic real-world driving.

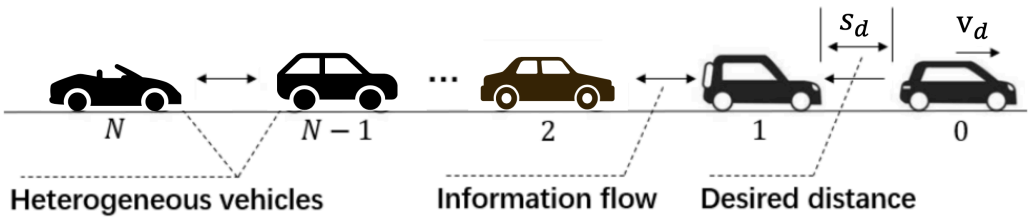

Figure 3.3: Cooperative control architecture of a heterogeneous vehicle platoon. s_d, v_d are the desired following distances and the target velocity of the platoon at the steady state, respectively.

By incorporating the advanced V2X communications, ACC can be extended to the cooperative adaptive cruise control (CACC) with a faster response time that enables a tighter vehicle following distance, as illustrated in Fig 3.3. In mixed urban traffic environments, the mixed platoons will naturally form when the vehicles tend to keep a tighter distance, where CAVs can positively influence the surrounding HDVs [180], [114], [181]. The formation of mixed platoons and how to make use of mixed platooning to benefit the overall urban traffic will be discussed in Chapter 4.

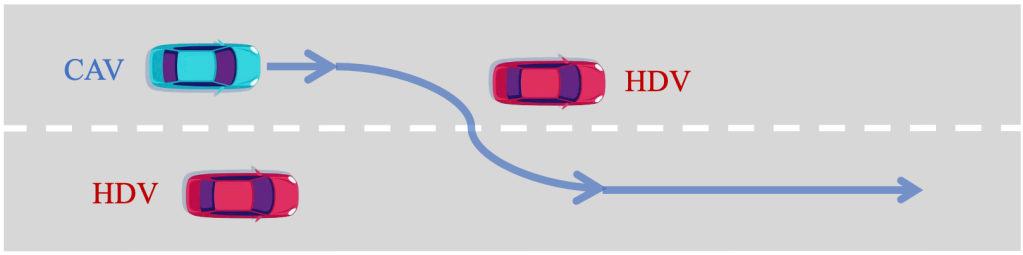

Figure 3.4: Lane-changing of the CAV in mixed traffic environments.

Moving on to the lane-changing zone of Fig. 1.4, this thesis utilizes the Stackelberg game to strategically model the previously neglected CAV-HDV interactions, which is illustrated in Fig. 3.4. In a Stackelberg game, the leader has a significant influence over the follower's behavior by moving first, effectively dictating the follower's optimal response based on the leader's chosen strategy. This strategic advantage allows the leader to anticipate and shape the follower's actions. By modeling the CAV as the leader and the HDV as the follower (without specifically controlling the HDV), a fully controllable CAV can be used to positively influence HDV behavior, improving overall traffic efficiency and safety. However, this level of control is not possible in a Nash game, where both players (CAV and HDV) are treated equally. In such a scenario, the controllability of CAVs in mixed-traffic environments cannot be fully leveraged. The feasibility of applying a Stackelberg framework in autonomous driving control has been demonstrated in previous studies [34, 35, 158, 182]. The game is solved using backward induction by

$$u_L^* = \underset{u_L \in \mathscr{U}_L}{\operatorname{argmin}} \left(\min_{u_F \in \mathscr{U}_F^*} J_L(x_0, u_L, u_F) \right) \tag{3.10}$$

$$\begin{aligned} \mathscr{U}_F^*(u_L) \triangleq \{ & u_F^* \in \mathscr{U}_F : J_F(x_0, u_L, u_F^*) \\ & \leq J_F(x_0, u_L, u_F), \forall u_L \in \mathscr{U}_L \} \end{aligned} \tag{3.11}$$

where x_0 denotes the initial state, u_L and u_F are the actions of the leader and follower, respectively, while u_L^* and u_F^* are the optimal actions. $\mathscr{U}_L$ and $\mathscr{U}_F$ are the action spaces. J_L and J_F stand for the leader's and follower's cost functions, respectively. From (3.10), (3.11), the definition of the Stackelberg equilibrium is given below, which will be the cornerstone of the forthcoming analysis.

Definition 3.1. *If there exists $u_F^* \in \mathscr{U}_F$ such that, for any fixed $u_L \in \mathscr{U}_L$*

$$J_F(x_0, u_F^*, u_L) \leq J_F(x_0, u_F, u_L) \tag{3.12}$$

and if there exists $u_L^* \in \mathscr{U}_L$ such that

$$J_L(x_0, u_F^*, u_L^*) \leq J_L(x_0, u_F^*, u_L) \tag{3.13}$$

for all $u_L \in \mathscr{U}_L$, then $\{u_L^*, u_F^*\} \in \mathscr{U}_L \times \mathscr{U}_F$ is called a Stackelberg equilibrium.

3.3 Conclusions

This chapter introduces general mathematical formulations and preliminary concepts needed for the urban traffic coordination discussed in this thesis. Starting from a generic trajectory planning problem, we introduce different vehicle motion models, including the double integrator model and the bicycle model. Then different control methods utilized to solve trajectory planning problems are introduced, i.e., LQR and MPC. ACC, IDM, and mixed platooning are introduced to characterize the car-following behaviors in mixed traffic environments. Finally, the Stackelberg game is introduced to model CAV-HDV interactions in lane-changing scenarios. All these will be specifically used in the development of the algorithms discussed in the following chapters. In particular, the mixed platooning and the IDM will be

employed in the signal-vehicle coupled coordination framework in Chapter 4. In Chapter 5, the Stackelberg game will be used for strategic interactive modeling of lane-changing behaviors in mixed traffic environments. Finally, in Chapter 6, an MPC-based method is applied to CAVs in multi-vehicle lane-changing scenarios.

Chapter 4

Intersection Signal-Vehicle Coupled Coordination

4.1 Introduction

In this chapter, the scalability and environmental impact issues in mixed traffic environments are investigated. An intersection signal-vehicle coupled coordination is proposed, which is utilized in the car following zone in Fig. 1.4. Some existing works use an integrated optimization framework to jointly control signal timing and vehicle trajectory, such as [20–22]. While these methods are capable of identifying the global optimum, the joint optimization structure incurs significant computational costs due to the problem's large scale [118, 119]. An alternative is to adopt the hierarchical control framework, with SPAT optimization performed at the higher level, followed by lower-level vehicle trajectory control that complies with the predetermined SPAT schemes [23, 24, 26]. The existing methods are mainly designed for maximizing travel time , whereas energy efficiency is either omitted or taken into account through conventional fuel consumption. As travel time and energy efficiency usually lead to contradicting optimal solutions, this chapter investigates the trade-off between intersection throughput and the energy efficiency of all vehicles by co-optimizing the traffic SPAT and CAV trajectories (whereby the velocities of HDVs are indirectly governed following the notation of "$1+N$" mixed platoon [180], [114]). Instead of using further alternative signal phases to pro-

mote CAV-led platoons (like [26]), the platoon formation is enforced by trajectory optimization in the present work. To avoid solving a complex joint optimization problem that is computationally demanding, a two-layer control architecture is designed, respectively, for finding the SPAT and vehicle speed plans. The novelty of the work in this chapter is as follows:

1. In contrast to the majority of existing SPAT control solutions that rely on macroscopic traffic flow models [26, 50, 183, 184], the proposed solution makes use of microscopic vehicle motion and queue discharging models instead. Therefore, the control solution tends to be more responsive to the time-varying traffic demands at a road intersection.

2. A novel signal-vehicle coupled optimal control strategy is proposed for mixed platoons, which can find the trade-off between the two key metrics: traffic throughput and vehicle energy consumption, unlike most of the existing methods, which solely focus on one aspect.

3. The benefit of the newly developed method is shown by comparisons with various traditional strategies [23]. Additionally, the impacts of intersection traffic density, flow distribution, and the penetration rates of CAV and EV are investigated by comprehensive simulation trials.

The remainder of this chapter is organized as follows. Section 4.2 introduces the problem and the intersection model. The mixed platoon-based hierarchical control framework entailing the mixed platoon model, traffic SPAT optimization and speed trajectory optimization is presented in Section 4.3. Simulation results and discussion are shown in Section 4.4. Finally, concluding remarks are given in Section 4.5.

4.2 Signalized Intersection Model

As illustrated in Fig. 4.1, this chapter considers a signalized road intersection with mixed traffic flow of CAVs and HDVs. The intersection layout studied in this work consists of two single-lane perpendicular and flat roads. The center of the intersec-

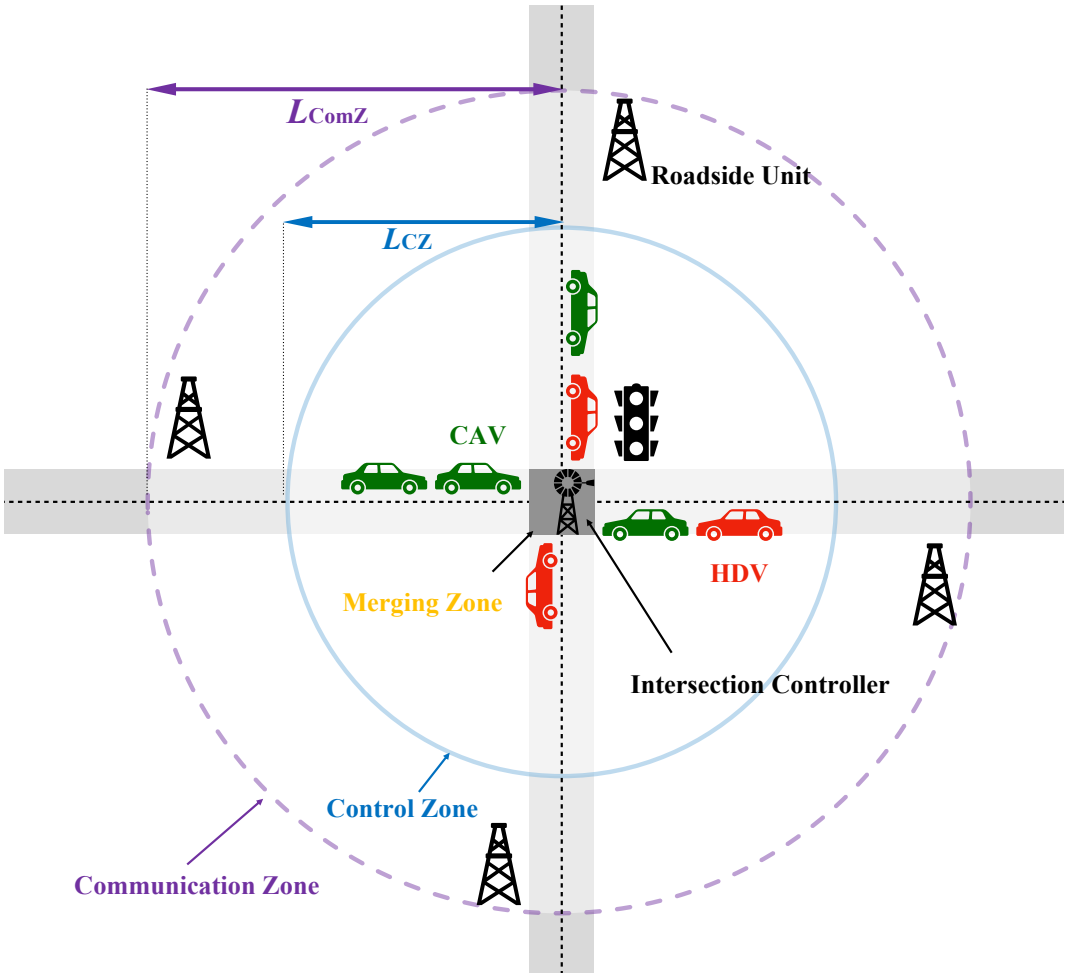

Figure 4.1: The system architecture of a signalized four-way road intersection problem with consideration of mixed traffic flow of CAVs and HDVs. This single-lane scenario can be easily extended into multi-lane scenarios, although still in the context of no turning and no lane changing.

tion is the *Merging Zone* (MZ). Outside the MZ is the *Control Zone* (CZ), where the motion of each CAV can be fully controlled by a central intersection controller (IC). The lengths of the CZ and MZ are L_{CZ} and L_{MZ}, respectively. In this framework, the IC is responsible for manipulating both the traffic SPAT and the trajectories of the CAVs to maximize the intersection traffic throughput and vehicle energy efficiency. Further from the center, there is a *Communication Zone* (ComZ), in which the IC can communicate with the CAVs. Moreover, there exist roadside units and sensors (camera, loop detector, etc.) at the entry points of the ComZ, where the entry speed, time, and length of the vehicles are measured and shared with the IC. For simplicity, turning is not considered in this framework, while lane changes are

only allowed outside the CZ. This may involve introducing an additional zone (centered at the intersection) beyond the control zone, where vehicles are allowed to perform lane changes in line with their turning intentions [185]. The Chapter 5 and the Chapter 6 will focus on the decision-making and control of lane-changing in mixed-traffic environments. As such, the control design for lane changes may be decoupled from the control design for the intersection crossing (as addressed in the present chapter). Fig. 4.2 shows a graphical representation of a typical signal

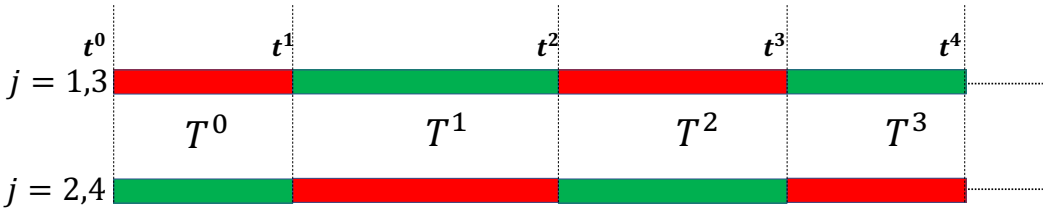

Figure 4.2: Graphical representation of signal cycles.

cycle for every approach at the intersection. In each phase the signal indicator is either green or red, while the amber phase is integrated into the red phase for safety purposes. Let $I_j^q \in \{0,1\}$ be the signal indicator at the qth ($q \in \mathbb{N}$) phase for the jth direction with $j \in \mathscr{J} = \{1,2,3,4\}$, which collects the four approaches of the intersection, with $\{1,3\}$ perpendicular to $\{2,4\}$. $I_j^q = 1$ is the green light and $I_j^q = 0$ is the red light. For the sake of further discussion, let $\mathscr{S}_j^q$ be the SPAT information set at the qth phase for the jth direction, it is defined as:

$$\mathscr{S}_j^q = \{T^q, I_j^q\},\ q \in \mathbb{N} \tag{4.1}$$

where $\mathscr{S}_j^0 = \{T^0, I_j^0\}$ is the predefined initial condition and T^q is the time duration of the qth signal phase. Then, let

$$t^q = t^0 + \sum_{k=0}^{q-1} T^k \tag{4.2}$$

be the start time of the qth SPAT provided t^0 is the initial time. The signal indication of the two perpendicular roads in this work are always reversed, and therefore, when

the SPAT is determined for one direction, the other is determined accordingly. To complete the intersection model, the following assumptions are also needed.

Assumption 4.1. *Each CAV can communicate with the IC without errors and delays once the vehicles enter the control zone.*

Assumption 4.2. *After entering the CZ, all CAVs are fully controllable and capable of precisely following the trajectories provided by the IC.*

Assumption 4.3. *The communication zone is large enough, such that any vehicle that enters the ComZ at a green phase will not reach the stop line within the same phase.*

Assumptions 4.1 and 4.2 are commonly used in existing works, such as [25, 114, 186]. In this context, the IC can be informed of the type (whether it is a CAV or HDV) and the length of each vehicle upon arrival at ComZ. Assumption 4.3 is added to enable the formulation such that the corresponding optimization problem (the algorithm will be introduced in Section 4.3) does not depend on unknown information outside the ComZ. Given the maximum vehicle speed $v_{\max}$ at a road intersection and the upper time duration limit of a signal phase $T_{\max}$ chosen in the present work, it is straightforward to determine the appropriate radius of the ComZ (i.e., $L_{\text{ComZ}} \geq v_{\max} T_{\max}$ which may be realized by multi-hop communication), such that Assumptions 4.3 is satisfied. For instance, when $v_{\max} = 15$ m/s and $T_{\max} = 50$s, Assumption 4.3 holds if $L_{\text{ComZ}} \geq 750$ m.

4.3 Mixed Platoon-based Signal-Vehicle Coupled Coordination Scheme

Mixed platooning is well established and frequently used in urban traffic control [23,26,114]. Recent research shows a growing trend of using CAVs as administrative vehicles to lead HDVs [187], which can be extended to platooning scenarios. In each platoon, CAVs can positively influence the behavior of surrounding HDVs, improving overall traffic performance at the platoon level. Meanwhile, treating

groups of vehicles as coordinated platoons offers computational advantages, making it a practical solution for managing large-scale traffic in complex urban environments. Thus, to address the signalized intersection coordination problem with mixed autonomy vehicles as illustrated in Fig. 4.1, this chapter exploits the notion of the "$1+N$" mixed platoon [114, 180] where "1" represents the CAV leading a platoon and "N" collects the following HDVs with $N \in \mathbb{N}$. In particular, when $N = 0$, it represents a platoon with only a single CAV. As such, any mixed traffic flow can be decoupled into multiple mixed platoons with individual CAV leads. The mixed platoon model will be introduced in Section 4.3.1, followed by the proposed signal-vehicle coupled control algorithm that is based on the concept of mixed platoons. The control algorithm follows a hierarchical architecture, where the upper layer is the traffic SPAT controller (see Section 4.3.2) and the lower layer is the speed trajectories controller of CAVs (while the HDVs are indirectly controlled). The two layers are respectively presented in Section 4.3.2 and Section 4.3.3. The overall control scheme is sketched in Fig. 4.3. The upper-level is designed to find the optimal light duration for the next phase T^{q*}, the number of mixed platoons allowed to cross the intersection within the phase l_j^{q*} and the target equilibrium speed (i.e., crossing speed) of the mixed platoons v_j^{q*} in terms of maximizing the intersection throughput. Note that a single v_j^{q*} is used for all crossing platoons to avoid rear-end collision between platoons. Then, at the lower-level, the optimal speed trajectories of each CAV are determined according to T^{q*}, l_j^{q*}, v_j^{q*} obtained at the upper-level so as to minimize the control effort of all each mixed platoon.

Before the introduction of the upper-level SPAT optimization, some preliminaries are introduced first. Let us consider $\mathscr{J}_1 = \{j \mid I_j^q = 1, \forall q \in 2\mathbb{N}+1\}$ and $\mathscr{J}_2 = \{j \mid I_j^q = 0, , \forall q \in 2\mathbb{N}+2\}$ with $\mathscr{J} = \mathscr{J}_1 \cup \mathscr{J}_2$. Without loss of generality, in the rest of Section 4.3 we assume $q \in 2\mathbb{N}+1$ in the proposed method, although the method can be easily applied to $q \in 2\mathbb{N}+2$. Let the set $\mathscr{V}^q$ represent the set of all vehicles inside the ComZ at $t = t^q$, then $\mathscr{V}^q = \cup_{j\in\mathscr{J}} \mathscr{V}_j^q$ where $\mathscr{V}_j^q$ collects the vehicles in direction j. The set $\mathscr{V}_j^q, \forall j \in \mathscr{J}_1$ is formed by the remaining vehicles $\tilde{\mathscr{V}}_j^q$ after the last green phase $t \in (t^{q-2}, t^{q-1}], \forall q \geq 2$ and the vehicles $\bar{\mathscr{V}}_j^q$ arriving at

the ComZ during the subsequent red phase $t \in (t^{q-1}, t^q]$. Note that $\tilde{\mathscr{V}}_j^1$, $j \in \mathscr{J}_1$ represents the vehicles in the ComZ at $t = t^0$ that is predefined. With reference to the $1+N$ mixed platoon model, $\bar{\mathscr{V}}_j^q$ can be decomposed into multiple CAV-led mixed platoons and some HDVs ahead of the first CAV, such that $\bar{\mathscr{V}}_j^q = \mathscr{H}_j^q \cup_{l \in \bar{\mathscr{L}}_j^q} \mathscr{P}_{l,j}^q$, where $\mathscr{H}_j^q$ is the set of HDVs ahead of the first CAV in $\bar{\mathscr{V}}_j^q$ and $\mathscr{H}_j^q = \emptyset$ if the first element in $\bar{\mathscr{V}}_j^q$ is a CAV, $\mathscr{P}_{l,j}^q = \{1, 2, \ldots, |\mathscr{P}_{l,j}^q|\}$ the set of lth mixed platoon vehicles in $\bar{\mathscr{V}}_j^q$ and $\bar{\mathscr{L}}_j^q = \{1, 2, \cdots \bar{l}_j^q\}$ is the set of mixed platoons with the maximum platoon number denoted by $\bar{l}_j^q$. By combining the uncontrollable HDVs $\mathscr{H}_j^q$ with the awaiting vehicles $\tilde{\mathscr{V}}_j^q$ and letting $\mathscr{P}_{0,j}^q = \mathscr{H}_j^q \cup \tilde{\mathscr{V}}_j^q$, we have $\mathscr{V}_j^q = \cup_{l \in \mathscr{L}_j^q} \mathscr{P}_{l,j}^q$ with $\mathscr{L}_j^q = 0 \cup \bar{\mathscr{L}}_j^q$. Finally, $\mathscr{V}_j, \forall j \in \mathscr{J}_2$ only collects the residual vehicles after the green phase $t \in (t^{q-1}, t^q]$, thus $\mathscr{P}_{0,j}^q = \mathscr{V}_j, \forall j \in \mathscr{J}_2$. For ease of notation, one sets $n_{l,j}^q = |\mathscr{P}_{l,j}^q|$ that is the number of vehicles involved in a platoon $\mathscr{P}_{l,j}^q$.

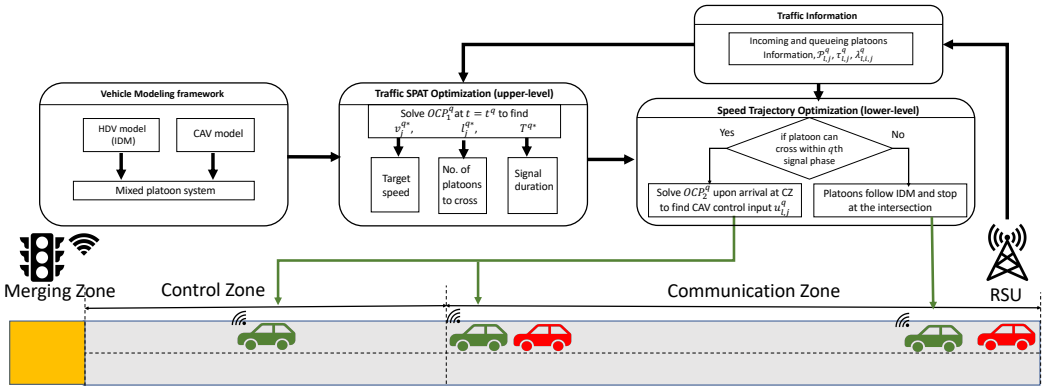

Figure 4.3: The scheme of the hierarchical mixed platoon control framework with traffic SPAT optimization and speed trajectory optimization for the signalized mixed intersection problem sketched in Fig. 4.1. CAVs and HDVs are represented by green and red vehicles, respectively. The optimization problems in upper and lower level are formulated in (4.22) and (4.33), respectively. Note that HDVs are not controlled and they always follow IDM with $v_d = v_{\max}$ (4.3).

4.3.1 Modeling of a mixed platoon system

The following assumption is invoked to model the mixed platoon system.

Assumption 4.4. *The motion of the HDVs can be characterized by the IDM car-following model.*

By organizing vehicles into mixed platoons, lane-changing and overtaking

behaviors can be reasonably restricted, allowing these maneuvers to be specifically managed within designated lane-changing zones, as discussed in the following chapters. Such formulation can be supported by many of the existing works [24, 25, 114, 188].

For the sake of further analysis, let us denote $p^q_{l,i,j}(t)$, $v^q_{l,i,j}(t)$ and $a^q_{l,i,j}(t)$ respectively the (front-end) position, velocity and acceleration of the ith vehicle within the lth mixed platoon approaching from the direction j during qth signal phase. In particular, $p^q_{l,i,j} = 0$ refers to the entry point of the ComZ. Under Assumption 4.4, the acceleration of each HDV follows the equation (3.8), which can be expressed as

$$\dot{a}^q_{l,i,j}(t) = F\left(s^q_{l,i,j}(t), \dot{s}^q_{l,i,j}(t), v^q_{l,i,j}(t)\right). \tag{4.3}$$

where $F\left(s^q_{l,i,j}(t), \dot{s}^q_{l,i,j}(t), v^q_{l,i,j}(t)\right)$ is a nonlinear function of the following distance $s^q_{l,i,j}(t) = p^q_{l,i-1,j}(t) - p^q_{l,i,j}(t)$ and the velocity difference $\dot{s}^q_{l,i,j}(t) = v^q_{l,i-1,j}(t) - v^q_{l,i,j}(t)$ between the preceding vehicle $i-1$ and the vehicle i. $a_{\max}$ is the maximum vehicle acceleration, δ is the acceleration exponent, and v_d is the desired constant following velocity of an individual HDV. In the present chapter, $\delta = 4$ and $v_d = v_{\max}$ are utilized, which are common choices in the literature to represent realistic driving behavior [68]. s_0 the standstill spacing between consecutive vehicles, a_b the comfortable deceleration of each HDV, and T_0 the safe time headway.

It is worth remembering that HDVs are not controllable. Conversely, CAVs are fully controllable, and their longitudinal motion is modeled by a commonly used third-order model [189]:

$$\begin{cases} \dot{p}^q_{l,1,j}(t) = v^q_{l,1,j}(t), \\ \dot{v}^q_{l,1,j}(t) = a^q_{l,1,j}(t), \\ \dot{a}^q_{l,1,j}(t) = \dfrac{1}{\tau^q_{l,j}} u^q_{l,j}(t) - \dfrac{1}{\tau^q_{l,j}} a^q_{l,1,j}(t) \end{cases} \tag{4.4}$$

where $\tau^q_{l,j}$ and $u^q_{l,j}(t)$ are the inertial time-lag and the control input of the lth platoon leading CAVs in approach j of the qth phase, respectively. As it can be noticed, the heterogeneity of CAVs can be taken into account by $\tau^q_{l,j}$, which can be shared with

the IC when the CAV enters the ComZ.

Considering v_j^{q*} the equilibrium speed of the mixed platoon and s_j^{q*} the equilibrium following distance, it holds that

$$\dot{v}_{l,i,j}^q = F\left(s_j^{q*}, 0, v_j^{q*}\right) = 0. \tag{4.5}$$

By introducing the error variables $\tilde{s}_{l,i,j}^q(t) = s_{l,i,j}^q(t) - s_j^{q*}$ and $\tilde{v}_{l,i,j}^q(t) = v_{l,i,j}^q(t) - v_j^{q*}$, the IDM model for an HDV (4.3)-(3.8) can be linearized around the equilibrium point, leading to

$$\begin{cases} \dot{\tilde{s}}_{l,i,j}^q(t) = \tilde{v}_{l,i-1,j}^q(t) - \tilde{v}_{l,i,j}^q(t), \\ \dot{\tilde{v}}_{l,i,j}^q(t) = \alpha_1 \tilde{s}_{l,i,j}^q(t) - \alpha_2 \tilde{v}_{l,i,j}^q(t) + \alpha_3 \tilde{v}_{l,i-1,j}^q(t) \end{cases} \tag{4.6}$$

where $\alpha_1 = \frac{\partial F}{\partial s_{l,i,j}^q}, \alpha_2 = \frac{\partial F}{\partial \dot{s}_{l,i,j}^q} - \frac{\partial F}{\partial v_{l,i,j}^q}, \alpha_3 = \frac{\partial F}{\partial \dot{s}_{l,i,j}^q}$ evaluated at the equilibrium state (v_j^{q*}, s_j^{q*}).

Consider an arbitrary mixed platoon $\mathscr{P}_{l,j}^q$ (which involves $n_{l,j}^q - 1$ HDV followers by definition). By combining the system equations (4.4) and (4.6) for all $n_{l,j}^q$ vehicles within the mixed platoon, the mixed platoon system can be recast into a single state-space model:

$$\dot{x}_{l,j}^q(t) = A_{l,j}^q x_{l,j}^q(t) + B_{l,j}^q u_{l,j}^q(t) \tag{4.7}$$

where the aggregated state and input vectors are

$$\begin{aligned} x_{l,j}^q(t) = \Big[& p_{l,1,j}^q(t), v_{l,1,j}^q(t), a_{l,1,j}^q(t), \tilde{s}_{l,2,j}^q(t), \tilde{v}_{l,2,j}^q(t), \\ & \tilde{s}_{l,3,j}^q(t), \tilde{v}_{l,3,j}^q(t), \ldots, \tilde{s}_{l,n_{l,j}^q-1,j}^q(t), \tilde{v}_{l,n_{l,j}^q-1,j}^q(t) \Big]^\top \in \mathbb{R}^{2n_{l,j}^q+1}. \end{aligned} \tag{4.8}$$

and $A^q_{l,j} \in \mathbb{R}^{(2n^q_{l,j}+1)\times(2n^q_{l,j}+1)}$ and $B^q_{l,j} \in \mathbb{R}^{(2n^q_{l,j}+1)}$ are given as follows

$$A^q_{l,j} = \begin{bmatrix} A_{l,1} & 0 & \dots & \dots & 0 & 0 \\ H_2 & H_1 & 0 & \dots & \dots & 0 \\ 0 & H_2 & H_1 & 0 & \dots & 0 \\ \vdots & \ddots & \ddots & \ddots & \ddots & \vdots \\ 0 & \dots & 0 & H_2 & H_1 & 0 \\ 0 & \dots & \dots & 0 & H_2 & H_1 \end{bmatrix}, \tag{4.9}$$

$$B^q_{l,j} = \begin{bmatrix} 0 & 0 & \frac{1}{\tau_{l,j}} & 0 & 0 & \dots & 0 \end{bmatrix}^\top, \tag{4.10}$$

with

$$A_{l,1} = \begin{bmatrix} 0 & 1 & 0 \\ 0 & 0 & 1 \\ 0 & 0 & -\frac{1}{\tau_{l,j}} \end{bmatrix}, H_1 = \begin{bmatrix} 0 & -1 \\ \alpha_1 & -\alpha_2 \end{bmatrix}, H_2 = \begin{bmatrix} 0 & 1 \\ 0 & \alpha_3 \end{bmatrix}. \tag{4.11}$$

The controllability of the mixed platoon system (4.7) is characterized by the following Lemma [114].

Lemma 4.1. *The $1+N$ mixed platoon system is controllable when the following condition holds*

$$\alpha_1 - \alpha_2\alpha_3 + \alpha_3^2 \neq 0 \tag{4.12}$$

4.3.2 Traffic SPAT planner

In the SPAT optimization, vehicles belonging to $\mathscr{P}^q_{0,j}$ are assumed static, and it yields a queue of $n^q_{0,j}$ vehicles ahead of the $\bar{l}^q_j$ platoons. In the following, we denote by $\lambda^q_{l,i,j}$ the length of the ith vehicle in $\mathscr{P}^q_{l,j}$. The objective of the SPAT optimization is to minimize the total waiting time of all vehicles. The waiting time $T^{wait}_{l,j}$ of a vehicle in the lth mixed platoon to enter the MZ can be evaluated for all $l \in \mathscr{L}^q_j$ by:

$$T^{q,wait}_{l,j} = \begin{cases} T^{q*} - \hat{T}^{q,stop}_{l,j}, & \text{if } j \in \mathscr{J}_2, \\ \beta^q_{l,j}(T^{q*} + \hat{T}^{q+1} - \hat{T}^{q,stop}_{l,j}), & \text{if } j \in \mathscr{J}_1, \end{cases} \tag{4.13}$$

where $\hat{T}_{l,j}^{q,stop}$ is the minimum time required for lth platoon to reach the stop line

$$\hat{T}_{l,j}^{q,stop} = \frac{L_{\text{ComZ}} - p_{l,1,j}^{q}(t^q)}{v_{\max}}$$

The elimination of $\hat{T}_{l,j}^{q,stop}$ is motivated by the fact that the initial distance to the stop line of a platoon is an indispensable part of the mission regardless of the crossing decision. In addition, $\beta_{l,j}^{q}$ is a binary indicator given by

$$\beta_{l,j}^{q} = \begin{cases} 0, & \text{if } l \leq l_j^{q*}, \\ 1, & \text{if } l > l_j^{q*}, \end{cases} \tag{4.14}$$

where $\beta_{l,j}^{q}=0$ represents platoon l can complete the intersection crossing during the qth green signal light phase. Conversely, $\beta_{l,j}^{q}=1$ is the case that the platoon cannot pass through the intersection within the current phase and has to wait for another red phase T^{q+1}. $\hat{T}^{q+1}$ is the estimate of T^{q+1}, and is approximated by the prior red light duration time, $\hat{T}^{q+1} = T^{q-1}$, when evaluating the waiting time in the SPAT optimization (4.22), which is compatible with the traffic flow that does not change suddenly.

To determine the number of vehicles that can pass through the intersection, the queue discharge time at the intersection needs to be estimated. The initial distance (at $t = t^q$) from the rear end of the last vehicle in the queue $\mathscr{P}_{0,j}^{q}$ to the exit of the MZ is defined as $D_{0,j}^{q}$, which is calculated by

$$D_{0,j}^{q} = L_{\text{MZ}} + \sum_{i=1}^{n_{0,j}^{q}} \left(\lambda_{0,i,j}^{q} + s_0 \right) - s_0 \tag{4.15}$$

For computational efficiency of the prediction, when the traffic signal turns to green indication, we simply assume that all the vehicles in the queue follow a constant acceleration a_d ($a_d \leq a_{\max}$) until $v_{\max}$ is reached, where $v_{\max}$ is the maximum speed limit. Being a_d a tuneable parameter, it is possible to design a suitable a_d to ensure safety and comfort [190]. In this context, the time required for the last vehicle in

the queue to leave the MZ can be estimated by:

$$T_{n_j^q} = \begin{cases} \sum_{i=1}^{n_{0,j}^q} \kappa_{0,i,j}^q + \dfrac{\sqrt{2a_d D_{0,j}^q}}{a_d} & \text{if } D_{0,j}^q \leq \dfrac{v_{\max}^2}{2a_d} \\ \sum_{i=1}^{n_{0,j}^q} \kappa_{0,i,j}^q + \dfrac{v_{\max}}{a_d} + \dfrac{D_{0,j}^q - \frac{v_{\max}^2}{2a_d}}{v_{\max}} & \text{otherwise} \end{cases} \tag{4.16}$$

where $\kappa_{0,i,j}^q$ represents the anticipated response delay of a human driver. Therefore, $\kappa_{0,i,j}^q = \kappa_0$ when the queueing vehicle i is an HDV and $\kappa_{0,i,j}^q = 0$ in the case of a CAV, with $\kappa_0 \in \mathbb{R}_{>0}$ being a tunable parameter.

To ensure that the first mixed platoon $\mathscr{P}_{1,j}^q$, $j \in \mathscr{J}_1$ does not (rear-end) collide with the last vehicle in the discharge queue and to maximize the traveling speed of all platoons, the target crossing speed v_j^{q*} of the first platoon is set to

$$v_j^{q*} = \min\left(v_{\max}, \frac{L_{\text{ComZ}} + L_{\text{MZ}} - p_{1,1,j}^q(t^q)}{T_{n_j^q}}\right) \tag{4.17}$$

which is then utilized for all platoons allowed to cross during the qth phase for safety consideration as the movement of the remaining platoons is constrained by the first one. The length of the lth mixed platoon, $D_{l,j}^q$, at steady state with target velocity v_j^{q*} can be determined by

$$D_{l,j}^q = \sum_{i=1}^{n_{l,j}^q} \left(\lambda_{l,i,j}^q + s_j^{q*}\right) \tag{4.18}$$

where the steady state headway s_j^{q*} can be expressed as a function of v_j^{q*} owing to (4.5), as given by:

$$s_j^{q*} = \frac{s_0 + v_j^{q*} T_0}{\sqrt{1 - \left(v_j^{q*}/v_{\max}\right)^4}}. \tag{4.19}$$

The SPAT optimization aims to find the optimal signal phase T^{q*} that allows a certain number of mixed platoons l_j^{q*}, $j \in \mathscr{J}_1$ to cross the intersection. To this end, let us define $T_{\min,l,j}^q$ the minimum time required for the entire lth platoon to pass the

intersection. It can be represented as a function of v_j^{q*}, as follows:

$$T^q_{\min,l,j} = \begin{cases} T_{n_j^q}, & l = 0 \\ \dfrac{L_{\text{ComZ}} + L_{\text{MZ}} - p^q_{l,1,j} + D^q_{l,j}}{v_j^{q*}}, & l \in \bar{\mathscr{L}}_j^q \end{cases} \tag{4.20}$$

where $j \in \mathscr{J}_1$. It is evident that a platoon l can cross the intersection if $T^q_{\min,l,j} \leq T_{\max}$. For the sake of further discussion, consider $\mathscr{L}^q_{j,f} = \{l \mid T^q_{\min,l,j} \leq T_{\max}, j \in \mathscr{J}_1\} \subset \mathbb{N}$ the feasible set of platoons that could potentially cross the intersection within the upcoming green phase. Furthermore, given the optimal number of platoons that are allowed to cross the intersection in both green phase directions, l_j^{q*}, $j \in \mathscr{J}_1$ and the resulting $T^{q*}_{\min,l,j}$ by (4.20), the optimal signal phase duration is defined by

$$T^{q*} = \max_{j \in \mathscr{J}_1} (T^{q*}_{\min,l,j}) \tag{4.21}$$

We now have all ingredients to formulate the upper-level SPAT optimization, which has now been reduced to find the optimal number of crossing platoons l_j^{q*}, $j \in \mathscr{J}_1$ so as to minimize the total waiting time of all vehicles approaching from the four directions for each traffic signal cycle. This leads to an integer programming problem:

$$\mathscr{OC}\,\mathscr{P}_1^q : \min_{l_j^{q*} \in \mathscr{L}^q_{j,f}} \quad \sum_{j \in \mathscr{J}} \sum_{l \in \mathscr{L}_j^q} n^q_{l,j} T^{q,wait}_{l,j} \tag{4.22}$$

where $T^{q,wait}_{l,j}$ can be determined by (4.13)-(4.21) utlizing T^{q*} determined by (4.21). The minimum solution of problem $\mathscr{OC}\,\mathscr{P}_1^q$ can be found by searching over the space $\mathscr{L}^q_{j,f}$.

Remark 4.1. *The optimization problem* (4.22) *may be infeasible if there does not exist a* T^{q*} *(following* (4.21)*) that satisfies the constraint* $[0, T_{\max}]$ *(e.g., the initial waiting queue* $\mathscr{P}^q_{0,j}$ *is extremely long, which implies heavy traffic). In such a circumstance, the optimal phase duration follows* $T^{q*} = T_{\max}$.

4.3.3 Speed trajectory controller

Given the optimal v_j^{q*}, T^{q*}, l_j^{q*} determined at the upper-level, the aim of the speed trajectory planning at the lower level is to ensure that the vehicles in $\mathscr{P}_{l,j}^q$ can efficiently form a mixed platoon at the steady state velocity v_j^{q*} and complete the intersection crossing within the time duration T^{q*} of the green signal light phase if $l \leq l_j^{q*}$ or otherwise stop properly.

Let us first focus on the platoons $l \leq l_j^{q*}$ that are permitted to cross within the qth signal phase. According to Assumption 4.3, the optimal decisions v_j^{q*}, T^{q*}, l_j^{q*} are not available when a mixed platoon $\mathscr{P}_{l,j}^q$ enters the ComZ. To facilitate the platoon control inside the CZ, the IC will suggest each leading CAV of a platoon that has not yet entered the CZ a target velocity, $\hat{v}_{l,j}^{q*}$, and the movement of those CAVs will be governed by IDM as with uncontrolled HDVs.

With the aim of maximizing the throughput and avoiding rear-end collisions, $\hat{v}_{l,j}^{q*}, \forall l \in \bar{\mathscr{L}}_j^q$ is calculated by:

$$\hat{v}_{l,j}^{q*} = \min\left(v_{\max}, \frac{L_{\text{ComZ}}+L_{\text{MZ}}}{\hat{t}_{l,j}^q - \tilde{t}_{l,j}^q}\right) \tag{4.23}$$

where $\tilde{t}_{l,j}^q$ is the ComZ entering time of the platoon $\mathscr{P}_{l,j}^q$ and $\hat{t}_{l,j}^q$ is the estimated arriving time of the lead vehicle of the lth platoon at the exit point of the MZ. $\hat{t}_{l,j}^q$ is estimated by

$$\hat{t}_{l,j}^q = \begin{cases} t^q + \hat{T}_{0,n_j^q}, & l = 1 \\ \hat{t}_{l-1,j}^q + \hat{T}_{l-1,n_j^q}, & l \in \bar{\mathscr{L}}_j^q \backslash 1 \end{cases} \tag{4.24}$$

where $\hat{T}_{l-1,n_j^q}$ is the estimated discharging time required for the $(l-1)$th platoon, which is determined as follows:

$$\hat{T}_{l-1,n_j^q} = \begin{cases} T_{n_j^q}, & l = 1, \\ \dfrac{\sum_{i=1}^{n_{l-1,j}^q}\left(\lambda_{l-1,i,j}^q + \hat{s}_{l-1,j}^{q*}\right) - \hat{s}_{l-1,j}^{q*}}{\hat{v}_{l-1,j}^{q*}}, & \text{otherwise}, \end{cases} \tag{4.25}$$

where $T_{n_j^q}$ is the queue discharging time defined in (4.16), $\hat{s}_{l,j}^{q*}$ is the steady state

headway associated with $\hat{v}_{l,j}^{q*}$, determined by (4.19). In view of (4.23)-(4.25), given $T_{n_j^q}$, then $\hat{T}_{l-1,n_j^q}$, $\hat{t}_{l,j}^q$ and $\hat{v}_{l,j}^{q*}$ can be recursively determined for each l.

For every platoon entering the CZ, the IC optimizes its trajectory by solving an individual OCP (for the speed trajectory optimization) based on v_j^{q*}, T^{q*} and l_j^{q*} from the upper layer obtained at t^q. Consider $\bar{t}_{l,j}^q$ the CZ entering time of the platoon $\mathscr{P}_{l,j}^q$. For the sake of further discussion, let us denote $\tilde{\mathscr{L}}_j^q = \{l|\bar{t}_{l,j}^q \geq t^q\}$ the index of platoons that can be informed of the target speed v_j^{q*} and the signal phase T^q by the upper-level SPAT planner upon arrival at the CZ. Then, $\bar{\mathscr{L}}_j^q \backslash \tilde{\mathscr{L}}_j^q$ represents the platoons which enter the CZ before t^q, and therefore can not be informed. In this framework, the lower-level speed trajectory optimization is activated at $t = \bar{t}_{l,j}^q$ for $l \in \tilde{\mathscr{L}}_j^q$, while for $l \in \bar{\mathscr{L}}_j^q \backslash \tilde{\mathscr{L}}_j^q$, it is triggered at $t = t^q$, and for $t \in [\bar{t}_{l,j}^q, t^q)$ (when the mixed platoon is in the CZ but the results of upper-level optimization are not available), the leading CAV of each of those platoons will continue following the IDM with the target speed specified in (4.23). Before introducing the OCP for speed optimization, let us define the coordination constraints.

To avoid rear-end collisions between vehicles in a platoon, and the lead vehicle of the lth platoon and the last vehicle in its preceding platoon, the following collision avoidance constraints are enforced, respectively:

$$\tilde{s}_{l,i,j}^q(t) + s_j^{q*} \geq s_0 + v_{l,i,j}^q(t) T_0 \tag{4.26}$$

$$p_{l,1,j}^q(t) \leq p_{l-1,n_{l-1,j}^q,j}^q(t) - (s_0 + v_{l,1,j}^q(t) T_0), \forall l \in \bar{\mathscr{L}}_j^q \tag{4.27}$$

Moreover, for safety purposes, the velocity of any vehicles and the control input of the leading CAV of any platoon are constrained by:

$$0 < v_{l,1,j}^q \leq v_{\max}, \tag{4.28a}$$

$$a_{\min} \leq a_{l,1,j}^q \leq a_{\max}, \tag{4.28b}$$

$$0 < \tilde{v}_{l,i,j}(t) + v_j^{q*} \leq v_{\max}, i \in \mathscr{P}_{l,j}^q \backslash 1 \tag{4.28c}$$

$$u_{\min} \leq u_{l,j}^q(t) \leq u_{\max}, \tag{4.28d}$$

where $u_{\min}$ and $u_{\max}$ are the minimum and maximum CAV control input, respectively.

To ensure that the full body length of the last vehicle in a platoon (that is allowed to cross) can leave the MZ within the green phase, the following constraint is also required:

$$L_{\text{ComZ}} + L_{\text{MZ}} - \bar{p}^q_{l,n^q_{l,j},j} + \lambda^q_{l,n^q_{l,j},j} \leq d^q_{l,n^q_{l,j},j} \tag{4.29}$$

where $\bar{p}^q_{l,n^q_{l,j},j}$ is the position of the last vehicle in $\mathscr{P}^q_{l,j}$ when the speed optimization is triggered

$$\bar{p}^q_{l,n^q_{l,j},j} = \begin{cases} p^q_{l,n^q_{l,j},j}(\bar{t}^q_{l,j}), & l \in \tilde{\mathscr{L}}^q_j \\ p^q_{l,n^q_{l,j},j}(t^q), & l \in \bar{\mathscr{L}}^q_j \backslash \tilde{\mathscr{L}}^q_j \end{cases}$$

$\bar{p}^q_{l,n^q_{l,j},j}$ is available to the IC by vehicular communication if the vehicle is connected (CAVs and connected HDVs) or by prediction through IDM refer to Assumption 4.4 (unconnected HDVs). $d^q_{l,n^q_{l,j},j}$ is the total distance traveled by the last car in the platoon during the entire time horizon of the optimization, that is $[\bar{t}^q_{l,j},\, t^q_{f,l,j}]$ for $l \in \tilde{\mathscr{L}}^q_j$ and $[t^q,\, t^q_{f,l,j}]$ for $l \in \bar{\mathscr{L}}^q_j \backslash \tilde{\mathscr{L}}^q_j$ with $t^q_{f,l,j}$ the terminal (MZ exit) time of the lth platoon in jth direction and qth phase. Instead of enforcing a prescribed terminal time, which might be restrictive, in this work, a time slot for a platoon to leave the MZ is assigned (i.e., a constraint for the terminal time):

$$\begin{cases} t^q_{f,l,j} \in [\max(\underline{\hat{t}}^q_{l,j}, t^q + T_{n^q_j}), \min(\bar{\hat{t}}^q_{l,j}, t^q + T^{q*})], l = 1 \\ t^q_{f,l,j} \in [\max(\underline{\hat{t}}^q_{l,j}, t^{q*}_{f,l-1,j}), \min(\bar{\hat{t}}^q_{l,j}, t^q + T^{q*})], l > 1 \end{cases} \tag{4.30}$$

where $t^{q*}_{f,l,j}$ is the optimal terminal time for lth platoon and

$$\underline{\hat{t}}^q_{l,j} = \begin{cases} \dfrac{L_{\text{ComZ}} + L_{\text{MZ}} - \bar{p}^q_{l,n^q_{l,j},j} + \lambda^q_{l,n^q_{l,j},j}}{v_{\max}} + \bar{t}^q_{l,j}, & l \in \tilde{\mathscr{L}}^q_j \\ \dfrac{L_{\text{ComZ}} + L_{\text{MZ}} - \bar{p}^q_{l,n^q_{l,j},j} + \lambda^q_{l,n^q_{l,j},j}}{v_{\max}} + t^q, & l \in \bar{\mathscr{L}}^q_j \backslash \tilde{\mathscr{L}}^q_j \end{cases} \tag{4.31}$$

$$\bar{t}_{l,j}^{q}=\begin{cases}\dfrac{L_{\mathrm{ComZ}}+L_{\mathrm{MZ}}-\bar{p}_{l,n_{l,j}^{q},j}^{q}+\lambda_{l,n_{l,j}^{q},j}^{q}}{\min(v_{j}^{q*},\hat{v}_{l,j}^{q*})}+\bar{t}_{l,j}^{q}, & l\in\tilde{\mathscr{L}}_{j}^{q}\\ \dfrac{L_{\mathrm{ComZ}}+L_{\mathrm{MZ}}-\bar{p}_{l,n_{l,j}^{q},j}^{q}+\lambda_{l,n_{l,j}^{q},j}^{q}}{\min(v_{j}^{q*},\hat{v}_{l,j}^{q*})}+t^{q}, & l\in\bar{\mathscr{L}}_{j}^{q}\backslash\tilde{\mathscr{L}}_{j}^{q}\end{cases}\tag{4.32}$$

Note that consideration of $t^q+T_{n_j^q}$, $t_{f,l,j}^{q*}$ and t^q+T^{q*} can prevent overlaps between time slots and late MZ exit time ($>t^q+T^{q*}$), which may lead to infeasibility.

Now, we can formulate the OCP to optimize the trajectory of a platoon $\mathscr{P}_{l,j}^{q}$. The problem is given by

$$\mathscr{CCP}_{2}^{q}:\min_{\mathbf{u}_{l,j}^{q},t_{f,l,j}^{q}} W_1\|\mathbf{u}_{l,j}^{q}(t)\|+W_2\|\mathbf{v}_{l,j}^{q}(t)-v_j^{q*}\|$$
$$+W_3\|\mathbf{s}_{l,j}^{q}(t)-s_j^{q*}\|,\tag{4.33a}$$
$$\textbf{s.t. } (4.7)-(4.11),(4.24)-(4.32)\tag{4.33b}$$
$$\textbf{given: } \bar{x}_{l,j}^{q},v_j^{q*},S_j^{q},\mathscr{P}_{l,j}^{q}\tag{4.33c}$$

where $\mathbf{u}_{l,j}^{q}(t)$ is the control input of the leading CAV in the mixed platoon $\mathscr{P}_{l,j}^{q}$, $\mathbf{v}_{l,j}^{q}(t)=[v_{l,1,j}^{q},v_{l,2,j}^{q},...,v_{l,n_{l,j}^{q},j}^{q}]^{\top}\in\mathbb{R}^{n_{l,j}^{q}}$ and $\mathbf{s}_{l,j}^{q}(t)=[s_{l,2,j}^{q},s_{l,3,j}^{q},...,s_{l,n_{l,j}^{q},j}^{q}]^{\top}\in\mathbb{R}^{n_{l,j}^{q}-1}$ are stacked vectors of the velocity and inter-vehicle distance of each vehicle in the platoon $\mathscr{P}_{l,j}^{q}$ respectively. $\bar{x}_{l,j}^{q}$ is the initial condition of the platoon system (4.7), expressed as:

$$\bar{x}_{l,j}^{q}=\begin{cases}x_{l,j}^{q}(\bar{t}_{l,j}^{q}), & l\in\tilde{\mathscr{L}}_{j}^{q}\\ x_{l,j}^{q}(t^{q}), & l\in\bar{\mathscr{L}}_{j}^{q}\backslash\tilde{\mathscr{L}}_{j}^{q}\end{cases}$$

The objective function in (4.33a) is designed to minimize the control effort (which is loosely related to the energy consumption) and the deviations from the target speed v_j^{q*} and headway distance s_j^{q*} so that the platoon is formed. W_1, W_2 and W_3 are the weighting coefficients respective for the three objectives. The optimization problem (4.33) involves quadratic cost function and linear constants and can be solved efficiently by standard convex optimization tools.

During $[t^{q-1},t^{q+1}]$, the platoons arriving at the ComZ after the l_j^{q*}th platoon

are not permitted to cross the intersection within the qth signal phase. Conversely, they will form the waiting queue, $\mathscr{P}_{0,j}^{q+2}$, for the $(q+2)$th signal phase. In the proposed framework, these vehicles will be informed of the decision (at $t = t^q$ for platoons arriving at the ComZ before $t = t^q$ or upon arrival at the ComZ), and they will follow the IDM model subject to a desired velocity v_d to form the queue. In the proposed framework, v_d is set to $v_{\max}$ (as with the HDV model (3.8)) to conforms with the assumption – the queue $\mathscr{P}_{0,j}^{q}$ is static – imposed in the upper layer SPAT planner at the price of potentially increasing energy usage. Further optimal design of v_d corresponds to another optimization problem, which is beyond the scope of the present article. For instance, to avoid stops at the red light, v_d can be optimized by taking into account the present green and upcoming red phases (see, for example, [114]). Nevertheless, this could lead to an extremely small target velocity, thereby reducing the inflow speed at the intersection, and such a slow speed may not be preferred by human drivers.

Remark 4.2. *$\mathscr{OC}\,\mathscr{P}_2^q$ may be infeasible due to the bi-level optimization structure. For example, the l_j^{q*}th platoon can not fully cross the intersection by the end of the green phase. To deal with this limitation, the first platoon that can not yield a feasible solution of $\mathscr{OC}\,\mathscr{P}_2^q$ will be truncated by dropping the last HDV and re-solving $\mathscr{OC}\,\mathscr{P}_2^q$. This will be repeated recursively until a feasible solution is found, and the truncated vehicles and platoons after that will be added to $\mathscr{P}_{0,j}^{q+2}$.*

4.4 Simulation Validation

In this section, the performance of the proposed control framework is evaluated and compared with a recently proposed coupled vehicle-signal control (CVSC) method [23] and two traditional benchmark methods in terms of traffic throughput and energy economy. In contrast to the proposed signal-vehicle co-control method, the two benchmark methods involve either SPAT or vehicle speed optimization only whereas the other layer in both methods is pre-defined, respectively. The two methods are defined below in Section 4.4.1 followed by the introduction of the energy consumption model and the simulation environment. The impact of EV penetra-

tion rate on energy consumption is also studied. In addition, the impacts of traffic volume distribution across the perpendicular directions (i.e., either the same or different arrival rates of the horizontal directions from the vertical directions) and CAV penetration rate on the traffic energy economy and throughput are investigated. The robustness of the proposed method is also validated by introducing uncertainties to the mixed platoons.

4.4.1 Benchmark algorithms and comparison metrics

Fixed SPAT and Speed Optimization (F-SPAT) This benchmark method finds the optimal velocity trajectories of all vehicles by following the proposed lower-layer optimal control scheme (4.33) subject to a fixed (non-optimized) SPAT policy. Herein, the fixed SPAT follows a constant time duration for all signal phases, which is set to $T_{\max}/2$, the middle value of the time duration limits of a signal indication.

Optimized SPAT and IDM (O-SPAT) This method adopts the SPAT optimization algorithm (4.22) to find an optimized SPAT. However, the vehicle speed trajectories are not optimized. Instead, both CAVs and HDVs follow the IDM car-following model (3.8) with $v_d = v_{\max}$.

To fairly compare the eco-driving performance of all algorithms, the fuel consumption model developed in [191] is utilized for post-evaluation of the resulting traditional vehicles' energy usage of the speed trajectories in all algorithms. Considering a vehicle i in platoon $\mathscr{P}^q_{l,j}$, the fuel consumption rate of this vehicle $\phi^q_{l,i,j}$ (in milliliters per second) can be estimated by

$$\phi^q_{l,i,j} = b_0 + b_1 v^q_{l,i,j} + b_2 (v^q_{l,i,j})^2 + b_3 (v^q_{l,i,j})^3 + \hat{a}\left(c_0 + c_1 v^q_{l,i,j} + c_2 (v^q_{l,i,j})^2\right) \quad (4.34)$$

where $\hat{a}$ is the estimated "total" acceleration required by each vehicle to follow the specified speed trajectory, which includes the actual vehicle acceleration $a^q_{l,i,j}$ and the "acceleration" required to counterbalance friction forces due to the air drag and tire rolling resistances. Therefore, $\hat{a} = a^q_{l,i,j} + \frac{1}{2m} C_D \rho_a A_V (v^q_{l,i,j})^2 + \mu g$, where m is the vehicle mass, A_V is the vehicle frontal area, ρ_a is the air density, C_D and μ are air drag and tire rolling resistance coefficients, respectively. Note

that the parameters A_V, C_D, μ, m are fixed (that represents a general-purpose car, see Table 4.1) in the post-evaluation for simplicity. The fitting parameters in (4.35), (4.34) are $b_0 = 0.1569$, $b_1 = 2.450 \times 10^{-2}$, $b_2 = -7.415 \times 10^{-4}$, $b_3 = 5.975 \times 10^{-5}$, $c_0 = 0.07224$, $c_1 = 9.681 \times 10^{-2}$, and $c_2 = 1.075 \times 10^{-3}$, which are obtained by fitting the map of a 1.3L engine [191].

To study the influence EV penetration rate on the energy efficiency, the commonly used energy consumption (in watt) model for an electric drive is introduced:

$$\phi^q_{l,i,j} = e_1 m v^q_{l,i,j} a^q_{l,i,j} + e_2 (m a^q_{l,i,j})^2 \tag{4.35}$$

where $e_1 = 1.052 \times 10^{-3}, e_2 = 4.458 \times 10^{-7}$ are obtained by fitting the experimental data [192].

Eventually, the fuel/energy consumption of an individual vehicle is calculated by

$$\Phi^q_{l,i,j} = \int_{\mathscr{T}^q_{l,i,j}} \phi^q_{l,i,j} \mathrm{d}t, \tag{4.36}$$

where $\mathscr{T}^q_{l,i,j}$ is the time duration required by the vehicle to leave the MZ from the entry point of the ComZ, available once each vehicle leaves the MZ. By introducing the calorific value of the gasoline C_f, the fuel consumption (in milliliters) can be transformed into energy consumption (in KJ) for a fair comparison.

Without loss of generality, the control problem is initialized with randomized ComZ arrival conditions (time and speed for each vehicle), vehicle lengths and the inertial time-lags (only for CAVs, see (4.4)) in the following case studies. In particular, the inertial time-lags and the vehicle lengths are generated within suitable sets (see Table 4.1), which can represent internal combustion engine vehicles with similar car dimensions so that the two parameters are compatible with the fuel consumption model (4.34) and its overall parameter choices. Moreover, the arrival (initial) speeds of the vehicles follow a uniform distribution within $(0, v_{\max}]$, while their arrival times follow a Poisson distribution. Finally, the vehicle and intersection parameters are summarized in Table 4.1, and all simulation case studies are carried out in the Matlab environment.

Table 4.1: Vehicle and intersection parameters

symbol	value	description
m	1200 kg	vehicle mass
T_0	0.5 s	safe time headway
s_0	1 m	standstill distance
$\lambda^q_{l,i,j}$	[4 m, 5 m]	car length
Δt	0.1 s	sampling time interval for vehicle
T_s	1 s	sampling time interval for IC
L_{CZ}	300 m	length of control zone
L_{ComZ}	750 m	length of communication zone
L_{MZ}	10 m	length of merging zone
$T_{\max}$	50 s	upper time limit of a signal light phase
$v_{\max}$	15 m/s	maximum velocity
$a_{\min}/a_{\max}$	$-6/4$ m/s^2	maximum deceleration and acceleration
a_d	3 m/s^2	acceleration of the discharging queue
a_b	-2 m/s^2	comfortable deceleration
$\tau^q_{l,i,j}$	[0.4, 0.7]	CAV inertial time-lag
A_V	2.5 m^2	vehicle frontal area
ρ_a	1.184 kg	air density
C_d	0.32	air drag coefficient
C_f	34.5 kJ/mL	calorific value of the gasoline
μ	0.015	tire rolling resistance coefficient
κ_0	0.7 s	response delay of a human driver
W_1	1000	Weighting parameter of $\mathscr{OCP}^q_2$
W_2, W_3	10	Weighting parameter of $\mathscr{OCP}^q_2$

4.4.2 Simulation Results

In the first instance, the proposed SPAT and vehicle co-control method is simulated in a scenario where the vehicle arrival rate in each direction (lane) is 1000 veh/h/lane (vehicles per hour per lane) with an overall penetration rate of CAV of 50%. The position trajectories of all vehicles (from the entry point of the CZ to the exit of the MZ) and the phases of the traffic signals are shown in Fig. 4.4. Note that for clarity of the figure, only two perpendicular approaches are shown here.

As it can be seen, there are no rear-end (the position trajectories do not intersect each other) and lateral collisions (vehicles from the two perpendicular directions do not appear in the MZ at the same time) and all vehicles follow the traffic lights, which verifies the feasibility of the proposed approach. Additionally, considering that all vehicles are conventional, the resulting intersection vehicle throughput and

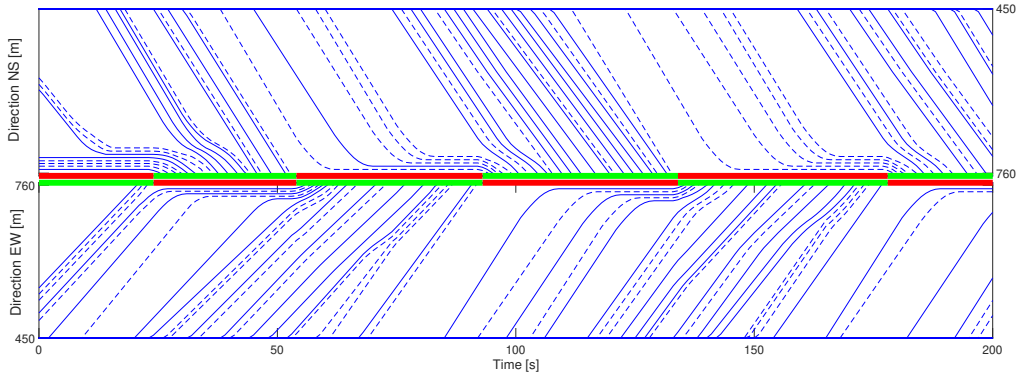

Figure 4.4: Traffic SPAT and vehicle position trajectories (from the entry point of the CZ at 450 m to the exit of MZ at 760 m, note that the entry of the MZ is at 750 m) for 200 s solved by the proposed methodology subject to a CAV penetration rate of 50% and a balanced traffic volume of 1000 veh/h across all lanes. The trajectories of HDVs are denoted by dashed lines, and the trajectories of CAVs are represented by solid lines. Only two perpendicular lanes, NS refers to the direction from north-to-south, and EW is the direction from east-to-west, are shown for clarity of the figure.

average vehicle fuel consumption of the proposed method are compared with the results of the baseline approaches. As shown in Table 4.2, an increase of 7.92% in the traffic throughput of intersections compared to the F-SPAT, while the proposed method achieves a similar result to O-SPAT and CVSC. The results imply that the throughput mainly depends on the signal control.

Table 4.2: Vehicle throughput and average fuel usage comparison between the proposed method and the benchmark methods for a 200 s simulation trial.

	Vehicle throughput [veh]	Average fuel usage [mL]
Proposed	218	64.596
F-SPAT	202	68.558
O-SPAT	218	72.663
CVSC	218	68.691

The comparative results also show a reduction in average fuel consumption of 12.49%, 6.13% and 6.34% when comparing the proposed method with F-SPAT, O-SPAT and CVSC, respectively. It can be understood that the speed optimization of CAVs plays a more critical role than the SPAT optimization in terms of fuel economy. In contrast to CVSC in [23], where speed profiles are determined by empirical rules, the proposed optimization of the speed trajectory can lead to more

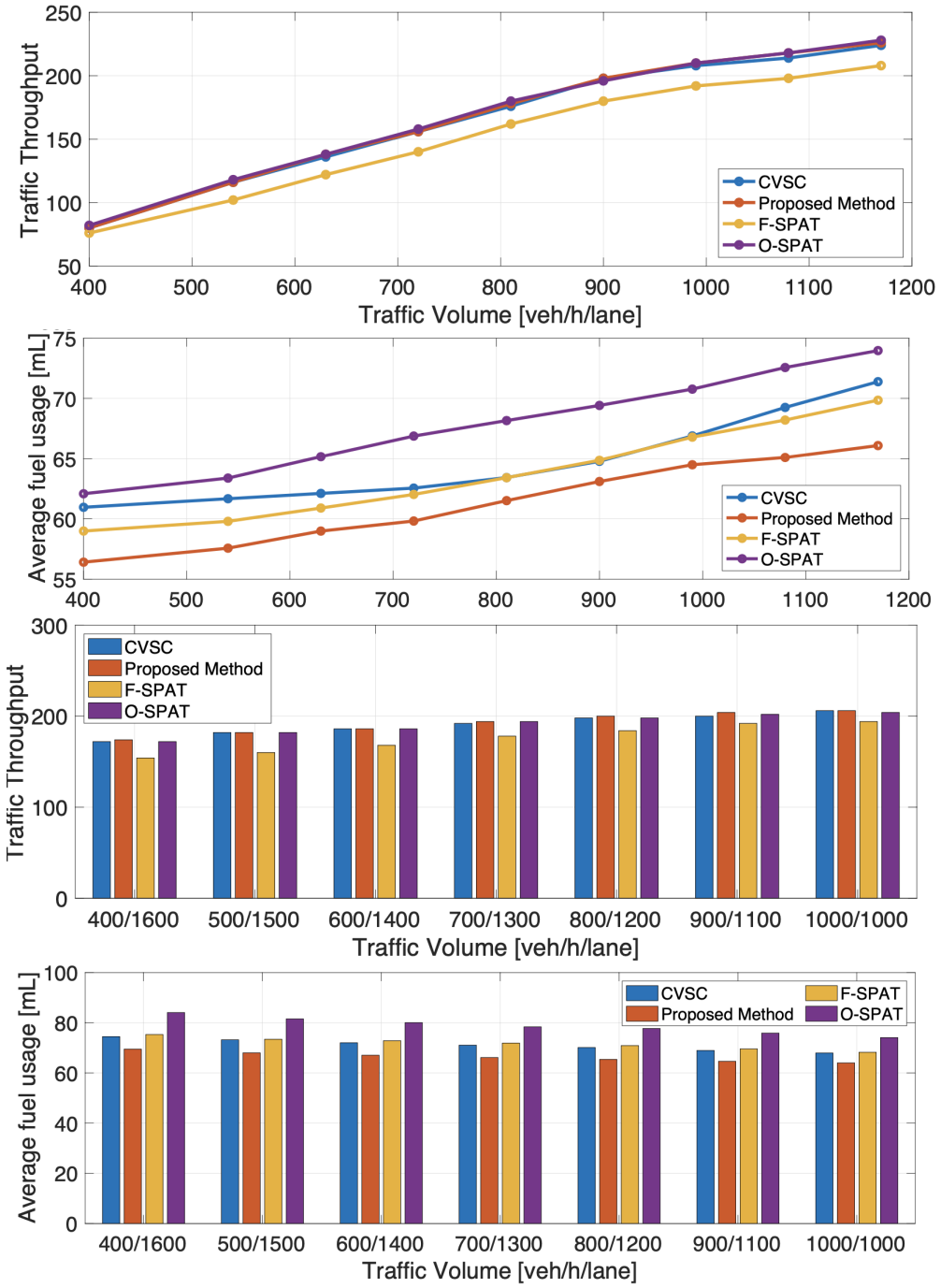

Figure 4.5: Intersection traffic throughput and average fuel consumption of the proposed and benchmark methods under balanced and unbalanced traffic volume across the lanes subject to a CAV penetration rate of 60%. Top two: balanced cases. Bottom two: unbalanced across a pair of perpendicular lanes with an aggregated arrival rate of 2000 veh/h. The opposite directions have the same traffic volume.

energy efficiency results without sacrificing traffic efficiency.

To examine the influence of traffic volume (arrival rate), we further compare the proposed approach with the three baseline algorithms under various scenarios, considering both balanced and unbalanced arrival rates across all lanes. Without loss of generality, the CAV penetration rate is set to 60%. The two top figures in Fig. 4.5 present the control solutions for three methods with a balanced arrival rate in all directions. The three methods exhibit comparable performance when dealing with a low traffic volume case, 400 veh/h/lane. As traffic volume increases, the proposed method, CVSC [23] and O-SPAT can result in better throughput compared to F-SPAT, and the maximum benefit of 8.65% is achieved at 1170 veh/h/lane. In addition, the proposed method costs the least fuel due to joint control of the SPAT and the vehicle speed trajectory. As traffic volume increases, the proposed method shows an improved energy efficiency compared to O-SPAT, and the benefit is maximized at 12.65% when the arrival rate reaches 1170 veh/h/lane. Compared to CVSC, the proposed method can achieve a maximum improvement of 8.67% in fuel consumption. Although the fuel savings of the proposed method are not as high when compared to F-SPAT, it remains the best for all arrival rates.

The unbalanced cases are illustrated at the bottom of Fig. 4.5. The aggregated arrival rates of any two perpendicular approaches are fixed at 2000 veh/h whereas the arrival rates for any two opposite directions are identical. It is important to highlight that only F-SPAT and the CVSC are depicted for comparison, whereas O-SPAT can attain comparable throughput to the proposed method; however, its energy efficiency is significantly compromised, as observed in the top two plots in Fig. 4.5 and Table 4.2. The proposed method results in a traffic throughput performance comparable to that of the CVSC method while showing a significant improvement compared to F-SPAT. The improvement of the proposed method in terms of throughput becomes more pronounced as the level of imbalance intensifies. In particular, in the scenario with a volume distribution of 400/1600 veh/h/lane, the benefit amounts to 14.10%, which is significantly higher than the 7.12% achieved in the case of 1000/1000 veh/h/lane. Regarding fuel consumption, a similar con-

clusion can be drawn based on the results compared to F-SPAT and CVSC, where maximum improvements of 8. 33% and 7.22% are observed, respectively, when the volume distribution follows 400/1600 veh/h/lane.

Fig. 4.6 presents a speed comparison between the proposed method and the other three benchmark algorithms. The balanced case is shown on the left, where the CAV penetration rate is set to 60%. The proposed algorithm can lead to a higher average speed compared to the other three methods in all cases.

In the balanced case, F-SPAT can outperform O-SPAT when the volume is low, but as the volume of traffic increases, the performance of F-SPAT degrades and becomes the least-performing method. The proposed method and CVSC [23] can outperform both F-SPAT and O-SPAT for all traffic volumes, while the fastest average speed is always achieved by the proposed method. More specifically, the proposed method shows an improved average speed compared to O-SPAT, which is maximized at 2.95% when the arrival rate reaches 1080 veh/h/lane. Compared to CVSC, the proposed method can achieve a maximum improvement of 2.20% in average speed.

The unbalanced case is illustrated on the right. The proposed method results in slightly faster average speed performance compared to the other three methods when the level of imbalance is low. The improvement of the proposed method in terms of average speed becomes more significant as the level of imbalance increases. In particular, in the scenario with a volume distribution of 400/1600 veh/h/lane, the benefit amounts to 6.55%, 4.71%, and 2.77% when compared with the F-SPAT, the O-SPAT, and the CVSC method, respectively.

To assess how the adoption of EVs impacts the energy efficiency of the proposed method, three different scenarios with 100%, 50%, and 0% EV penetration rates are examined. For illustrative purposes, we base our analysis on a scenario featuring an evenly distributed traffic volume of 1000 veh/h across all lanes, and a CAV penetration rate of 60%. We subsequently evaluate energy consumption using equations (4.34) to (4.36). It is noteworthy that in the 50% EV penetration scenario, all EVs are also CAVs, as automation often coincides with electrification. As illus-

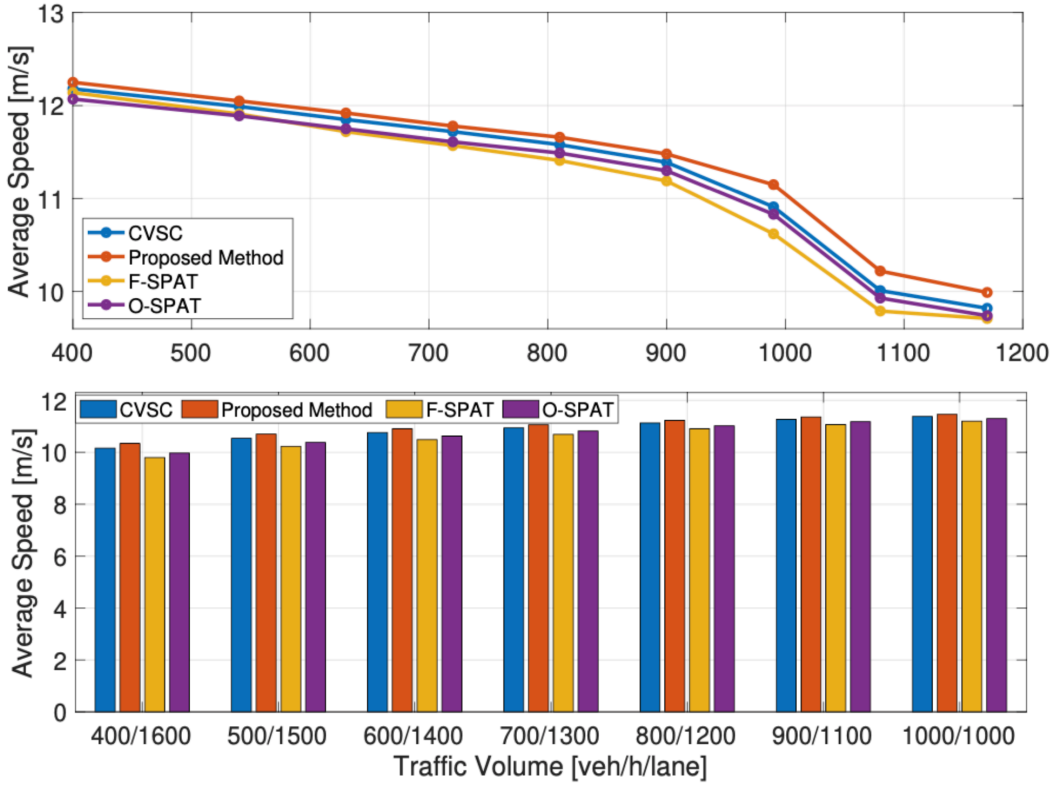

Figure 4.6: Average speed of the proposed and benchmark methods under balanced and unbalanced traffic volume across the lanes subject to a CAV penetration rate of 60%. Top: balanced cases. Bottom: unbalanced across a pair of perpendicular lanes with an aggregated arrival rate of 2000 veh/h. The opposite directions have the same traffic volume.

trated in Fig.4.7, an increase in the penetration of EVs leads to a substantial reduction in energy consumption. This is because of the improved efficiency of electric drives and the occurrence of numerous stop-and-go situations at intersections.

In addition, the influence of the CAV penetration rate, ranging from 30% to 100%, on the energy consumption and vehicle throughput of the proposed method is investigated under a fully electric environment. In this specific case, it is assumed that the volume of vehicles is evenly distributed in all directions. As shown in the left plot of Fig. 4.8, the traffic throughput is primarily influenced by traffic volume rather than penetration rate. In principle, the throughput increases linearly as the volume rises, but it peaks at about 1200 veh/h/lane, which represents the capacity for the lane. As previously mentioned, the traffic throughput is heavily influenced by SPAT control, which greatly relies on the knowledge of the vehicle location.

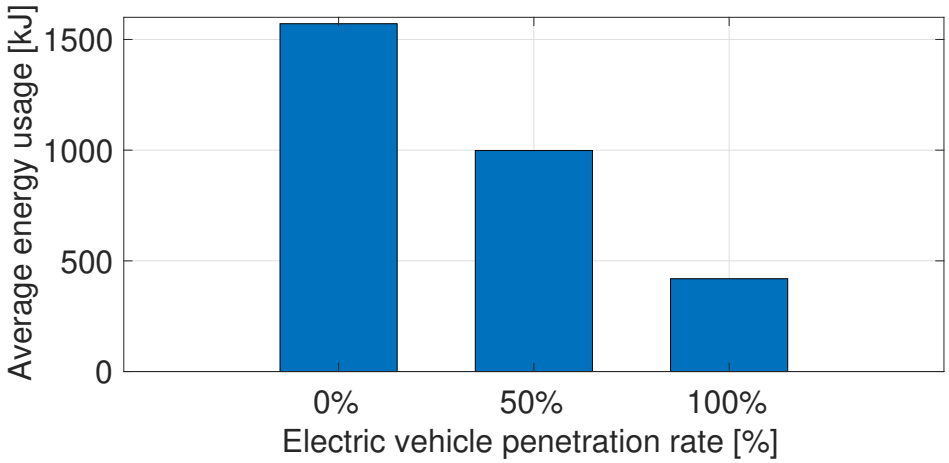

Figure 4.7: The impact of EV penetration rate on the vehicle energy efficiency subject to a 1000 veh/h/lane traffic volume and a fixed 60% CAV penetration rate.

As uncertainties are not considered in the present work, the benefit of additional automation may not be readily apparent, particularly when the traffic volume is low. However, in high-traffic volume scenarios, an increased number of CAVs can have a more positive impact on SPAT optimization, thereby improving traffic throughput. The impact of the penetration rate on traffic throughput becomes most evident when the traffic volume reaches 1000 veh/h/lane. With a penetration rate of 100%, traffic throughput can be improved by 5.03% compared to the 30% case.

In contrast, the average electricity consumption, as presented in the right plot of Fig. 4.8, can be reduced when the CAV penetration rises, given the same traffic volume. This reduction becomes slightly more pronounced with higher traffic volumes. This can be understood as follows: 1) the energy cost is primarily influenced by optimizing speed trajectories, and as the penetration rate increases, more vehicles can be precisely controlled, allowing for faster platoon formation, and therefore greater energy savings; and 2) vehicle movement is less restrained by safety constraints in low traffic volume cases, thereby fewer acceleration and deceleration during driving are required. The most apparent energy reduction caused by an increase in the penetration rate occurs when the traffic volume is 1200 veh/h/lane, with a reduction of 11.47%.

Finally, the robustness of the proposed method is also assessed. An input dis-

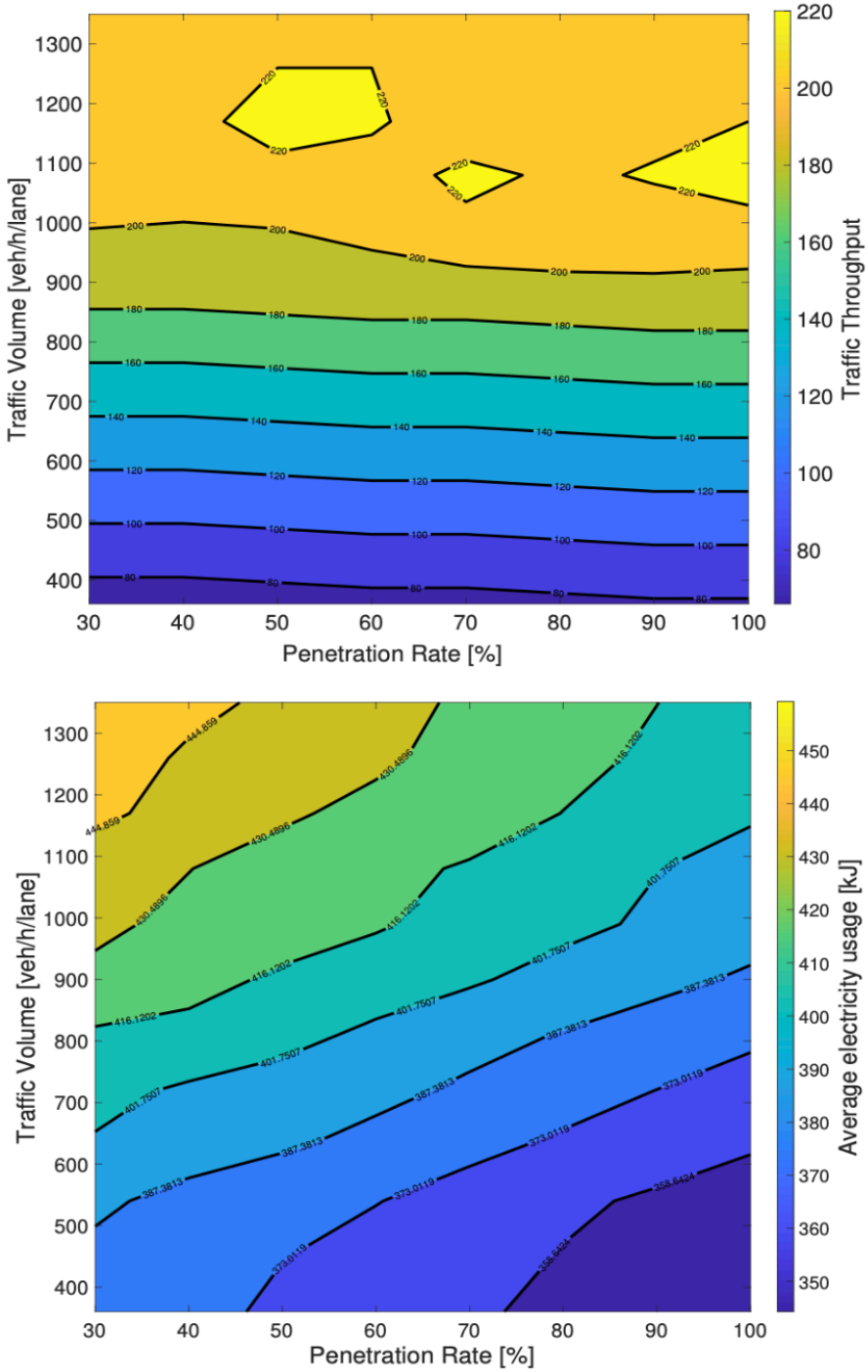

Figure 4.8: Intersection traffic throughput and average electricity consumption of the proposed method obtained under different CAV penetration rates and traffic volumes.

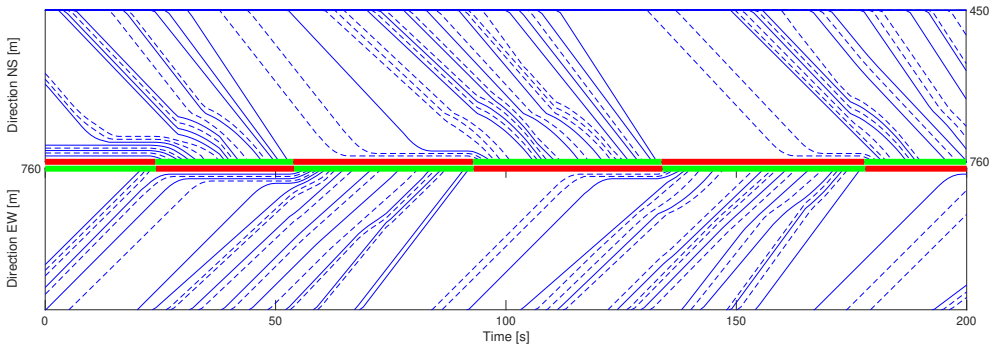

Figure 4.9: Traffic SPAT and vehicle position trajectories. The trajectories of HDVs are denoted by dashed lines, and the trajectories of CAVs are represented by solid lines. Only two perpendicular lanes, NS refers to the direction from north-to-south, and EW is the direction from east-to-west, are shown for clarity of the figure.

turbance is added to the mixed platoon model (4.7) to simulate the uncertainty of HDVs. This disturbance follows a Gaussian distribution with zero mean and a variance of 0.01. Traffic SPAT and vehicle position trajectories (from the entry point of the CZ at 450 m to the exit of MZ at 760 m) for 200 s solved by the proposed methodology subject to a CAV penetration rate of 50% and a balanced traffic volume of 1000 veh/h across all lanes. As can be seen in Fig. 4.9, there are no rear-end (the position trajectories do not intersect each other) and lateral collisions (vehicles from the two perpendicular directions do not appear in the MZ at the same time), and all vehicles follow the traffic lights, which shows the robustness of the proposed approach.

4.5 CONCLUSIONS

Following the control framework in Fig. 1.4, this chapter introduces a two-layer intersection signal-vehicle coupled coordination scheme for joint control of the intersection SPAT and speed trajectory of CAV and HDV for traffic management within the car-following zone. The method is developed based on a CAV-led mixed platoon model, where the motion of the HDVs is governed by a linearized intelligent driver model. In addition to the SPAT, the target platoon velocity and the number of passing platoons are continuously updated in the upper layer to minimize the total waiting time. Subsequently, the intersection controller utilizes the SPAT infor-

mation to conduct optimal control of the mixed platoon within the control zone by manipulating the speed of the leading CAVs.

A comparative analysis is performed, contrasting the proposed method with conventional approaches focusing solely on optimizing signal duration or vehicle trajectory, as well as a recently proposed coupled vehicle-signal control method [23]. Through these comparisons, the advantages of the proposed method are revealed in terms of average fuel consumption and traffic throughput. The proposed method improves throughput by 7.92% while achieving additional fuel savings of 5.97% compared to the method with optimized vehicle trajectories only. Furthermore, it reduces fuel consumption by 11.54% compared to the benchmark method, which solely optimizes SPTA, and shows a reduction of 6.34% compared to a state-of-the-art method [23] while maintaining a similar traffic throughput. The simulation results also highlight the significant roles of SPAT control and vehicle trajectory control in enhancing throughput and achieving energy savings, respectively. The benefits of the proposed control solution are further amplified in the presence of unbalanced traffic volumes across the intersection lanes. Lastly, the simulation results validate the advantages of increasing the CAV market penetration rate, particularly in terms of electricity savings, which can reach as high as 11.47% when the penetration is escalated from 30% to 100% in the given simulation.

As lane-changing and overtaking are not allowed in the concerned zone, the interaction between CAVs and HDVs is not investigated here. In Chapters 5 and 6, we will focus on the lane-changing zone, where the human-machine interactions are thoroughly studied.

Chapter 5

A Game-based Optimal and Safe Lane Change control of single CAV

5.1 Introduction

In the previous chapter, lane changing is not allowed inside the car following zone, which neglects the interactions between CAVs and HDVs. However, this neglected interaction is crucial in ensuring safety in mixed traffic environments. To find out how to model the CAV-HDV interaction in a realistic and safe way, the overtaking and lane-changing behaviors in the lane-changing zone of Fig. 1.4 will be investigated in this chapter.

Game-theoretic methods are commonly used to model and analyze conflict behaviors among multiple intelligent agents or players [193], which provides a valid tool for addressing the interaction problem between CAVs and HDVs [194–196]. Different types of games have been investigated, such as the inverse differential game [151], the mixed strategy Nash game [155], the Stackelberg game [152, 153, 158,159,196]. Despite the rich literature, there remains a lack of theoretical analysis concerning the equilibria of game-theoretic lane-changing strategies. To address this gap, this chapter proposes a Stackelberg game-based optimal lane-changing control framework, with a particular focus on theoretical analysis. Specifically, lane-changing scenarios involving one CAV and one HDV are investigated in detail. The work in this chapter has the following novelty:

1. Unlike many existing works, the HDV in this study is capable of changing lanes while the CAV is changing lanes. The interaction of both is taken into account by a Stackelberg game, which yields an unconstrained optimal control solution by the Hamilton–Jacobi equation (HJE).

2. A theoretical proof is provided to show that the unconstrained optimal strategy is the asymptotically stable equilibrium, and with a suitable design of the weight matrices, safety can be guaranteed by the obtained optimal strategy.

The remainder of this chapter is organized as follows. Section 5.2 introduces the overall framework for changing lanes. In Section 5.3, the Stackelberg game-based control scheme is introduced. A theoretical proof is presented to show that with a suitable choice of the weighting parameters of the CAV's reward function, safety can be ensured by the derived strategy. The simulation results and the discussion are shown in Section 5.4. Finally, concluding remarks are given in Section 5.5.

5.2 Problem Formulation

This chapter focuses on the autonomous lane-changing of CAV on roads in the presence of a potential conflict HDV. This scenario is fundamental for studying CAV-HDV interactions, as more complex maneuvers like overtaking, turning, and roundabout driving can be derived from it. As shown in Fig. 5.1, this chapter considers a scenario where there is a fully controllable CAV and an uncontrollable HDV traveling in the neighboring lane. The CAV intends to make a lane change while the HDV either keeps driving on its original lane or turns to its destination lane. To successfully and safely change lanes, the CAV must decide whether to merge in front or behind the HDV depending on the initial conditions (position, velocity, etc.) of both vehicles, the intention of the HDV, and how the HDV interacts with the CAV. In particular, depending on the intention of the HDV, there are two lane-changing interactions between the two vehicles, which are illustrated in Fig. 5.1. As can be seen in Figs. 5.1 (a)-(b), only the CAV changes the lane, while the HDV continues to drive in its original lane. In Fig. 5.1 (a), when the relative distance between the two vehicles is small and the CAV is faster than the HDV, the CAV can choose to

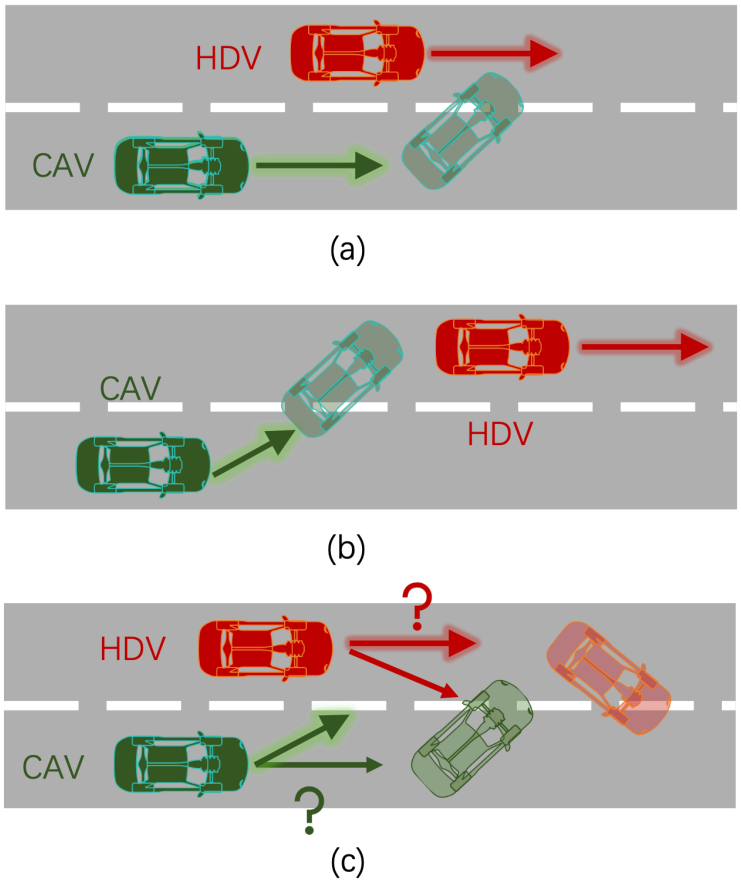

Figure 5.1: The complex lane-changing decision in mixed traffic scenarios involving HDV and CAV.

accelerate and overtake the HDV. Meanwhile, the HDV may maintain its current speed or even decelerate to facilitate the CAV. In Fig. 5.1 (b), if the HDV is faster than the CAV or the relative distance between the two vehicles is large, the CAV will choose to merge behind the HDV. To leave enough space for the CAV to merge into the lane, the HDV may choose to accelerate in such circumstances. In Fig. 5.1 (c), both HDV and CAV decide to change lanes, which yields a more challenging case. In this case, both vehicles need to determine individual lane-changing according to their driving preferences, which could include driving efficiency, comfort, and safety concerns.

The chapter aims to address the problem of lane change control for the CAV by designing a decision-making and trajectory control method. To make the de-

rived control solution more realistic and considering the lane-changing maneuver, we use the bicycle model illustrated in Fig. 3.1 to model the vehicle dynamics, with the details given in (3.3). The vehicle state is denoted by $x_k(t) = \begin{bmatrix} p_{k,x}(t) & p_{k,y}(t) & \theta_k(t) & v_k(t) \end{bmatrix}^\top$, where the CAV and the HDV are indexed by $k = 0$ and $k = 1$, respectively. $p_{k,x}(t)$ and $p_{k,y}(t)$ represent the longitudinal and lateral position of each vehicle in the global coordinate, respectively, and L_B is the length of the wheelbase. $\theta_k(t)$ is the vehicle heading angle and $v_k(t)$ is the forward velocity. $\varphi_k(t)$ and $a_k(t)$ are the steering angle of the front wheels of the vehicle and the acceleration of the vehicle, which represent the manipulated variables of both vehicles.

Assumption 5.1. *It is assumed that the initial direction of both vehicles is straight ahead, with heading angles of* 0*, and during the task, the two vehicles can only move straight ahead or move toward the target (neighboring) lane.*

According to Assumption 5.1, considering that the heading angle of the CAV satisfies $\theta_0(t) \leq 0$, it can be inferred that the heading angle of the HDV satisfies $\theta_1(t) \geq 0$, under the same coordination system. To ensure the safety of the CAV lane change maneuver, it is requested to meet the velocity constraint $v_0(t) < v_{\max}, \forall t$ and the collision avoidance constraint against the HDV, as described below. To deal with collision avoidance, the vehicle will be viewed as a rectangle with length L and width L_W, which can be expressed as: $\mathbb{O}_k(t) = \left\{ p(t) \in \mathbb{R}^2 : A_k(t)p(t) \leq b_k(t) \right\}, k \in \{0,1\}$

The collision avoidance constraint can be written as

$$\operatorname{dist}\left(\mathbb{O}_0(t), \mathbb{O}_1(t)\right) \geq d_{\min} \tag{5.1}$$

with

$$\operatorname{dist}\left(\mathbb{O}_0(t), \mathbb{O}_1(t)\right) = \min_r \left\{ \|r\| : \left(\mathbb{O}_0(t) \bigoplus r \right) \cap \mathbb{O}_1(t) \neq \varnothing \right\}$$

denoting the distance between two vehicles in this chapter. $d_{\min} > 0$ denotes the minimum safe distance. $\bigoplus$ denotes the Minkowski sum, which can be expressed as $\mathscr{C} = \mathscr{A} \bigoplus \mathscr{B} = \{c : c = \alpha + \beta, \alpha \in \mathscr{A}, \beta \in \mathscr{B}\}$. The equivalent conditions of this

collision avoidance constraint are given in the following lemma, which is based on the existing work [197].

Lemma 5.1. *[197] The constraint* (5.1) *holds if there exist* $\lambda(t) \in \mathbb{R}^4, \nu(t) \in \mathbb{R}^4$ *belongs to constraint set* $\mathscr{D}(b_0(t), b_1(t), A_0(t), A_1(t), d_{\min})$ *with parameter matrices* $b_0(t), b_1(t) \in \mathbb{R}^4$, $A_0(t), A_1(t) \in \mathbb{R}^{4\times 2}$, *which can be expressed as*

$$-b_0^\top(t)\nu(t) - b_1^\top\lambda(t) \geq d_{min}, \tag{5.2a}$$

$$A_0^\top(t)\nu(t) + A_1^\top(t)\lambda(t) = 0, \tag{5.2b}$$

$$\lambda(t) \succeq 0, \nu(t) \succeq 0, \tag{5.2c}$$

$$\left\| A_1^\top(t)\lambda(t) \right\| \leq 1. \tag{5.2d}$$

To simplify the notation, we have dropped the dependence of all variables on t in the subsequent equations. Given the lateral and longitudinal positions of CAV $(p_{0,x}, p_{0,y})$ and HDV $(p_{1,x}, p_{1,y})$, the driving angle of two vehicles θ_0, θ_1, respectively. With L being the vehicle length and L_W being the vehicle width, the matrices A_k, b_k, where $k \in \{0,1\}$ can be expressed as follows:

$$b_k = \begin{bmatrix} p_{k,x}\cos\theta_k + p_{k,y}\sin\theta_k + \frac{L}{2} \\ -p_{k,x}\cos\theta_k - p_{k,y}\sin\theta_k + \frac{L}{2} \\ -p_{k,x}\sin\theta_k + p_{k,y}\cos\theta_k + \frac{L_W}{2} \\ p_{k,x}\sin\theta_k - p_{k,y}\cos\theta_k + \frac{L_W}{2} \end{bmatrix}$$

$$A_k = \begin{bmatrix} \cos\theta_k & -\cos\theta_k & -\sin\theta_k & \sin\theta_k \\ \sin\theta_k & -\sin\theta_k & \cos\theta_k & -\cos\theta_k \end{bmatrix}^\top$$

5.3 Game-based lane-changing strategy

5.3.1 Stackelberg Game

To model the interaction between CAV and HDV appears in the lane change scenario shown in Fig. 5.1, the Stackelberg game model will be utilized. The reason to adopt the Stackelberg game has been elaborated in Chapter 3. To introduce the

game-based control strategy, consider $x = [x_0^\top \; x_1^\top]^\top \in \mathbb{R}^8$ and $u_k = [\tan\varphi_k \; a_k]^\top$, $k \in \{0,1\}$. Note that $\tan\varphi_k$ is used as a control instead of φ for ease of analysis. The joint dynamics of both vehicles can be recast in the following form:

$$\dot{x} = f(x) + g_0(x)u_0 + g_1(x)u_1 \tag{5.3}$$

where $f(x) = [v_0\cos\theta_0 \; v_0\sin\theta_0 \; 0 \; 0 \; v_1\cos\theta_1 \; v_1\sin\theta_1 \; 0 \; 0]^\top$

$$g_0(x) = \begin{bmatrix} 0 & 0 & L_B^{-1}v_0 & 0 & 0 & 0 & 0 & 0 \\ 0 & 0 & 0 & 1 & 0 & 0 & 0 & 0 \end{bmatrix}^\top.$$

$$g_1(x) = \begin{bmatrix} 0 & 0 & 0 & 0 & 0 & 0 & L_B^{-1}v_1 & 0 \\ 0 & 0 & 0 & 0 & 0 & 0 & 0 & 1 \end{bmatrix}^\top$$

are all verified to be Lipschitz continuous.

As can be seen in Chapter 3, the Stackelberg game model allows for optimal control of the CAV subject to optimal response of the HDV. Compared to some of the existing works that model the HDV using a macroscopic driver model, the HDV involved in the proposed game-based framework does not necessarily follow a specific car-following model. Instead, the optimized response of HDV tends to be more realistic and, in turn, could yield more reliable control solutions of the CAV. Denote $x_i = x(0)$ the initial state of the vehicles, u_0 and u_1 are the actions (acceleration) of the leader and follower actions, respectively, while u_0^* and u_1^* are the optimal actions for the leader and follower. $\mathscr{U}_0$ and $\mathscr{U}_1$ are the action spaces of the leader and follower. J_0 and J_1 stand for the leader's and follower's cost functions, respectively. The solution of the game gives a planned trajectory for the lane change vehicles to change lanes successfully (in the absence of a collision avoidance constraint (5.1)).

5.3.2 Stackelberg Game-Based CAV Lane Changing Strategy

In this article, the cost function of each player J_k is designed as

$$J_k(x_i, u_0, u_1) = \int_0^\infty r_k(x, u_0, u_1)\, dt,\ k \in \{0,1\} \tag{5.4}$$

where the reward functions of both vehicles follow

$$r_k(x, u_0, u_1) = \|x - x_d\|^2_{Q_k} + \|u_k\|^2_{R_k},\ k \in \{0,1\} \tag{5.5}$$

where $Q_k = \text{diag}\{q_{k,j}\}$, $j = 1,2,\ldots,8$, $R_k = \text{diag}\{r_{k,l}\}$, $l = 1,2$ with $q_{k,j} \geq 0$, $r_{k,l} > 0$ are design weights of the rewards. $x_d \in \mathbb{R}^8$ is the desired state of two vehicles after the lane change maneuver of the CAV. Next, we have the individual value function.

$$V_k(x, u_0, u_1) = \int_t^\infty r_k(x(\tau), u_0(\tau), u_1(\tau)) d\tau,\ k \in \{0,1\} \tag{5.6}$$

In this context, the associated Hamiltonians can be constructed as:

$$\mathscr{H}_k(x, \nabla V_k, u_0, u_1) = r_k(x, u_0, u_1) + \nabla V_k^\top (f(x) + g_0(x)u_0 + g_1(x)u_1) \tag{5.7}$$

where $\nabla V_k = (\partial V_k(x)/\partial x)$, $k \in \{0,1\}$.

Given (5.5), (5.6) and (5.7), it is immediate to show that $\mathscr{H}_k$ is convex with respect to u_k. Therefore, the first optimality condition holds, and the optimal control can be obtained by solving $\frac{\partial \mathscr{H}_0}{\partial u_0} = \frac{\partial \mathscr{H}_1}{\partial u_1} = 0$. In particular, the optimal action for the follower is

$$u_1^*(u_0) = \arg\min_{u_1} \mathscr{H}_1(x, \nabla \bar{V}_1, u_0, u_1) = -\frac{1}{2} R_1^{-1} g_1(x)^\top \nabla \bar{V}_1 \tag{5.8}$$

where $\bar{V}_1$ is the value function evaluate with u_0 and $u_1^*(u_0)$. In the case $u_0 = u_0^*$, we have

$$u_1^* = u_1^*(u_0^*) = -\frac{1}{2} R_1^{-1} g_1(x)^\top \nabla V_1^* \tag{5.9}$$

where $\nabla V_k^*, k \in \{0,1\}$ is obtained when u_0^* and u_1^* are applied. Similarly, according

to the definition of the Stackelberg game, the optimal action of the leader can also be determined

$$u_0^* = \arg\min_{u_0} \mathscr{H}_0(x, \nabla V_0^*, u_0, u_1^*(u_0)) = -\frac{1}{2} R_0^{-1} g_0(x)^\top \nabla V_0^* \tag{5.10}$$

According to the HJE, the following holds for u_0^*, u_1^*

$$\mathscr{H}_k(x, \nabla V_k^*, u_0^*, u_1^*) = r_k(x, u_0^*, u_1^*) + \nabla V_k^{*T} \times (f(x) + g_0(x)u_0^* + g_1(x)u_1^*) = 0, k \in \{0,1\}. \tag{5.11}$$

Theorem 5.1. *The system* (5.3) *is asymptotically stable, such that* $||x - x_d|| = 0, t \to \infty$ *under the control* u_k^*, $k \in \{0,1\}$ *given by* (5.9), (5.10). *Furthermore,* u_k^* *is the equilibrium of this Stackelberg game with the game values being* $V_k^*(x_i)$, *where* V_k^*, $k \in \{0,1\}$ *are the smooth solutions to* (5.11)

Proof. According to the chain rule, it holds that

$$\dot{V}_k = \nabla V_k^\top \dot{x} = \nabla V_k^\top (f(x) + g_0(x)u_0 + g_1(x)u_1)$$

From (5.11), we also have

$$\nabla V_k^{*\top} (f(x) + g_0(x)u_0^* + g_1(x)u_1^*) = -r_k(x, u_0^*, u_1^*)$$

which implies $\dot{V}_k^* = -r_k\left(x, u_0^*, u_1^*\right) < 0$ Let $e = x - x_d$, it can be shown that V_k^* is a valid Lyapunov candidate with respect to e (V_k^* is semi-positive definite and $V_k^* = 0$ only when $e = 0$). As a consequence, the system (5.3) is asymptotically stable. In view of (5.4), the cost function $J_k(x_i, u_0, u_1)$ can be written as

$$J_k(x_i, u_0, u_1) = \int_0^\infty r_k(x, u_0, u_1)\, dt + V_k^*(x_i) + \int_0^\infty \dot{V}_k^*(x) dt - V_k^*(\infty) = \int_0^\infty \mathscr{H}_k(x, \nabla V_k^*, u_0, u_1)\, dt + V_k^*(x_i) \tag{5.12}$$

where $V_k(\infty)$ is dropped due to the convergence of the system. As $\mathscr{H}_0\left(x, \nabla V_0, u_0^*, u_1^*\right) =$

0, for the leader CAV, it can be inferred that $J_0\left(x_i, u_0^*, u_1^*\right) = V_0^*\left(x_i\right)$. By (5.8) and (5.10), it also holds that

$$\mathscr{H}_k\left(x, \nabla V_k^*, u_0, u_1\right) \geq \mathscr{H}_k\left(x, \nabla V_k^*, u_0^*, u_1^*\right), k \in \{0,1\} \tag{5.13}$$

In view of (5.12), it can be derived that

$$\begin{aligned} J_0\left(x_i, u_0, u_1^*(u_0)\right) &= \int_0^\infty \mathscr{H}_0\left(x, \nabla V_0^*, u_0, u_1^*(u_0)\right) dt + V_0^*\left(x_i\right) \\ &\geq \int_0^\infty \mathscr{H}_0\left(x, \nabla V_0^*, u_0^*, u_1^*\right) dt + V_0^*\left(x_i\right) = J_0\left(x_i, u_0^*, u_1^*\right) \end{aligned} \tag{5.14}$$

where the inequality is inferred from (5.13). Similarly, for the follower vehicle, we have $J_1\left(x_i, u_0^*, u_1^*\right) = V_1^*\left(x_i\right)$ Given the optimal action of the leader u_0^*, suppose the follower takes the action u_1 other than u_1^*, then we have

$$\begin{aligned} J_1\left(x_i, u_0^*, u_1\right) &= \int_0^\infty \mathscr{H}_i\left(x, \nabla V_1^*, u_0^*, u_1\right) dt + V_1^*\left(x_i\right) \\ &\geq \int_0^\infty \mathscr{H}_1\left(x, \nabla V_1^*, u_0^*, u_1^*\right) dt + V_1^*\left(x_i\right) = J_1\left(x_i, u_0^*, u_1^*\right) \end{aligned} \tag{5.15}$$

By (3.13) and (3.12) in Definition 3.1, u_0^* and u_1^* are the equilibrium of this Stackelberg game with the game values being $V_k^*(x_i)$.

□

From Theorem 5.1, the optimal lane changing control u_0^* for the CAV can be obtained by solving two sequential optimization problems described below:

$$u_1^* = \underset{u_1 \in \mathscr{U}_1}{\operatorname{argmin}} J_1\left(x_i, u_0 \in \mathscr{U}_0, u_1\right) \tag{5.16a}$$

$$u_0^* = \underset{u_0 \in \mathscr{U}_0}{\operatorname{argmin}} J_0\left(x_i, u_0, u_1^*\right) \tag{5.16b}$$

5.3.3 Safety Guarantees

Note that the optimal control strategy obtained in (5.9) and (5.10) is obtained without considering collision avoidance and velocity constraints. In this section, we show that by appropriately choosing the weighting parameters of the CAV reward

function, the optimal lane change control action u_k^*, $k \in \{0,1\}$ can avoid collisions between the two vehicles using the notion of zeroing control barrier function (ZCBF).

Lemma 5.2. *(ZCBF) [198]. Consider a dynamical system $\dot{x} = f(x)$ with f locally Lipschitz continuous. Let $\mathscr{C} = \{x \in \mathbb{R}^n : h(x) \geq 0\}$ be the 0-super level set of a constraint function h. h is a zeroing control barrier function (ZCBF) if there exists a $\mathscr{K}$ function γ and there exists $u \in \mathscr{U}$ such that*

$$\sup_{u \in \mathscr{U}} \left[L_f h(x) + L_g h(x) u + \gamma(h(x)) \right] \geq 0, \forall x \in \mathscr{C} \tag{5.17}$$

Then, for any u that belongs to the following set:

$$\{u \in \mathscr{U} : \left[L_f h(x) + L_g h(x) u + \gamma(h(x)) \right] \geq 0\} \tag{5.18}$$

will guarantee the forward invariance of $\mathscr{C}$.

Next, we will show how to construct a ZCBF for system (5.3) based on the collision avoidance constraints defined previously in (5.2) so that the resulting set $\mathscr{C}$ is forward invariant and thus the lane changing control is safe. The following assumption is needed for the main result.

Assumption 5.2. *The desired speed of the CAV is $v_{\max}$, such that $v_d = v_{\max}$. The CAV starts with an initial speed strictly below this limit $v_0(0) < v_{\max}$.*

Consider a candidate control barrier function from (5.2a)

$$B(t) = -b_0^\top \nu - b_1^\top \lambda - d_{min} + c_1(v_0(0) - v_d) + \theta_0 \sqrt{p_{0,x}^2 + p_{0,y}^2} - \theta_1 \sqrt{p_{1,x}^2 + p_{1,y}^2} \tag{5.19}$$

where $c_1 \geq 0$ is a tunable constant. Being $v_0(0) < v_d$ (see Assumption 5.2), $\theta_0 \leq 0$ and $\theta_1 \geq 0$ (see Assumption 5.1), the last three terms are negative, which makes $B(t) \geq 0$ a more strict collision avoidance condition. In the following, it will be verified that $B(x,u)$ indeed satisfies the required CBF properties (i.e., (5.17)) subject to (5.2b)-(5.2d).

Lemma 5.3. *Given system* (5.3) *and the control* u_0^**, the velocity of the CAV* v_0^* *asymptotically converges to* v_d*.*

Proof. Let $e_v = v_0^* - v_d$ and consider a candidate Lyapunov function $\Omega(e_v) = \int_t^\infty e_v^2 d\tau$ and $\Omega(0) = 0$, it holds that

$$\dot{\Omega} = \dot{e}_v \int_t^\infty 2e_v d\tau = \dot{v}_0^* \int_t^\infty 2e_v d\tau = a_0^* \int_t^\infty 2e_v d\tau$$

where a_0^* is the optimal acceleration of the CAV (second element in u_0^*). Given (5.9) and (5.10), it can be derived that $a_0^* = -w_1 \int_t^\infty (v_0 - v_d) d\tau^\top$ with $w_1 = q_{0,4}/r_{0,2}$. Then we have the following:

$$\dot{\Omega} = -w_1 \left(\int_t^\infty e_v d\tau \right)^2 \leq 0$$

Thus, we can conclude that v_0^* asymptotically converges to v_d. Under Assumption 5.2, the CAV can comply with the velocity restriction during the maneuver. □

Theorem 5.2. *Under Assumptions 5.1 and 5.2, given the system* (5.3) *and the control* u_k^**,* $k \in \{0,1\}$*,* $B(t)$ *defined by* (5.19) *is a ZCBF if* w_1 *is designed such that the following condition is satisfied.*

$$w_1 \geq \frac{2\sqrt{3} a_{max} v_{max}}{\Delta v^2 c_1} \tag{5.20}$$

where $\Delta v = v_{\max} - v_0(0)$ *and* a_{max} *is the maximum acceleration of the CAV.*

Proof. In view of (5.2d), it holds that

$$(\lambda_1 - \lambda_2)^2 + (\lambda_3 - \lambda_4)^2 \leq 1 \tag{5.21}$$

where $\lambda_i, i = \{1,2,3,4\}$ represents ith entry of λ. Then, from (5.2b), we have $A_0^\top \nu = -A_1^\top \lambda$, and similarly to (5.21), it can be shown that

$$(\nu_1 - \nu_2)^2 + (\nu_3 - \nu_4)^2 \leq 1 \tag{5.22}$$

where ν_i, $i = \{1,2,3,4\}$ represents ith entry of ν. To ensure (5.17) is satisfied for the control u_k^* obtained in (5.9) and (5.10), it is required that

$$\nabla B(t)^\top (f(x) + g_0(x)u_0^* + g_1(x)u_1^*) \geq 0 \tag{5.23}$$

with $\lambda \geq 0$, $\nu \geq 0$ from (5.2c). After some cumbersome algebra, full expressions of $\nabla B(t)$, $g_1(x)u_1^*$ and $g_0(x)u_0^*$ can be calculated and given as follows

$$\nabla B(t) = \begin{bmatrix} -((\nu_1-\nu_2)\cos\theta_0 + (\nu_4-\nu_3)\sin\theta_0) \\ -((\nu_1-\nu_2)\sin\theta_0 + (\nu_3-\nu_4)\cos\theta_0) \\ -((\nu_1-\nu_2)p_{0,y} + (\nu_4-\nu_3)p_{0,x})\cos\theta_0 - \\ ((\nu_2-\nu_1)p_{0,x} + (\nu_4-\nu_3)p_{0,y})\sin\theta_0 + \sqrt{p_{0,x}^2 + p_{0,y}^2} \\ c_1 \\ -((\lambda_1-\lambda_2)\cos\theta_1 + (\lambda_4-\lambda_3)\sin\theta_1) \\ -((\lambda_1-\lambda_2)\sin\theta_1 + (\lambda_3-\lambda_4)\cos\theta_1) \\ -((\lambda_1-\lambda_2)p_{1,y} + (\lambda_4-\lambda_3)p_{1,x})\cos\theta_1 - \\ ((\lambda_2-\lambda_1)p_{1,x} + (\lambda_4-\lambda_3)p_{1,y})\sin\theta_1 - \sqrt{p_{1,x}^2 + p_{1,y}^2} \\ 0 \end{bmatrix} \tag{5.24}$$

$$\begin{aligned} g_1(x)u_1^* &= -0.5 g_1(x) R_1^{-1} g_1(x)^\top \nabla V_1^* = -0.5 g_1(x) R_1^{-1} g_1(x)^\top Q_1 \int_t^\infty (x - x_d) d\tau \\ &= -\begin{bmatrix} 0 & \cdots & 0 & \frac{v_1^2}{L_B^2} w_4 \int_t^\infty \theta_1 d\tau & w_3 \int_t^\infty (v_1 - v_d) d\tau \end{bmatrix}^\top, \end{aligned} \tag{5.25}$$

and

$$g_0(x)u_0^* = -\begin{bmatrix} 0 & 0 & \frac{v_0^2}{L_B^2} w_2 \int_t^\infty \theta_0 d\tau & w_1 \int_t^\infty (v_0 - v_d) d\tau & 0 & \cdots & 0 \end{bmatrix}^\top \tag{5.26}$$

where $w_2 = q_{1,8}/r_{1,2}$, $w_3 = q_{0,3}/r_{0,1}$, $w_4 = q_{1,7}/r_{1,1}$. By applying (5.24)-(5.26) and after some algebra, the condition (5.23) can be rewritten, as follows

$$\sum_{i=1}^{3} \eta_i + c_1 w_1 \int_t^\infty (v_d - v_0) d\tau \geq 0 \tag{5.27}$$

with

$$\eta_1 = ((\lambda_1-\lambda_2)\cos\theta_1+(\lambda_4-\lambda_3)\sin\theta_1)(v_0\cos\theta_0-v_1\cos\theta_1)$$
$$+((\lambda_1-\lambda_2)\sin\theta_1+(\lambda_3-\lambda_4)\cos\theta_1)(v_0\sin\theta_0-v_1\sin\theta_1)$$
$$\eta_2 = \frac{v_0^2}{L_B^2}w_2[\sqrt{p_{0,x}^2+p_{0,y}^2}-((v_1-v_2)p_{0,y}+(v_4-v_3)p_{0,x})$$
$$\times\cos\theta_0-((v_2-v_1)p_{0,x}+(v_4-v_3)p_{0,y})\sin\theta_0]\int_t^\infty -\theta_0 d\tau$$
$$\eta_3 = \frac{v_1^2}{L_B^2}w_4\left[-((\lambda_1-\lambda_2)p_{1,y}+(\lambda_4-\lambda_3)p_{1,x})\cos\theta_1\right.$$
$$\left.-((\lambda_2-\lambda_1)p_{1,x}+(\lambda_4-\lambda_3)p_{1,y})\sin\theta_1-\sqrt{p_{1,x}^2+p_{1,y}^2}\right]\int_t^\infty -\theta_1 d\tau$$

Considering η_1 in (5.27), from the Cauchy-Schwartz inequality, it can be shown that

$$\begin{aligned}&|\ ((\lambda_1-\lambda_2)\cos\theta_1+(\lambda_4-\lambda_3)\sin\theta_1)(v_0\cos\theta_0-v_1\cos\theta_1)+\\&\qquad((\lambda_1-\lambda_2)\sin\theta_1+(\lambda_3-\lambda_4)\cos\theta_1)(v_0\sin\theta_0-v_1\sin\theta_1)\ |\leq\\&\sqrt{((\lambda_1-\lambda_2)^2+(\lambda_3-\lambda_4)^2)(v_0^2+v_1^2-v_0v_1\cos(\theta_0-\theta_1))}\leq\sqrt{v_0^2+v_1^2+v_0v_1}\leq\sqrt{3}v_{max}\end{aligned} \tag{5.28}$$

where the second inequality is obtained by (5.21). Consider η_2 in (5.27). Similarly, by using (5.22) it can be shown that

$$\begin{aligned}&|\ ((v_1-v_2)p_{0,y}+(v_4-v_3)p_{0,x})\cos\theta_0\\&\qquad+((v_2-v_1)p_{0,x}+(v_4-v_3)p_{0,y})\sin\theta_0\ |\leq\\&\sqrt{(\cos\theta_0^2+\sin\theta_0^2)(((v_1-v_2)^2+(v_3-v_4)^2))(p_{0,x}^2+p_{0,y}^2)}\leq\sqrt{p_{0,x}^2+p_{0,y}^2}\end{aligned} \tag{5.29}$$

Being $\theta_0\leq 0$, we can conclude that η_2 is always non-negative. Similarly, η_3 in (5.27) is also non-negative. Due to the asymptotic convergence of v_0^* to v_d, it can be inferred that

$$\int_t^\infty (v_{\max}-v_0)d\tau\geq\frac{\Delta v^2}{2a_{max}} \tag{5.30}$$

Therefore, (5.27) holds if

$$c_1 w_1 \int_t^{\infty} (v_{\max} - v_0) d\tau - \sqrt{3} v_{max} \geq 0 \tag{5.31}$$

Therefore, we reach the conclusion that provided (5.20), condition (5.23) is satisfied. According to Lemma 5.2, $B(t)$ is a ZCBF, and the control u_k^* obtained in (5.9) and (5.10) render the set $\mathscr{C}$ forward invariant. □

Theorem 5.2 implies that collision avoidance is guaranteed, provided the CAV and HDV are controlled by (5.16). As there is no disturbance considered in this work, when provided two players exactly follow the optimal strategies of the Stackelberg game, then deadlock is naturally avoided, according to Theorem 5.1 and Theorem 5.2.

5.4 Simulation Validation

5.4.1 Simulation setup

In this section, the performance of the proposed control framework is evaluated considering only one CAV and one HDV, which travel in two separate lanes, as shown in Fig. 5.1. All other surrounding vehicles are not considered. Two case studies are conducted. In case one, only the CAV changes lanes, whereas the HDV stays in its initial lane throughout the simulation. On the contrary, both vehicles intend to change lanes in the second case. In both case studies, the initial lateral position of the CAV (that is, the center of the lane on which the CAV initially drives) is 0 m, and the initial lateral position of the HDV is 5 m, which also represents the center of the destination lane of the CAV. In both case studies, it is reasonable to set the desired velocities of both vehicles at the maximum allowed speed, $v_{\max}$ (for a reduced travel time), and the desired heading angles at $t = 0$. For vehicles attempting to change lanes, the desired lateral positions are the center of the destination lanes; otherwise, the desired lateral positions are the center of the original lanes. With the target lateral positions, velocity, and steering angle, the desired state x_d can be specified for the problem.

The first case study involves two different scenarios with the same initial longitudinal position of the CAV, 10 m, and the HDV, 14 m, but different initial velocities for the sake of comparison. More specifically, in Scenario 1, the initial speeds of the CAV and the HDV are close to each other, set to 16 m/s and 15 m/s, respectively. In scenario two, the initial speeds of CAV is set to 19 m/s, which is much faster than the HDV's initial speed of 10 m/s. In the second case study where both the CAV and the HDV change lanes, the initial speed of the CAV and the HDV is set to 15m/s and 14m/s, respectively. The initial longitudinal position of the CAV and the HDV is 10m and 15m, respectively. As both vehicles change lanes in this case, the target lateral position of the HDV is 0m whereas the target for the CAV is 5m. The remaining vehicle parameters are summarized in Table 5.1.

Table 5.1: Simulation parameters

symbol	value	description
Δt	0.1 s	sampling time interval
L	4.6 m	vehicle length
L_B	2.7 m	vehicle wheelbase
L_W	1.8 m	vehicle width
$v_{\max}$	20 m/s	maximum velocity
$a_{\max}$	5 m/s^2	maximum acceleration

In addition, the robustness of the proposed method is also tested based on case study 2. A disturbance is added to the optimal control of HDV u_1^* derived from equation (5.9) to simulate human uncertainties. This disturbance follows a Gaussian distribution with zero mean and a variance of 0.05.

5.4.2 Analysis of simulation results

Following the approach designed in Section 5.3.2, simulation results are obtained by solving unconstrained optimizations (5.16), and the solutions are supposed to satisfy the collision avoidance constraints as justified in Section 5.3.3

As shown in Fig. 5.2 (a), the CAV conducted a successful lane-changing in the first scenario of case one. The convergence of the cost of each player is shown in Fig. 5.3 (a), which implies that both vehicles reach their desired velocity and target lanes. Although the CAV is slightly faster than the HDV at first, the CAV chooses

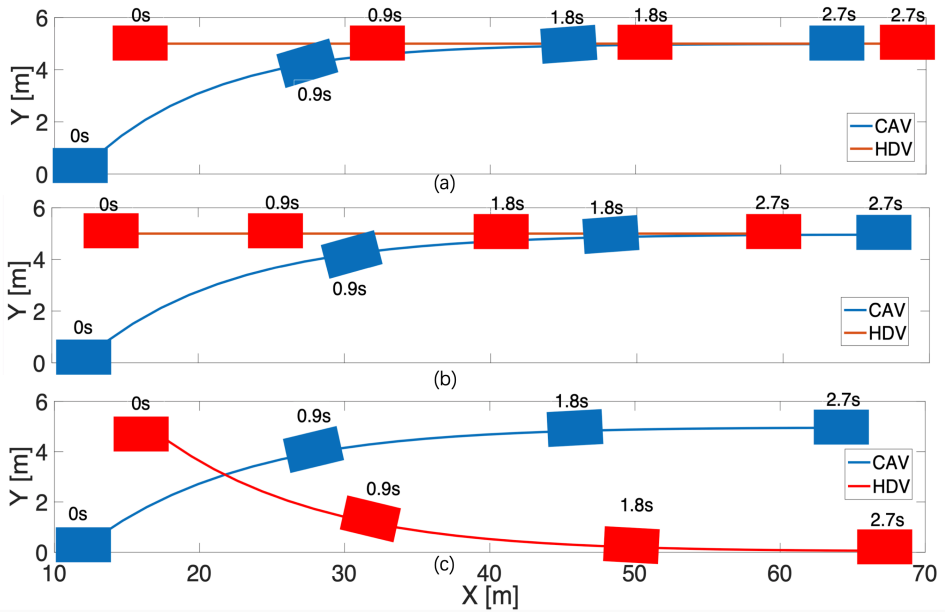

Figure 5.2: (a) is the trajectory of both vehicles in case study 1 scenario 1, (b) is the trajectory of both vehicles in case study 1 scenario 2, and (c) is the trajectory of both vehicles in case study 2.

to merge behind the HDV. It can be understood that the CAV is not sufficiently fast to overtake the HDV in a short time interval and therefore merges behind to accomplish the lane change and reach its desired state more quickly. Furthermore, collision avoidance is also guaranteed, which can be illustrated by the distance between the two vehicles in Fig. 5.3 (a).

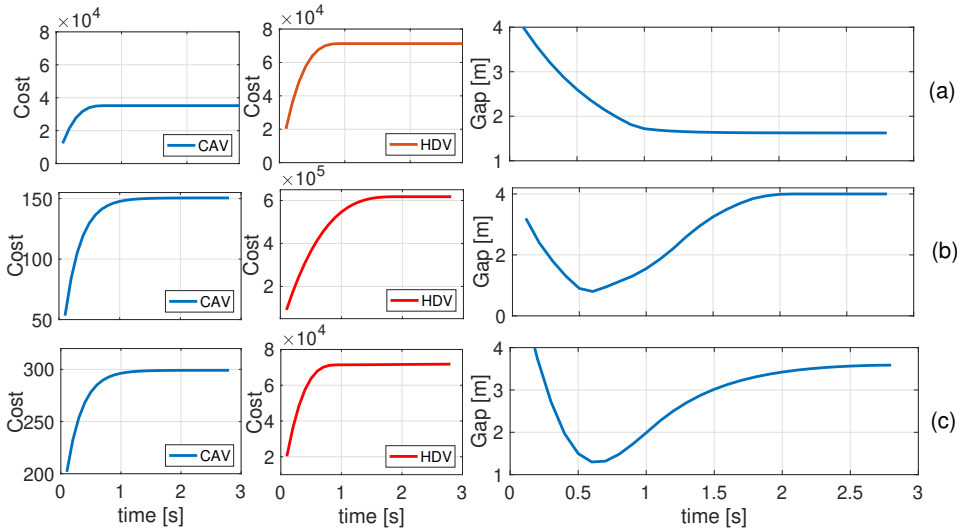

Figure 5.3: Results for the two case studies. (a) is the result of Case Study 1 scenario 1, (b) is the result of Case Study 1 scenario 2, and (c) is the result of the case study 2

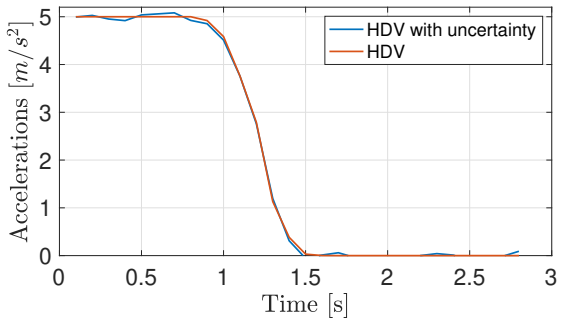

Figure 5.4: The Gaussian disturbance is added to the optimal strategy of HDV in case study 2 that is derived from equation (5.9). The blue line is the optimal strategy with the added disturbance, while the red line is original optimal strategy.

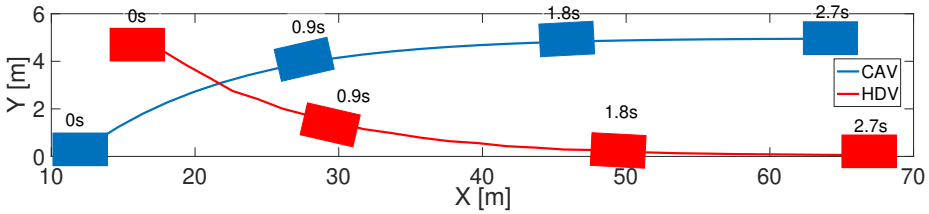

Figure 5.5: Robustness test of the proposed method under disturbances. The trajectory of both vehicles in case study 2 under the added disturbances.

In the second scenario, the CAV also performs a successful lane change, which can be validated in Fig. 5.2 (b), and Fig. 5.3 (b). The CAV performs an overtaking maneuver to complete the lane change, while collision avoidance is also guaranteed. The convergence of each vehicle's cost indicates that each vehicle reaches its desired velocity and target lane. In the case study in which both the CAV and the HDV need to change lanes, each vehicle successfully reaches its target lane, as can be seen in Fig. 5.2 (c). Both vehicles are steered to their destination lanes without collision and reach their desired speed, which is validated by Fig. 5.3 (c). All these simulation results show the validity of the lane-changing scheme.

The robustness test results are shown in Fig. 5.4 and Fig. 5.5. As can be seen in Fig. 5.5, both vehicles conducted a successful lane-changing without collision when a Gaussian disturbance with zero mean and a variance of 0.05 is added to the optimal control of HDV in case study 2 to emulate human uncertainty. This result shows that the proposed game-based lane-changing method is robust to a certain level of uncertainties. The theoretical analysis on the robustness remains further

investigation.

5.5 CONCLUSIONS

In this chapter, a game-based lane change framework is proposed for complex traffic environments mixed with HDVs and CAVs. A Stackelberg game method is used to model the interaction between HDVs and CAVs. An optimal strategy is designed, which is further shown to provide the asymptotically stable equilibrium point. The condition under which the optimal strategy can render the collision avoidance set invariant is provided. Numerical results show that the CAV can conduct a successful and safe lane change without colliding with the HDV.

This chapter mainly focuses on the fundamental analysis of the Stackelberg game-based lane-changing strategies. Therefore, a simplified mixed traffic scenario that only contains one CAV and one HDV is studied. However, the single CAV-HDV interaction is not sufficient in the real-world mixed traffic environments where there is a large number of vehicles. To further improve this work, the multi-vehicle lane-changing decision-making and control will be investigated in Chapter 6.

Chapter 6

A Game-Theoretical Framework for Safe Decision-Making and Control of Multi-CAV

6.1 Introduction

Following the results presented in Chapter 5 regarding a single pair of CAV and HDV, this chapter introduces a two-layer coalitional decision-making and control strategy for multi-vehicle lane-changing.

Although various game-theoretical approaches have been proposed to investigate interactive coordination of multiple CAVs and HDVs [158, 159, 182, 196], several limitations remain. In particular, most existing methods focus on small-scale scenarios with a limited number of vehicles, often neglecting the challenges of large-scale traffic environments. To deal with these limitations, a two-layer coalitional decision-making and control strategy for multi-vehicle lane-changing is proposed. As different vehicles have different driving intentions and conducting global optimal control is infeasible, a game-based coalition control is applied to group the vehicles in the upper layer. Then the interactions between HDVs and CAVs are modeled by the Stackelberg game, and data-enabled predictive control is applied to CAVs to enhance robustness against modeling uncertainty. The real-world applicability of the proposed method is validated by HIL experiments. The novelty of the

work in this chapter is as follows.

1. In the upper layer, a game-based coalition structure is proposed to group the vehicles involved in lane-changing based on their positions and initial conditions. Such a method can avoid exhaustive computation compared with the method that optimizes the trajectories of all vehicles involved in lane-changing as a whole while maintaining a comparably good performance.

2. In the lower layer, unlike many existing works [158, 182], the HDVs in this study are capable of changing lanes while the CAVs are changing lanes. The interaction of CAVs and HDVs is taken into account by a Stackelberg game in each coalition, which is more realistic.

3. To enhance robustness against modeling uncertainty, the data-enabled predictive control is applied to the CAVs. The dual collision avoidance constraint is also incorporated to ensure lane-changing safety. The effectiveness of the proposed method is validated by utilizing data representing different driving aggressiveness in a large number of experiments.

The remainder of this chapter is organized as follows. Section 6.2 introduces the overall framework for the multi-vehicle lane-changing scenario. In Section 6.3, the hierarchical game-based data-enabled control framework is proposed. In the upper layer, the vehicles are split into different coalitions based on game-theoretical strategy. In the lower layer, a Stackelberg game-based control scheme is introduced. Considering the uncertainty of human drivers, the data-enabled predictive control is applied to CAVs. The simulation results and discussion are shown in Section 6.4. Moreover, HIL experiments are also included. Finally, concluding remarks are given in Section 6.5.

6.2 Problem Formulation

As shown in Fig. 6.1, this chapter considers a scenario where there are fully controllable CAVs and uncontrollable HDVs traveling in the neighboring lane. As can be seen, there exist roadside units (RSU) and sensors (camera, loop detector, etc.)

along the road, which can gather HDVs' information such as positions, velocities, and lane-changing intentions and forward them to CAVs. The CAV in the second lane intends to make a lane change while the surrounding vehicles continue to drive in their original lanes or turn to their destination lanes. Then the central coordinator (CC) will plan the trajectory for this CAV to successfully change the lane.

It is infeasible and ineffective for the CC to consider all the vehicles on the road when planning the lane-changing for a CAV. Thus it needs to decide which cars are more likely to influence lane-changing and how many cars should be involved in order to ensure the safety and efficiency of lane change with the help of the roadside units (RSU). Moreover, the CC will decide this CAV whether to merge in front or behind a vehicle in the target lane depending on the states (position, velocity, lane-changing intention, etc.) of the involved vehicles, and how these vehicles interact with it.

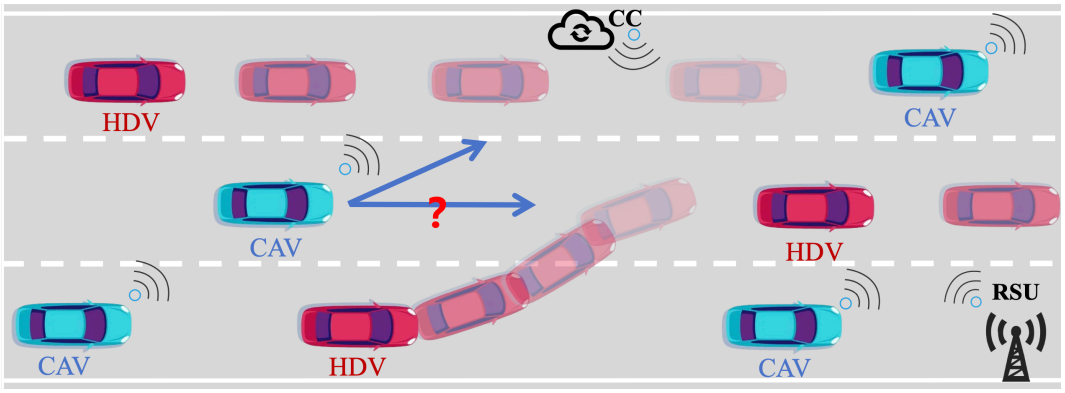

Figure 6.1: The complex lane-changing decision in mixed traffic scenarios involving HDVs and CAVs.

Assumption 6.1. *The lane-changing intention, position, and velocity of the HDVs involved in lane-changing can be collected by RSUs without error and delay.*

Assumption 6.1 is commonly used in existing works, such as [25, 114, 186]. Here, we assume HDVs are rational, which means HDVs will activate turn signals when intending to change lanes; otherwise, they remain in their current lane. Under this assumption, the turning intention, along with velocity and position, can be detected by RSUs.

6.3 Hierarchical Game-based Data-enabled Predictive Control Scheme

To address the multi-vehicle lane-changing problems depicted in Fig. 6.1, a two-layer hierarchical control architecture is proposed in this chapter. In reality, it is impractical to conduct the global optimal control for all vehicles on the road. Alternatively, it is reasonable to consider a group of vehicles that may influence and interact with each other during lane-changing. In this context, a coalition establishing method is proposed in the upper layer, which will be introduced in Section 6.3.1. In the lower layer, after the CC determines the coalition structure, it will provide each CAV with a trajectory to change lanes. As there may be HDVs within each coalition, the Stackelberg game will be utilized to model the interaction between CAVs and HDVs, which will be introduced in Section 6.3.2. Then the data-enabled predictive control is applied to CAVs which is introduced in Section 6.3.3. The overall control scheme is sketched in Fig. 6.2.

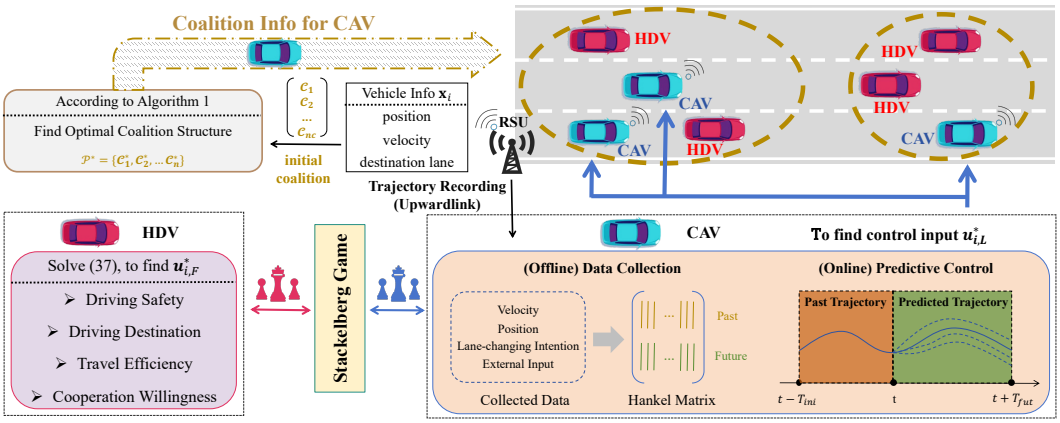

Figure 6.2: The scheme of the learning-and-game-based coalitional decision-making and control strategy for multi-vehicle lane-changing. In the upper layer, a coalition establishing optimization is proposed. In the lower layer, the interaction between HDVs and CAVs is modeled by the Stackelberg game, and CAV driving strategies are solved by data-enabled predictive control.

6.3.1 Coalition Establishing

In the multi-vehicle lane-changing problem, cooperation between each vehicle translates into better performance. However, this comes at the expense of higher

computation and communication requirements. The effort required for coordination increases with the number of vehicles involved in a coalition, which brings a heavy computation burden to the CC and CAVs. As such, our aim is to split all the vehicles into different coalitions, which can largely reduce the computation complexity and meanwhile maintain good control performance for lane-changing. In this section, we propose a game theoretical framework for the coalition establishing of a multi-vehicle system, where each coalition contains at least one CAV. The establishing of coalitions is conducted by the CC and CAVs involved in lane-changing together, and such a coalition structure is only formulated once.

Consider the ith coalition $\mathscr{C}_i$ with $|\mathscr{C}_i|$ individual vehicles, the dynamic of jth vehicle, $j \in \{1, \cdots, |\mathscr{C}_i|\}$ is given as

$$\dot{x}_j(t) = \begin{bmatrix} v_{j,x}(t) & v_{j,y}(t) & a_{j,x}(t) & a_{j,y}(t) \end{bmatrix}^\top \tag{6.1}$$

with

$$x_j(t) = \begin{bmatrix} p_{j,x}(t) & p_{j,y}(t) & v_{j,x}(t) & v_{j,y}(t) \end{bmatrix}^\top$$

where $p_{j,x}(t)$ and $p_{j,y}(t)$ represent the longitudinal and lateral position of each vehicle in the global coordinate, respectively, while $v_{j,x}(t)$ and $v_{j,y}(t)$ represent the longitudinal and lateral velocity of each vehicle. $u_j(t) = [a_{j,x}(t) a_{j,y}(t)]^\top$ where $a_{j,x}(t)$, $a_{j,y}(t)$ are the longitudinal and lateral acceleration. Thus, the overall dynamic of the ith coalition can be given as

$$\dot{\mathbf{x}}_i(t) = A_i^{coa}\mathbf{x}_i(t) + B_i^{coa}\mathbf{u}_i(t) \tag{6.2}$$

with $\mathbf{x}_i \in \mathbb{R}^{4|\mathscr{C}_i|}$, $\mathbf{u}_i \in \mathbb{R}^{4|\mathscr{C}_i|}$. $A_i^{coa} \in \mathbb{R}^{4|\mathscr{C}_i| \times 4|\mathscr{C}_i|}$, $B_i^{coa} \in \mathbb{R}^{4|\mathscr{C}_i| \times 2|\mathscr{C}_i|}$, which can be given as follows:

$$A_i^{coa} = \begin{bmatrix} H_1 & 0 & \dots & 0 \\ 0 & H_1 & \dots & 0 \\ \vdots & \ddots & \ddots & \vdots \\ 0 & \dots & \dots & H_1 \end{bmatrix}, B_i^{coa} = \begin{bmatrix} H_2 & 0 & \dots & 0 \\ 0 & H_2 & \dots & 0 \\ \vdots & \ddots & \ddots & \vdots \\ 0 & \dots & \dots & H_2 \end{bmatrix}, \tag{6.3}$$

with

$$H_1 = \begin{bmatrix} 0 & 0 & 1 & 0 \\ 0 & 0 & 0 & 1 \\ 0 & 0 & 0 & 0 \\ 0 & 0 & 0 & 0 \end{bmatrix}, H_2 = \begin{bmatrix} 0 & 0 & 1 & 0 \\ 0 & 0 & 0 & 1 \end{bmatrix}^\top. \tag{6.4}$$

Let us consider the vehicle j, $j \in \mathscr{C}_i$, conducting an optimal lane-changing policy aimed at minimizing its local cost $\ell_j(x_j, u_j)$, over a time interval T_F, where T_F denotes the time when the multi-vehicle lane-changing behavior is finished. Note that the local cost of each vehicle is implicitly a function of other vehicles' states, including positions, velocities, etc. In each coalition $\mathscr{C}_i$, the coalition stage cost is defined as $\Lambda_i(\mathbf{x}_i, \mathbf{u}_i)$. Based on the local objective of each vehicle, this coalitional objective allows for improvement by exploiting the shared vehicle information available at the coalition level and explicitly including the coupling variables in its formulation.

In the context of multi-vehicle lane changing, gathering information from each vehicle needs sufficient computation and communication resources. These costs are not negligible, and therefore constitute the cooperation costs for the coalitions. In the following, we will introduce a term that expresses the control performance and cooperation costs within a given vehicle coalition. The value of ith coalition $V(\mathscr{C}_i)$ is defined as follows:

$$V(\mathscr{C}_i) = \int_0^{T_F} \Lambda_i(\mathbf{x}_i(t), \mathbf{u}_i(t)) + \chi(|\mathscr{C}_i|)\, dt \tag{6.5}$$

where the cooperation cost $\chi(\cdot)$ depends on the number of vehicles in the coalition $\mathscr{C}_i$, and is monotonically increasing in the number of vehicles of the coalition. Define $\chi(|\mathscr{C}_i|)$ as:

$$\chi(|\mathscr{C}_i|) = w^{coal}|\mathscr{C}_i|^2 \tag{6.6}$$

with w^{coal} being the coefficient of the cooperation cost. The coalition stage cost of the ith coalition $\Lambda_i(\mathbf{x}_i(t), \mathbf{u}_i(t))$ can be expressed as the sum of the local cost of

vehicle $j \in \mathscr{C}_i$:

$$\Lambda_i(\mathbf{x}_i(t), \mathbf{u}_i(t)) = \sum_{j=1}^{|\mathscr{C}_i|} \ell_j(x_j(t), u_j(t)), j \in \mathscr{C}_i \tag{6.7}$$

To form an effective coalition for lane-changing control, the CC must consider various factors influencing vehicle's lane-changing behavior, including driving safety, comfort, target lane selection, and overall driving efficiency. Thus, the local cost ℓ_j of the jth vehicle in the coalition i consists of two parts, the cost of cooperation willingness ℓ_j^{wil} and the cost of individual driving comfort ℓ_j^{self}, which can be given as follows:

$$\ell_j(x_j, u_j) = \ell_j^{wil} + \ell_j^{self} \tag{6.8}$$

The cooperation willingness cost ℓ_j^{wil} represents a driver's intention to join a coalition, while the individual driving comfort cost ℓ_j^{self} shows that a driver wants to maintain a comfortable and successful lane-changing. To be specific, ℓ_j^{wil} takes into account the relative distance between vehicle j and each other vehicle $\eta, \eta \neq j, \eta \in \mathscr{C}_i, j \in \mathscr{C}_i$ in the coalition i. ℓ_j^{wil} can be expressed as:

$$\ell_j^{wil} = \sum_{\eta \neq j}^{\eta \in \mathscr{C}_i} \frac{w_j^{wil}((p_{j,y} - p_{\eta,y})^2 + (p_{j,x} - p_{\eta,x})^2)^2}{v_j} \tag{6.9}$$

where w_j^{wil} is the weight parameter for the cost of cooperation willingness, $(p_{j,x}, p_{j,y})$, $(p_{\eta,x}, p_{\eta,y})$ is the position of the vehicle j and vehicle η, respectively, v_j is the speed of vehicle j. When the vehicle is traveling at a higher speed, the relative distance between each vehicle can be larger. Thus, for a fair evaluation, we add the speed v_j to the denominator of the driving safety cost. Note that the cost ℓ_j^{wil} will increase with the number of vehicles in the coalition i. In addition, a larger relative distance between vehicles will increase ℓ_j^{wel}, which may reduce the possibility of forming a coalition. ℓ_j^{self} consists of three parts, which can be expressed as

$$\ell_j^{self} = \left\|u_j\right\|_{w_j^{com}}^2 + \left\|p_{j,y} - p_{j,d}\right\|_{w_j^{des}}^2 + \left\|v_j - v_d\right\|_{w_j^{eff}}^2 \tag{6.10}$$

where $w_j^{com}, w_j^{des}, w_j^{eff}$ is the weight parameter for the cost of driving comfort, des-

tination lane, and driving efficiency respectively. The term $\left\|u_j\right\|^2_{w_j^{com}}$ is to avoid excessive acceleration/deceleration behavior so that comfortable driving can be ensured. The term $\left\|p_{j,y}-p_{j,d}\right\|^2_{w_j^{des}}$ is to ensure that lane-changing maneuvers can be accomplished where $p_{j,d}$ is the lateral position of destination lane. The last term $\left\|v_j-v_d\right\|^2_{w_j^{eff}}$ is to consider the overall traffic efficiency where v_d is the desired velocity.

Given two vehicle subcoalitions $\mathscr{P}_1, \mathscr{P}_2, \mathscr{P}_1 \cup \mathscr{P}_2 = \mathscr{C}_i$, (6.5) is calculated separately for the two subcoalitions (unilateral strategies) and for their merger (coalition strategy for $\mathscr{C}_i$). In particular, for the coalition strategy relative to $\mathscr{P}_1 \cup \mathscr{P}_2$, $\Lambda_i(\cdot,\cdot)$ is calculated with the optimal lane-changing strategies $\mathbf{u}^*_{1\cup 2}$ and the associated $\mathbf{x}^*_{1\cup 2}$ obtained as a solution of (6.13). Note that the coalition value is an economic index, i.e., the surplus of the merger $V(\mathscr{P}_1)+V(\mathscr{P}_2)-V(\mathscr{P}_1\cup\mathscr{P}_2)$, can be reallocated between each vehicle [199]. A necessary condition for establishing a vehicle coalition requires that the benefit outperforms the total outcome of unilateral strategies, which can be expressed as:

$$V(\mathscr{P}_1 \cup \mathscr{P}_2) \leq V(\mathscr{P}_1) + V(\mathscr{P}_2) \tag{6.11}$$

In such a case, the establishment of the vehicle coalition expects a decrease in the control cost to (at least) compensate for the increased coordination effort. When a new coalition is formed, the value will be reallocated to each vehicle in this coalition, and it holds that $\sum_{j\in\mathscr{C}_i} rc_j^{(i)} = V(\mathscr{C}_i)$ where $rc_j^{(i)} \in \mathbb{R}$ is the cost reallocated to vehicle j in the coalition $\mathscr{C}_i$.

To complete the formulation, the constraints set consisting of the speed and acceleration limits has to be imposed.

$$0 < v_j \leq v_{\max}, \tag{6.12a}$$

$$a_{\min} \leq |u_j| \leq a_{\max}, \tag{6.12b}$$

where $a_{\max}, a_{\min}$ denote the maximum and the minimum acceleration respectively.

Now, we can formulate the OCP to find the optimal coalitional control for the

ith coalition:

$$\mathbf{u}_i^* = \arg\min_{\mathbf{u}_i} \int_0^{T_F} \Lambda_i\left(\mathbf{x}_i(t), \mathbf{u}_i(t)\right) dt \tag{6.13a}$$

$$\textbf{s.t. } (6.2), (6.12) \tag{6.13b}$$

The establishing of the coalition structure can be found in Algorithm 6.1. The initialization of $\{\mathscr{C}_1, \ldots, \mathscr{C}_{n_c}\}$ depends on the number of CAVs n_c. Each CAV will form a coalition, and an HDV will join the coalition held by the CAV nearest to it.

Algorithm 6.1 Overall Coalitional Control

Input: $\mathscr{P} = \{\mathscr{C}_1, \ldots, \mathscr{C}_{n_c}\}$
Output: coalition structure $\mathscr{P}^*$, allocation vector $rc^* \in \mathbb{R}^{|\mathscr{N}|}$
  if $n_c > 1$ **then**
    for all pairs $\mathscr{C}_i, \mathscr{C}_j \in \mathscr{P}$ where $i, j \in \{1, \ldots, n_c\}$ **do**
      Call Algorithm 6.2
    end for
  else
    Call Algorithm 6.3
  end if

Algorithm 6.2 Coalition Establishing

Input: $\mathscr{C}_i, \mathscr{C}_j \in \mathscr{P}$
Output: coalition structure $\mathscr{P}^+$, allocation vector $(rc_k)_{k \in \mathscr{C}_i \cup \mathscr{C}_j}$
  $V\left(\mathscr{C}_i \cup \mathscr{C}_j\right) \leftarrow$ minimize (6.13) over $\mathbf{u}_{i \cup j}$
  initialize $\mathbf{u}_i, \mathbf{u}_j$ with $\mathbf{u}_{i\cup j}^*$ respectively
  $V\left(\mathscr{C}_i\right) \leftarrow$ solve (6.13) over $\mathbf{u}_i$ w.r.t. $\mathbf{u}_j = \mathbf{u}_{i\cup j}^*|_j$
  $V\left(\mathscr{C}_j\right) \leftarrow$ solve (6.13) over $\mathbf{u}_j$ w.r.t. $\mathbf{u}_i = \mathbf{u}_{i\cup j}^*|_i$
  if (6.11)is verified **then**
    $\mathscr{P}^+ \leftarrow \mathscr{P} \backslash \left\{\mathscr{C}_i, \mathscr{C}_j\right\} \cup \left\{\mathscr{C}_i \cup \mathscr{C}_j\right\}$; Form Coalition
    $rc_k := V\left(\mathscr{C}_i \cup \mathscr{C}_j\right) / \left|\mathscr{C}_i \cup \mathscr{C}_j\right|$ for all $k \in \mathscr{C}_i \cup \mathscr{C}_j$
    $(rc_k)_{k \in \mathscr{C}_i \cup \mathscr{C}_j} \leftarrow$ Call Algorithm 6.3
  else
    Call Algorithm 6.3 for $\mathscr{C}_i$ and $\mathscr{C}_j$
  end if

Remark 6.1. *When there is a large number of vehicles, it is impractical to exhaustively evaluate all coalition pairs in* $\{\mathscr{C}_1, \ldots, \mathscr{C}_{n_c}\}$. *The outcome of the coalition structure might be influenced by the selection order of coalition splitting [199].*

Algorithm 6.3 Coalition Splitting

Input: $\mathscr{C}$, allocation vector $(rc_k)_{k\in\mathscr{C}}$, maxloop
Output: $\{\mathscr{C}'_1,\ldots,\mathscr{C}'_{n_m}\}$ where $\bigcup_i \mathscr{C}'_i = \mathscr{C}$, $\left(rc'_k\right)_{k\in\bigcup_i}\mathscr{C}'_i$

$n_m \leftarrow 0$; nloops $\leftarrow 0$; flag $\leftarrow$ FALSE
if $\mathscr{C}$ contains only one CAV **then**
break
end if
Repeat
randomly choose $\mathscr{S}_1 \subset \mathscr{C}$ and $\mathscr{S}_2 = \mathscr{C}\backslash\mathscr{S}_1$, where both $\mathscr{S}_1$ and $\mathscr{S}_2$ contain at least one CAV
$\pi_1 \leftarrow \sum_{k\in\mathscr{S}_1} rc_k$, $\pi_2 \leftarrow \sum_{k\in\mathscr{S}_2} rc_k$
$V(\mathscr{S}_1\cup\mathscr{S}_2) \leftarrow$ minimize (6.13) over $\mathbf{u}_{i\cup j}$
initialize $\mathbf{u}_1, \mathbf{u}_2$ with $\mathbf{u}^*_{1\cup 2}$ respectively
$V(\mathscr{S}_1) \leftarrow$ solve (6.13) over $\mathbf{u}_1$ w.r.t. $\mathbf{u}_2 = \mathbf{u}^*_{1\cup 2}|_2$
$V(\mathscr{S}_2) \leftarrow$ solve (6.13) over $\mathbf{u}_2$ w.r.t. $\mathbf{u}_1 = \mathbf{u}^*_{1\cup 2}|_1$
if $\pi_1+\pi_2 > V(\mathscr{S}_1)+V(\mathscr{S}_2)$ **then**
flag $\leftarrow$ TRUE; $\mathscr{P}$ splits into $\mathscr{S}_1$ and $\mathscr{S}_2$
for $i = 1,2$ **do**
$n_m \leftarrow n_m+1$; $\mathscr{C}_{n_m} \leftarrow \mathscr{S}_i$
Initialize payoff of every agent in $\mathscr{C}_{n_m}$
with egalitarian allocation
Call Algorithm 6.3 for $\mathscr{C}_{n_m}$
end for
else
if $\pi_1 > V(\mathscr{S}_1)$ **or** $\pi_2 > V(\mathscr{S}_2)$ **then**
$e \leftarrow \pi_1 - V(\mathscr{S}_1)$
$rc'_k \leftarrow rc_k - e/|\mathscr{S}_1|, k\in\mathscr{S}_1$
$rc'_k \leftarrow rc_k + e/|\mathscr{S}_2|, k\in\mathscr{S}_2$
end if
end if
nloops $\leftarrow$ nloops $+1$
Until flag=FALSE **and** nloops $<$ maxloop

Remark 6.2. *The coalition scheme is designed to group vehicles with potential conflicts while separating those that are more distant or have non-conflict intentions (see the cooperation willingness cost ℓ_j^{wil} in* (6.9)*). As a result, vehicles in different coalitions tend to be spatially separated, reducing the overall risk of collision. However, the collision avoidance can not be guaranteed by this coalition scheme.*

If condition (6.11) is satisfied for $\mathscr{C}_i$ and $\mathscr{C}_j$, then the coalition $\mathscr{C}_i \cup \mathscr{C}_j$ is established. The allocation of all vehicles in the new coalition is initialized by an equal share of the total cost. However, such allocation may violate the individual interests of some vehicles, thus Algorithm 6.3 is conducted. Algorithm 6.3 is performed also in the case where two coalitions fail to merge. Let $\mathscr{C}_i$ be the coalition under analysis and $\mathscr{S}_1, \mathscr{S}_2 \subset \mathscr{C}_i$. $\mathscr{S}_1$ and $\mathscr{S}_2$ can also leave the coalition if condition (6.11) is not satisfied. Therefore, while any coalition is established through a bilateral agreement, a vehicle can leave it unilaterally.

6.3.2 Stackelberg Game-based Lane-changing Strategy

After the coalition structure is determined, the CC plans the trajectory of each CAV in the coalition to change lanes. We will focus on a single coalition $\mathscr{C}_i$ as the lane change strategy is applicable to all coalitions. For the sake of further analysis, let us denote the set $\mathscr{C}_{c,i}$ consisting of all CAVs within the coalition $\mathscr{C}_i$, while the set $\mathscr{C}_{h,i}$ collects all HDVs within the coalition, such that $\mathscr{C}_{c,i} \cup \mathscr{C}_{h,i} = \mathscr{C}_i$. For the sake of brevity, the dependence on i of all variables will be dropped in the remainder of this section.

To account for the potential lane-changing maneuver, we use a bicycle model to describe the dynamics of vehicle j in the coalition $\mathscr{C}_i$, with the details given in (3.3). The vehicle state is given by $x_j(t) = \begin{bmatrix} p_{j,x}(t) & p_{j,y}(t) & \theta_j(t) & v_j(t) \end{bmatrix}^\top$, where L_b is the length of the wheelbase. $\theta_j(t)$ is the vehicle heading angle and $v_j(t)$ is the forward velocity. $\varphi_j(t)$ and $a_j(t)$ are the steering angle of the front wheels of the vehicle and the acceleration of the vehicle, which represent the manipulated variables of each vehicle. Denote $\mathbf{x} = [x_1^\top, \ldots, x_{|\mathscr{C}_i|}^\top]^\top \in \mathbb{R}^{4|\mathscr{C}_i|}$ and $\mathbf{u} = [u_1^\top, \ldots, u_{|\mathscr{C}_i|}^\top]^\top \in \mathbb{R}^{2|\mathscr{C}_i|}$ with $u_j = [\varphi_j \; a_j]^\top$, $j \in \{1, \ldots, |\mathscr{C}_i|\}$ the state and control input of coalition $\mathscr{C}_i$ re-

spectively.

To model the interaction between HDVs and CAVs that appears in the lane-changing scenario, the Stackelberg game model will be utilized [35], where all CAVs in $\mathscr{C}_{c,i}$ are considered as one leader and all HDVs in $\mathscr{C}_{h,i}$ are considered as one follower. In this context, HDVs can observe the CAVs' actions and accordingly choose their actions, while CAVs can optimize their actions based on the anticipated actions of HDVs. $\mathbf{x}_0$ denotes the initial state of all vehicles in the coalition $\mathscr{C}_i$. $\mathbf{u}^\top$ is rewritten as $\mathbf{u}^\top = [\mathbf{u}_L^\top, \mathbf{u}_F^\top]^\top$, where $\mathbf{u}_F \in \mathbb{R}^{2|\mathscr{C}_{h,i}|}$ and $\mathbf{u}_L \in \mathbb{R}^{2|\mathscr{C}_{c,i}|}$ denotes all the HDVs' control input and all the CAVs' control input respectively. $\mathbf{u}_L^*$ and $\mathbf{u}_F^*$ are the optimal actions. $((\mathscr{U}_L, \mathscr{U}_F), (J_L, J_F))$ denotes the single-leader single-follower game with $2|\mathscr{C}_{c,i}|$ CAVs (leader) and $2|\mathscr{C}_{h,i}|$ HDVs (follower). J_L and J_F represent the cost functions of the leader and follower, respectively. As can be seen in chapter 3, the Stackelberg game yields the optimal strategies of CAVs subject to the optimal response of the HDVs. The HDVs involved in the proposed game-based framework do not need to follow a specific car-following model. Instead, the optimized response of HDVs is more realistic and, as a result, could yield more reliable control strategies for the CAVs.

To introduce the game-based control strategy, the joint dynamics of all the vehicles in the coalition $\mathscr{C}_i$ based on (3.3) can be recast in the following form:

$$\dot{\mathbf{x}}(t) = f(\mathbf{x}(t), \mathbf{u}(t)) \tag{6.14}$$

where $f(\mathbf{x}(t), \mathbf{u}(t)) = \operatorname{col}\left(f_1, \ldots, f_{|\mathscr{C}_i|}\right) \in \mathbb{R}^{4|\mathscr{C}_i|}$ with

$$f_j = \begin{bmatrix} v_j \cos\theta_j & v_j \sin\theta_j & \frac{v_j \tan\varphi_j}{L_b} & a_j \end{bmatrix}^\top, j \in \mathscr{C}_i. \tag{6.15}$$

For the sake of further discussion, a linearized and discrete equation (6.14) is presented. The transformed linear system is expressed as:

$$\mathbf{x}(k+1) = A_\mathrm{d}\mathbf{x}(k) + B_\mathrm{d}\mathbf{u}(k), \tag{6.16}$$

where $A_{\mathrm{d}} = e^{A\Delta t} \in \mathbb{R}^{4|\mathscr{C}_i|\times 4|\mathscr{C}_i|}, B_{\mathrm{d}} = \int_0^{\Delta t} e^{At} B dt \in \mathbb{R}^{4|\mathscr{C}_i|\times 2|\mathscr{C}_i|}$. $\mathbf{x}_i(k) \in \mathbb{R}^{4|\mathscr{C}_i|}, \mathbf{u}_i(k) \in \mathbb{R}^{2|\mathscr{C}_i|}$ denote the state and control input, respectively. A and B are given by

$$A = \left.\frac{\partial f}{\partial \mathbf{x}_i}\right|_{\mathbf{x}(t),\mathbf{u}(t)}, \quad B = \left.\frac{\partial f}{\partial \mathbf{u}}\right|_{\mathbf{x}(t),\mathbf{u}(t)} \tag{6.17}$$

To tackle collision avoidance, each vehicle will be regarded as a convex hull shown in Fig. 6.3, which can be expressed as:

$$\mathbb{O}_j(k) = \left\{ p(k) \in \mathbb{R}^2 : C_j(k) p(k) \leq b_j(k) \right\} \ j \in \mathscr{C}_i \tag{6.18}$$

Given the lateral and longitudinal positions of j-th vehicle $(p_{j,x}, p_{j,y})$, and the driving angle θ_j, the matrices b_j, C_j can be expressed as follows:

$$b_j = \begin{bmatrix} p_{j,x}\cos\theta_j + p_{j,y}\sin\theta_j + L/2 \\ -p_{j,x}\cos\theta_j - p_{j,y}\sin\theta_j + L/2 \\ -p_{j,x}\sin\theta_j + p_{j,y}\cos\theta_j + L_w/2 \\ p_{j,x}\sin\theta_j - p_{j,y}\cos\theta_j + L_w/2 \end{bmatrix} \tag{6.19}$$

$$C_j = \begin{bmatrix} \cos\theta_j & -\cos\theta_j & -\sin\theta_j & \sin\theta_j \\ \sin\theta_j & -\sin\theta_j & \cos\theta_j & -\cos\theta_j \end{bmatrix}^\top \tag{6.20}$$

where L is the vehicle length, and L_w is the vehicle width.

Similarly, the road boundary set $\mathscr{B}$ containing two elements, the right boundary and the left boundary, with each one regarded as the convex hull, which can be given as:

$$\mathbb{B}_k(k) = \left\{ p(k) \in \mathbb{R}^2 : C_k(k) p(k) \leq b_k(k) \right\}, k \in \{r, l\} \tag{6.21}$$

with

$$C_k(k) = \begin{bmatrix} 0 & 0 & 0 & 0 \\ 1 & 0 & 0 & 0 \end{bmatrix}^\top, b_k(k) = \begin{bmatrix} B_k & 0 & 0 & 0 \end{bmatrix}^\top. \tag{6.22}$$

The collision avoidance constraint can be written as

$$\mathrm{dist}\left(\mathbb{O}_j(t), \mathbb{O}_\eta(t)\right) \geq \delta_\eta, \ \ j, \eta \in \mathscr{C}_i \tag{6.23}$$

with

$$\operatorname{dist}\left(\mathbb{O}_j(t),\mathbb{O}_\eta(t)\right)=\min_r\left\{\|r\|:\left(\mathbb{O}_j(t)\bigoplus r\right)\cap\mathbb{O}_\eta(t)\neq\varnothing\right\} \tag{6.24}$$

denoting the distance between two vehicles (similarly for the distance between road boundary and vehicles).

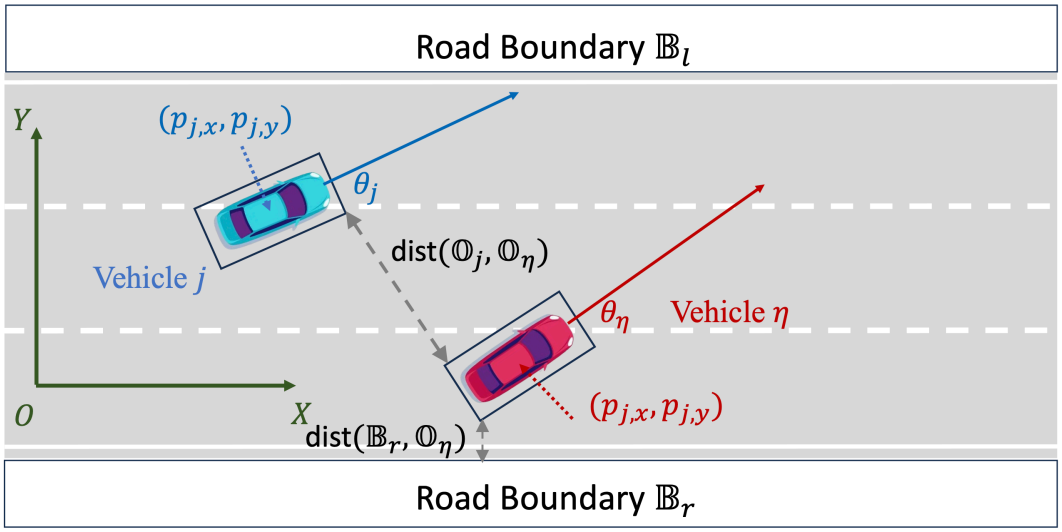

Figure 6.3: Convex hull of vehicles and road boundaries

According to [197], the collision avoidance can be guaranteed if the following condition holds for all $j\in\mathscr{C}_i$, $\eta\neq j,\eta\in\mathscr{C}_i\cup\mathscr{B}$

$$-b_\eta^\top(k)\nu_\eta(k)-b_j^\top\lambda_j(k)\geq\delta_\eta, \tag{6.25a}$$

$$C_\eta^\top(k)\nu_\eta(k)+C_j^\top(k)\lambda_j(k)=0, \tag{6.25b}$$

$$\lambda_j(k)\succeq 0,\nu_\eta(k)\succeq 0, \tag{6.25c}$$

$$\left\|C_j^\top(k)\lambda_j(k)\right\|\leq 1. \tag{6.25d}$$

Note δ_η is not a constant, instead it is a slack variable with

$$\delta_\eta\geq 0 \tag{6.26}$$

Instead of imposing a hard constraint, δ_η is introduced such that vehicles have more control freedom.

The cost function of the HDV j in the coalition $\mathscr{C}_i$ where $j \in \mathscr{C}_{h,i}$ should also include driving safety, driving comfort, driving destination, and traffic efficiency. Therefore, the cost $J_{F,j}(x_j, u_j)$ can be given as

$$J_{F,j}(x_j,u_j) = J_j^{saf} + \left\|u_j\right\|^2_{Q_j^{com}} + \left\|p_{j,y} - p_{j,d}\right\|^2_{Q_j^{des}} + \left\|v_j - v_d\right\|^2_{Q_j^{eff}} \tag{6.27}$$

where $Q_j^{com}, Q_j^{des}, Q_j^{eff}$ is the weight parameter for the driving comfort, destination lane, and driving efficiency respectively. The term $\left\|u_j\right\|^2_{Q_j^{com}}$ is to realize comfortable driving, $\left\|p_{j,y} - p_{j,d}\right\|^2_{Q_j^{des}}$ aims to achieve successful lane-changing behavior, and $\left\|v_j - v_d\right\|^2_{Q_j^{eff}}$ is to improve traffic efficiency. J_j^{saf} is a driving safety cost for the HDV j, it is defined as

$$J_j^{saf} = Q_j^{saf} \sum_{\eta \neq j}^{\eta \in \mathscr{C}_i \cup \mathscr{B}} \frac{1}{\delta_\eta^2 + \xi} \tag{6.28}$$

where Q_j^{saf} is the weight parameter for the driving safety, ξ is a small positive constant, and δ_η is a slack variable in (6.25).

Thus the overall cost function for the follower J_L in $\mathscr{C}_i$ will be expressed as

$$J_F(\mathbf{x}_i(k), \mathbf{u}_F(k)) = \sum_{j \in \mathscr{C}_{h,i}} J_{F,j}(x_j(k), u_j(k)) \tag{6.29}$$

In order to ensure safety during the lane-changing, vehicle j, $j \in \mathscr{C}_i$ needs to drive within its speed and acceleration limit, which can be expressed as

$$0 < v_j(k) \leq v_{\max}, \tag{6.30a}$$

$$[a_{\min}, \varphi_{\min}]^\top \leq \mathbf{u}(k) \leq [a_{\max}, \varphi_{\max}]^\top, \tag{6.30b}$$

where $\varphi_{\max}$ is the minimum and maximum steering angle of the front wheel, re-

spectively. Thus the following optimization problem can be obtained:

$$\mathbf{u}_F^* = \arg\min_{\mathbf{u}_{i,F}} \sum_{t=0}^{T_{fut}-1} J_F\left(\mathbf{x}(t \mid k), \mathbf{u}_F(t \mid k)\right) \tag{6.31a}$$

$$\textbf{s.t.}\ (6.16), (6.25), (6.26), (6.30) \tag{6.31b}$$

This optimization problem (6.31) will be solved for HDVs (follower) in the coalition i to find the optimal strategy. T_{fut} is the control horizon. The CAVs (leader) will then utilize this information to decide their optimal strategies based on data-enabled predictive control.

6.3.3 Data-Enabled Predictive Control

Data-enabled predictive control can bypass the need for model identification, ensuring safe and robust driving in unknown systems [44, 176, 179]. This approach is applied to CAVs, helping the CC manage the heterogeneity present in different CAVs, which are typically not accessible to the CC. In contrast, the movement of HDVs is predicted using a model-based approach through the Stackelberg game. Although numerous open datasets exist, accurately capturing the specific human driver behavior encountered by a CAV remains challenging. Therefore, instead of relying on data-driven control based on a predefined dataset, a general HDV model is utilized. However, the uncertainty introduced by HDVs (deviation from the game model) can be mitigated by incorporating a robustified design of the data-driven controller that will be elaborated later.

According to [44], a valid length-$L, (L \in \mathbb{N})$ trajectories of the linear system (6.16) can be constructed using a length-T $(T \in \mathbb{N})$ sequence, which consists of the CAV input sequence $\mathbf{u}_L^{\mathrm{d}} = \mathrm{col}\left(\mathbf{u}_L^{\mathrm{d}}(1), \ldots, \mathbf{u}_L^{\mathrm{d}}(T)\right) \in \mathbb{R}^{2|\mathscr{C}_{c,i}|T}$ and the corresponding state sequence $\mathbf{x}^{\mathrm{d}} = \mathrm{col}\left(\mathbf{x}^{\mathrm{d}}(1), \ldots, \mathbf{x}^{\mathrm{d}}(T)\right) \in \mathbb{R}^{4|\mathscr{C}_i|T}$. $T > N$. The Hankel matrix plays a key role in data-enabled predictive control, therefore defined below.

Definition 6.1. *The signal* $\omega = \mathrm{col}(\omega(1), \omega(2), \ldots, \omega(T))$ *of length* $T, (T \in \mathbb{N})$ *is*

exciting of order $l, (l \leq T, l \in \mathbb{N})$ *if the following Hankel matrix*

$$\mathscr{H}_l(\omega) := \begin{bmatrix} \omega(1) & \omega(2) & \cdots & \omega(T-l+1) \\ \omega(2) & \omega(3) & \cdots & \omega(T-l+2) \\ \vdots & \vdots & \ddots & \vdots \\ \omega(l) & \omega(l+1) & \cdots & \omega(T) \end{bmatrix} \tag{6.32}$$

is of full rank.

Denote $T_{ini} \in \mathbb{N}, T_{fut} \in \mathbb{N}$ as the time length of past and future data, respectively. Note that the length of future data T_{fut} is equal to the control horizon of HDVs (follower) in the Stackelberg game. The data Hankel matrices formulated from the collected data $(\mathbf{u}_L^{\mathrm{d}}, \mathbf{x}^{\mathrm{d}})$ are partitioned into two parts, which is corresponding to past data and future data respectively:

$$\begin{bmatrix} U_{\mathrm{p}} \\ U_{\mathrm{f}} \end{bmatrix} := \mathscr{H}_{T_{ini}+T_{fut}}\left(\mathbf{u}_L^{\mathrm{d}}\right), \begin{bmatrix} X_{\mathrm{p}} \\ X_{\mathrm{f}} \end{bmatrix} := \mathscr{H}_{T_{ini}+T_{fut}}\left(\mathbf{x}^{\mathrm{d}}\right), \tag{6.33}$$

where U_p contains the first T_{ini} block rows of $\mathscr{H}_{T_{ini}+T_{fut}}\left(\mathbf{u}_L^{\mathrm{d}}\right)$ and U_f contains the last T_{fut} block rows of $\mathscr{H}_{T_{ini}+T_{fut}}\left(\mathbf{u}_{i,L}^{\mathrm{d}}\right)$. Similarly, X_{p} and X_{f} consist of the first T_{ini} block rows and the last T_{fut} block rows of $\mathscr{H}_{T_{ini}+T_{fut}}\left(\mathbf{x}^{\mathrm{d}}\right)$ respectively. Each column represents a length-$T_{ini}+T_{fut}$ trajectory, with length-T_{ini} past trajectory and length-T_{fut} future trajectory.

At each time step k, denote $\mathbf{u}_{ini} = \mathrm{col}(\mathbf{u}_L(k-T_{ini}), \mathbf{u}_L(k-T_{ini}+1), \ldots, \mathbf{u}_L(k-1))$, $\mathbf{u}_f = \mathrm{col}(\mathbf{u}_L(k), \mathbf{u}_L(k+1), \ldots, \mathbf{u}_L(k+T_{fut}-1))$ as the past control sequence with length T_{ini}, and the future control sequence with length T_{fut} (similarly for $\mathbf{x}_{ini}$, $\mathbf{x}_f$).

Note that in our proposed framework, the future state of HDVs is inferred by the Stackelberg game. This future state of HDVs, i.e. positions, accelerations, and speeds will be used as future trajectories and control sequences in the data-enabled predictive control of CAVs.

According to [200], $\mathrm{col}(\mathbf{u}_{ini}, \mathbf{u}_f, \mathbf{x}_{ini}, \mathbf{x}_f)$ is a length-$T_{ini}+T_{fut}$ trajectory of sys-

tem (6.16) if and only if there exists $h \in \mathbb{R}^{T-T_{ini}-T_{fut}+1}$ such that

$$h^\top \begin{bmatrix} U_\mathrm{p}^\top & X_\mathrm{p}^\top & U_\mathrm{f}^\top & X_\mathrm{f}^\top \end{bmatrix}^\top = \begin{bmatrix} \mathbf{u}_{ini}^\top & \mathbf{x}_{ini}^\top & \mathbf{u}_f^\top & \mathbf{x}_f^\top \end{bmatrix}^\top \tag{6.34}$$

Equation (6.34) indicates that we can predict the future state sequence $\mathbf{x}_f$ under a future control input sequence $\mathbf{u}_f$ directly from the collected data $(\mathbf{u}_L^\mathrm{d}, \mathbf{x}^\mathrm{d})$, given the past trajectory $(\mathbf{u}_{ini}, \mathbf{x}_{ini})$. From (6.34), future state trajectory can be predicted without an explicit parametric model.

We consider the performance of all vehicles in the coalition i for controller design. In particular, we use a quadratic cost function $J_L^c(\mathbf{x}, \mathbf{u}_L)$ to quantify the overall performance by penalizing both the deviation from the desired state of all the vehicles after the lane change maneuvers and control effort of the CAV $\mathbf{u}_L$, defined as:

$$J_L^c(\mathbf{x}, \mathbf{u}_L) = \sum_{k=t}^{t+T_{fut}-1} \|\mathbf{x}(k) - \mathbf{x}_d\|_Q^2 + \|\mathbf{u}_L(k)\|_R^2 \tag{6.35}$$

where $Q = \mathrm{diag}\{q_j\}, j = 1, 2, \ldots, 4|\mathscr{C}_i|$ and $R = \mathrm{diag}\{r_l\}$, $l = 1, 2, \ldots, 2|\mathscr{C}_{c,i}|$ with $q_j \geq 0$, $r_l \geq 0$ are design weights of the rewards. Note that if a vehicle is HDV, its corresponding entries in the control weight matrix R are 0. $\mathbf{x}_d \in \mathbb{R}^{4|\mathscr{C}_i|}$ is the desired state of all vehicles in the coalition i after the lane change maneuvers are finished. It includes the target lateral positions, desired velocity, and the desired heading angle. The safety cost J_L^{saf} is designed similar with (6.28), which can be written as

$$J_L^{saf} = \sum_{j}^{j \in \mathscr{C}_{c,i}} J_j^{saf} \tag{6.36}$$

Next, several constraints will be introduced for this data-enabled predictive control. Firstly, for safety purposes, the velocity and the control input of each vehicle in the coalition i are constrained by:

$$0 < v_j(k) \leq v_\mathrm{max}, \tag{6.37a}$$

$$[a_\mathrm{min}, \varphi_\mathrm{min}]^\top \leq \mathbf{u}_L(k) \leq [a_\mathrm{max}, \varphi_\mathrm{max}]^\top, \tag{6.37b}$$

where $k \in \{1,\dots,T_{fut}\}$, $v_j, j \in \mathscr{C}_{c,i}$ is the velocity of each vehicle in the coalition i.

Note that given the cost function (6.8), the vehicles within each coalition are relatively close to each other. Thus, the information of the HDVs such as positions, velocities can be acquired by the CAV ζ via the roadside units without error and delay. The coalition scheme is designed to group vehicles with potential conflicts while separating those that are more distant or have non-conflict intentions (see the cooperation willingness cost ℓ_j^{wil} in (6.9)). As a result, vehicles in different coalitions tend to be spatially separated, reducing the overall risk of collision. Thus, collision avoidance of vehicles in different coalitions is not considered. To further enhance safety awareness, the weight parameter w_j^{wil} of ℓ_j^{wil} (see (6.9) and (6.10)) can be adjusted to place greater emphasis on cooperation willingness.

In practice, linearization of the system can make (6.34) inconsistent. Thus, we introduce a slack variable $\sigma \in \mathbb{R}^{6|\mathscr{C}_i|(T_{ini}+T_{fut})}$ for the state of the system, which guarantees the feasibility of the equality constraint (6.34), and then leads to the following optimization problem:

$$\begin{aligned} \min_{h,\mathbf{u}_L,\mathbf{x},\sigma} \quad & J_L^c(\mathbf{x},\mathbf{u}_L) + \lambda_h \|h\|_2^2 + \lambda \, \|\sigma\|_2^2 + J_L^{saf} \\ \textbf{s.t. } & h^\top \begin{bmatrix} U_\mathrm{p}^\top & X_\mathrm{p}^\top & U_\mathrm{f}^\top & X_\mathrm{f}^\top \end{bmatrix}^\top \\ & = \begin{bmatrix} \mathbf{u}_{ini}^\top & \mathbf{x}_{ini}^\top & \mathbf{u}_f^\top & \mathbf{x}_f^\top \end{bmatrix}^\top + \sigma^\top, \text{ (6.25), and (6.37).} \end{aligned} \tag{6.38}$$

Note (6.38) is a centralized optimization and is conducted by the CC. In (6.38), the slack variable σ is penalized with a weighted quadratic penalty function and the weight coefficient λ is chosen sufficiently large to ensure the feasibility of the equality constraint. Moreover, the norm penalty on h is also included to avoid overfitting and reduce the complexity of the data-centric representation. The constraints (6.25), (6.37) ensure the safety for the control of CAVs.

6.4 Simulation Validation

6.4.1 Simulation setup

In this section, the performance of the proposed control framework is evaluated considering a group of CAVs and HDVs, which travel in three separate lanes, as

shown in Fig. 6.4. Two case studies are conducted. In Case 1, there are 3 CAVs and 3 HDVs. In Case 2, there are only 2 CAVs and 3 HDVs. In each case, the initial lateral position of the vehicle in the first lane is 10 m, and the initial lateral position of the vehicle in the second lane is 5 m, which also represents the center of the destination lane of the CAV. Similarly, the initial lateral position of the vehicle in the third lane is 0 m. In each case, it is reasonable to set the desired velocities of each vehicle at the maximum allowed speed, $v_{\max}$ (for a reduced travel time). The dynamics of all HDVs follow the commonly used bicycle model. For vehicles intending to change lanes, the desired lateral positions are the center of the target lanes; otherwise, the desired lateral positions are the center of the original lanes. With the target lateral positions, velocity, and steering angle, the desired state $\mathbf{x}_{i,d}$ can be specified for the problem.

Case 1 involves two scenarios with the same number and initial positions of the vehicles but different velocities and lane-changing intentions. Each scenario contains two experiments, in which two sets of typical experimental data representing different driving aggressiveness are selected. The changes in acceleration decide the aggressiveness. In the first experiment, all HDVs are conservative, while in the second experiment, all HDVs are aggressive. In Case 1, the initial longitudinal position of CAV 1, HDV 2, CAV 3, HDV 4, HDV 5, and CAV 6 is 45m, 32m, 20m, 12m, 0m, 13m respectively. In the first scenario of Case 1 (Case 1.1), the initial speeds of CAV 1 and HDV 2 are set to 14 m/s, while the initial speeds of CAV 3, HDV 4, and HDV 5 are set to 13 m/s. The initial speed of CAV 6 is 12 m/s. In the second scenario of Case 1 (Case 1.2), the initial speed of CAV 1 is 13 m/s, while the initial speed of HDV 2, CAV 3, HDV 4, HDV 5, and CAV 6 is 14 m/s. The initial lateral positions and lane-changing intentions of each vehicle in Case 1 can be found in Fig. 6.4.

Similar to Case 1, two experiments based on two different data sets are conducted in Case 2. There are five vehicles, consisting of 2 CAVs and 3 HDVs. The initial longitudinal position of CAV 1, HDV 2, CAV 3, HDV 4, and HDV 5 is 43m, 28m, 13m, 0m, 13m respectively. The initial speed of CAV 1, HDV 2, and CAV 3 is

14m/s, while the initial speed of HDV 4 and HDV 5 is 13m/s. Similarly, the initial lateral positions and lane-changing intentions of each vehicle in Case 2 are shown in Fig. 6.4. The remaining vehicle parameters are summarized in Table 6.1.

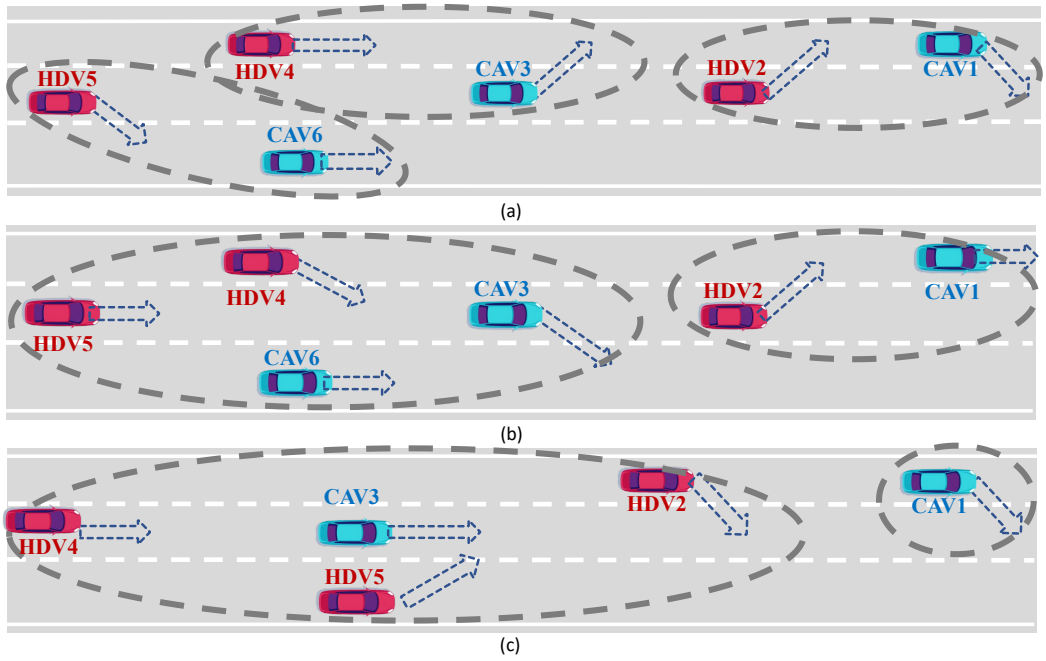

Figure 6.4: Lane-changing intentions of each vehicle and the final coalition structure in two case studies. (a) Case 1.1, (b) Case 1.2, and (c) Case 2

The parameter setup for data-enabled predictive control is as follows. Offline data collection: the length for the pre-collected trajectory is chosen as $T = 800$ with a sampling interval $\Delta t = 0.1s$. The data has been widely used in existing articles, modeling the vehicle lane-changing behaviors under the bicycle model. When the average acceleration of a vehicle is larger than 3m/s^2 it will be considered aggressive, and when the average acceleration of a vehicle is smaller than 1m/s^2 it will be considered conservative. Real-time predictive control: the time horizons for the future control sequence and past sequence are set to $T_{fut} = 5$, $T_{ini} = 20$ respectively. In (6.38), the parameters are set to $\lambda_i = 10000$ and $\lambda_h = 10$. In the cost function (6.35), the weight coefficient matrix Q_i and R_i are set to $Q_i = diag(Q_{i,j})$ with $Q_{i,j} = diag(0,10,1,2), j \in \mathscr{C}_i$, and $R_i = diag(R_{i,j})$ with $R_{i,j} = diag(10,1), j \in \mathscr{C}_i$.

Table 6.1: Simulation parameters

symbol	value	description
Δt	0.1 s	sampling time interval
L	4.6 m	vehicle length
L_b	2.7 m	vehicle wheelbase
L_w	1.8 m	vehicle width
$v_{\max}$	15 m/s	maximum velocity
$a_{\max}$	5 m/s^2	maximum acceleration
$a_{\min}$	-3 m/s^2	maximum acceleration
B_r/B_l	2-.5 m/12.5 m	right/left roadside boundary

6.4.2 Analysis of simulation results

As shown in Fig. 6.5, the total coalitional cost of two scenarios in Case 1 keeps reducing, which implies the establishment of coalitions. In addition, the different reducing trend means the different coalition structures. As can be seen in Fig. 6.4, two different coalition structures are formulated in Case 1. In Case 1.1, three coalitions are formulated, while there are only two coalitions formed in Case 1.2, despite the same initial positions of vehicles in the two scenarios. It can be concluded that the coalition establishment does not depend solely on the distance between each vehicle. Based on the settings of these two scenarios in Case 1, it can be inferred that the difference in coalition structures comes from the various initial speeds and the lane-changing intentions of each vehicle. For example, in Case 1.1, HDV 4 intends to keep driving in the third lane, while HDV 5 intends to change to the first lane, which has no conflict with the destination lane. These two vehicles have little chance of collision and thus tend to stay in different coalitions. Things are different in Case 1.2 when both HDV 4 and HDV5 intend to drive in the second lane. The incurred collision risk keeps these two vehicles in one coalition. Moreover, CAV 3 will interact with HDV 4 and CAV 6 during its lane-changing procedure, and under such circumstances, a coalition including CAV 3, HDV 4, HDV 5, and CAV 6 is formulated in Case 1.2. In the same way, CAV 1 and HDV 2 always form a coalition in Case 1.

In Case 2, two coalitions are formed, with a singleton coalition and another coalition containing the remaining vehicles, which can be seen in Fig. 6.4. Although

both CAV 1 and HDV 2 intend to drive to the second lane, a singleton coalition only consisting of CAV 1 is formulated. In particular, the collision risk between CAV 1 and HDV 2 is small, despite the shorter distance between the two vehicles. Therefore, CAV 1 and HDV 2 remain in different coalitions. In contrast, the initial longitudinal speed of HDV 2 is less than that of CAV 3 that continues to drive in the second lane. This may incur a larger collision risk, and thus these two vehicles stay in one coalition. HDV 5 has a high collision risk with both CAV 3 and HDV 4, which is obtained from their same destination lanes and a small distance between each vehicle. Hence, all four vehicles form one coalition.

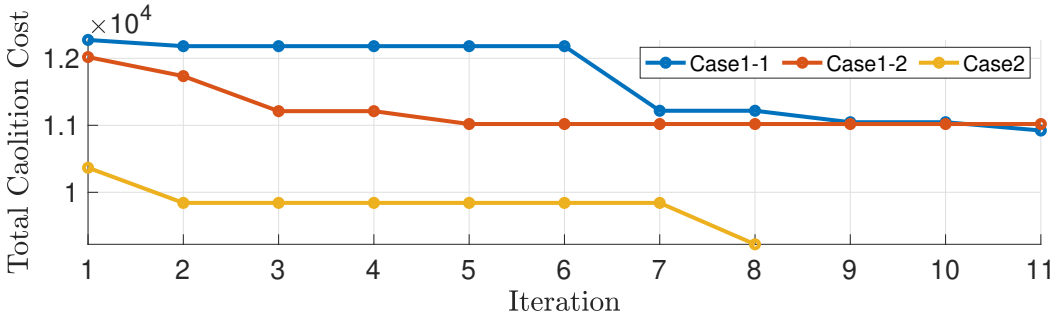

Figure 6.5: The total coalitional cost in three scenarios of two case studies

As can be seen in Figs. 6.6(a) and 6.7(a), each vehicle successfully changed lanes in both experiments of Case 1.1. The differences between Fig. 6.8(a) and Fig. 6.9(a), Fig. 6.10(a) and Fig. 6.11(a) show that CAVs adopt various lane change strategies when HDV driving behaviors differ. Both CAV 1 and HDV 2 accelerate to change lanes in each experiment. The difference is that HDV 2 in the second experiment drives more aggressively, and thus CAV 1 takes a larger acceleration to keep enough distance from HDV 2. The two vehicles adopt such strategies because they can reach their destination lanes faster and there is enough space to prevent collisions in both experiments. CAV 3 merges in front of HDV 4 in both experiments, although HDV 4 adopts different acceleration strategies. Specifically, conservative HDV 4 will decelerate and then maintain a relatively slow speed to give way to CAV 3 when they become closer to each other. On the contrary, the aggressive HDV 4 will accelerate in the beginning but decelerate when approaching CAV 3. Accordingly, CAV 3 takes a slower lane-changing in the first experiment than in the

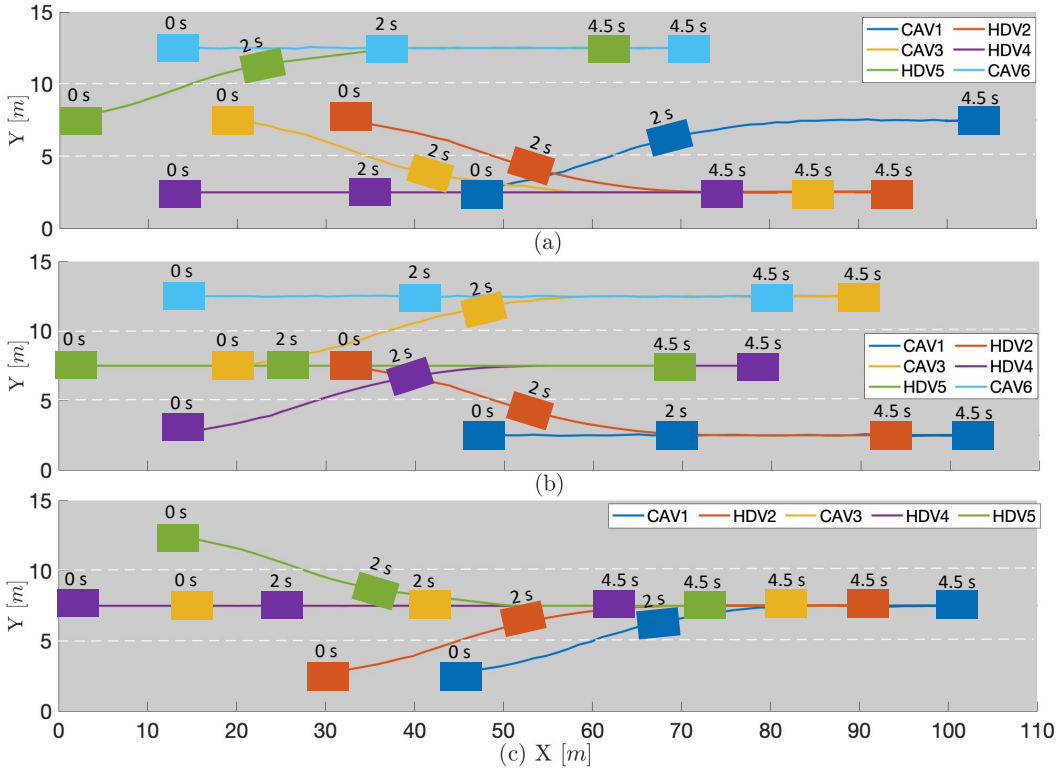

Figure 6.6: Trajectory of each vehicle in two case studies when HDVs are conservative. (a) is the result in Case 1.1, (b) is the result in Case 1.2, and (c) is the result in the Case 2

second. HDV 5 merges behind CAV 6 in both experiments despite its initial speed advantage over CAV 6. The aggressive HDV 5 in the second experiment changes to its destination lane with a larger acceleration compared to the conservative one in the first experiment. CAV 6 also drives faster in the second experiment to make enough space for HDV 5.

In both experiments of Case 1.2, all vehicles conduct successful lane-changing maneuvers, which is illustrated in Fig. 6.6(b), and Fig. 6.7(b). CAVs utilize different strategies in the two experiments, as shown by the differences between Fig. 6.8(b) and Fig. 6.9(b), Fig. 6.10(b) and Fig. 6.11(b). In the coalition consisting of CAV 1 and HDV 2, HDV 2 merges behind CAV 1 in both experiments, despite its faster initial speed. This is because the positional advantage of CAV 1 over HDV 2 is large, making it difficult for HDV 2 to overtake CAV 1 even for the aggressive one. As for the coalition consisting of the other four vehicles, HDV 4 merges in front of HDV 5 in both experiments, where HDV 4 adopts a larger acceleration in the

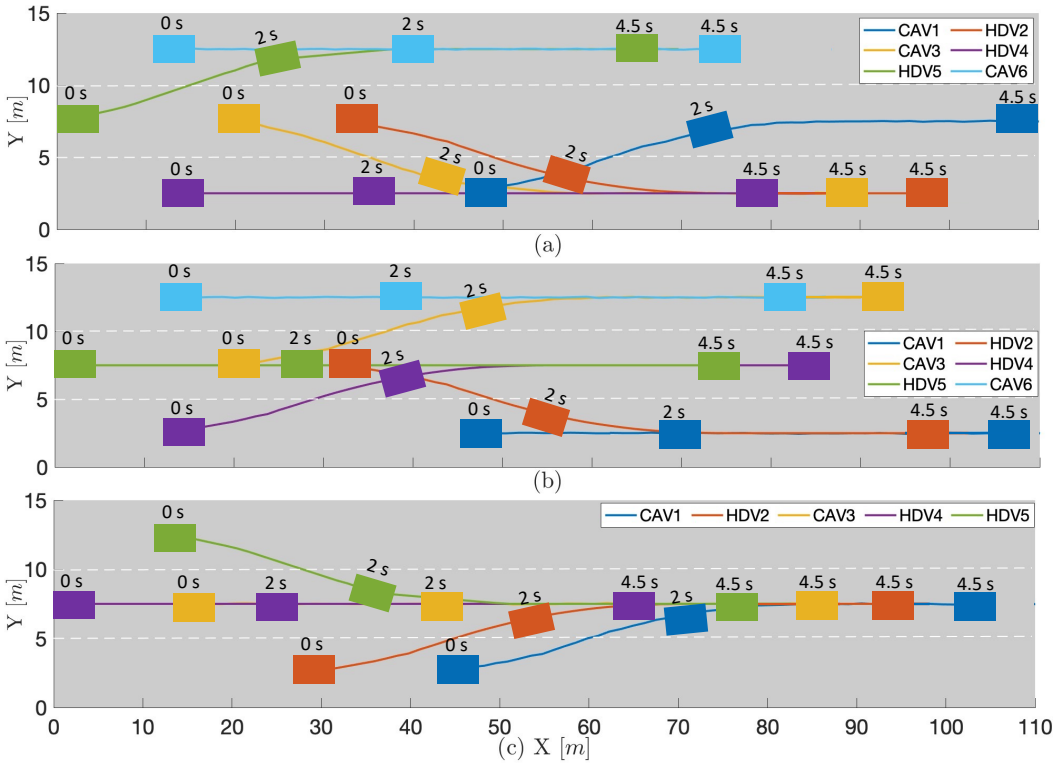

Figure 6.7: Trajectory of each vehicle in two case studies when HDVs are aggressive. (a) is the result of Case 1.1, (b) is the result of Case 1.2, and (c) is the result of Case 2

second experiment when HDV 5 is also aggressive. CAV 3 merges in front of CAV 6 in both experiments as its positional advantage over CAV 6 is enough to perform such a merging behavior. The difference is that CAV 3 takes a larger acceleration to facilitate the lane-changing of HDV 4 in the second experiment than in the first one. Consequently, CAV 6 reaches the desired velocity in a shorter time when CAV 3 ahead finishes the lane change with a higher acceleration.

As shown in Fig. 6.6(c), and Fig. 6.7(c), all vehicles in both experiments of Case 2 conduct successfully change lanes. As illustrated in Fig. 6.8(c), Fig. 6.9(c), Fig. 6.10(c) and Fig. 6.11(c), CAV 3 gives way to the lane-changing of HDV 2 in both experiments regardless of the different driving behaviors of HDV 2. In the first experiment, CAV 3 drives with a bigger acceleration than in the second experiment, as the aggressive HDV 2 changes to the second lane immediately and maintains enough distance from CAV 3. Unlike HDV 2, HDV 5 merges behind CAV 3 in both experiments. The reason is that there is no positional advantage of HDV 5 over

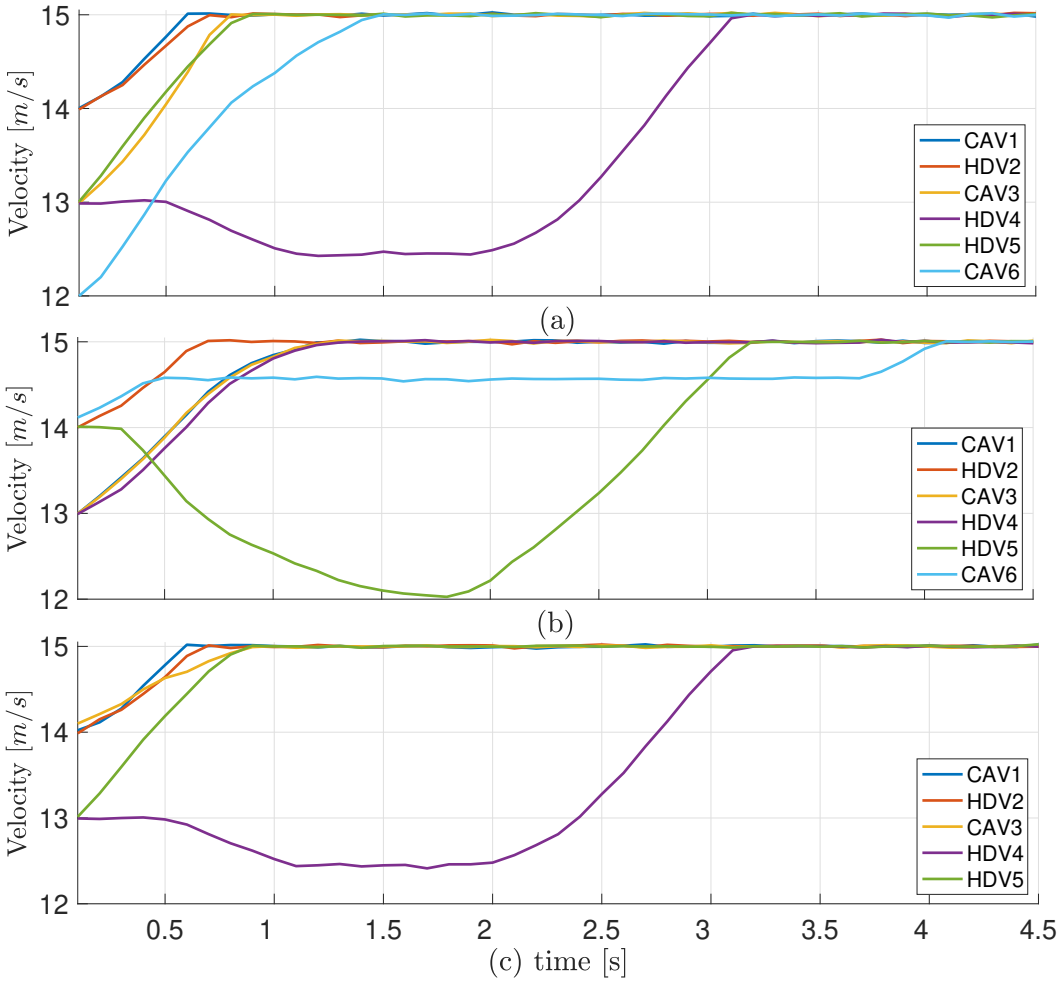

Figure 6.8: Speed of each vehicle in two case studies when HDVs are conservative. (a) is the result in Case 1.1, (b) is the result in Case 1.2, and (c) is the result in the Case 2

CAV 3 and the initial speed of HDV 5 is slower than that of CAV 3. It is impractical for HDV 5 to overtake CAV 3, even for the aggressive one. The conservative HDV 4 decelerates and then drives slowly to give way to the merging of HDV 5 in the first experiment, while the aggressive HDV 4 will accelerate at first and then decelerate when approaching HDV 5 in the second experiment. In both experiments, HDV 5 merges in front of HDV 4.

Further simulations are conducted to demonstrate the computational efficiency of our proposed method. For a fair comparison, the method that optimizes the trajectories of all vehicles involved in lane-changing as a whole is used as the benchmark. Each experiment runs 5 times to calculate the average running time for each step.

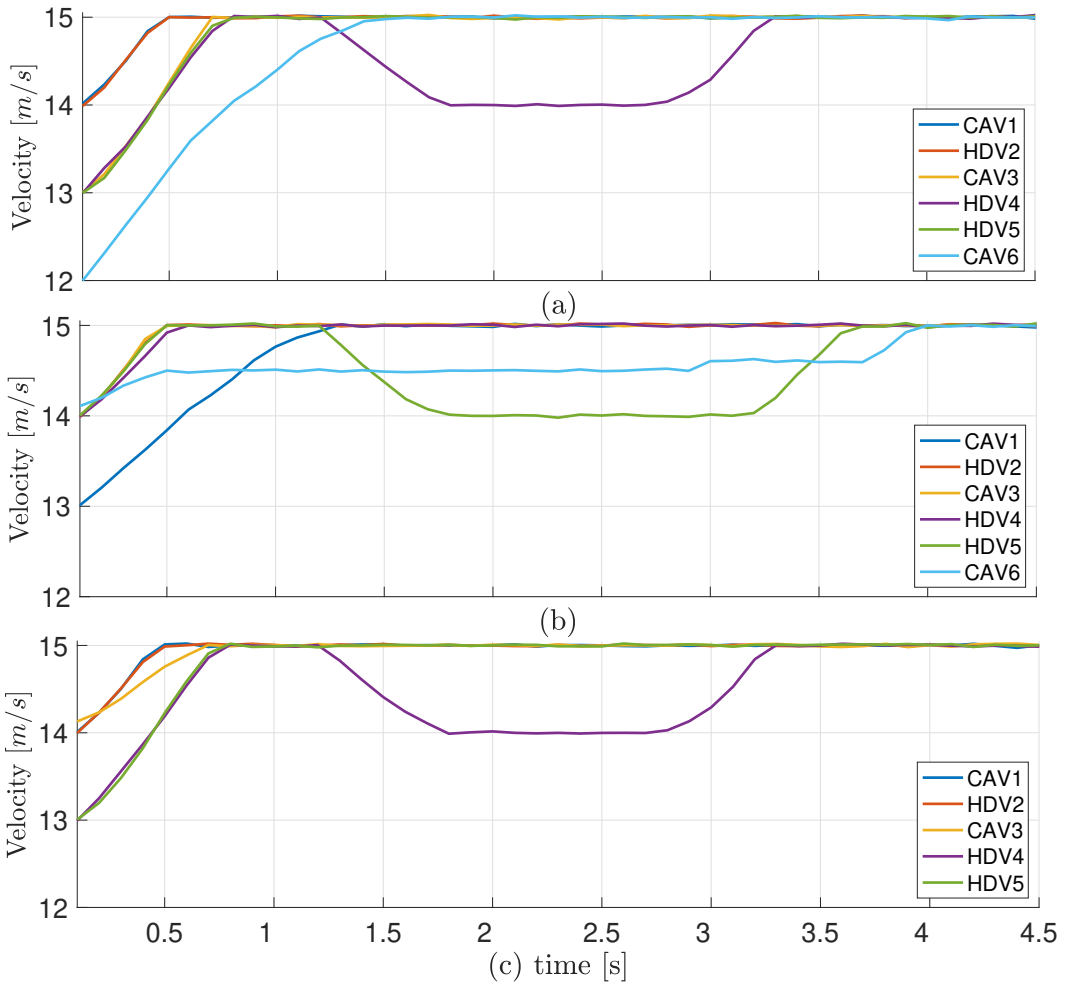

Figure 6.9: Speed of each vehicle in two case studies when HDVs are aggressive. (a) is the result in Case 1.1, (b) is the result in Case 1.2, and (c) is the result in the Case 2

The computation time of coalition establishment is also included. In addition, the average distance to finish lane-changing is also compared. The computation time for coalition establishment in Case 1.1, Case 1.2, and Case 2 are 1.67s, 1.59s, and 1.34s respectively. As shown in Table 6.2, the average running time for each step of our proposed method is about 60ms and slightly increases with the increased number of vehicles. This running time is smaller than the sampling time interval Δt, indicating the real-time applicability of the proposed method. Next, the benchmark method is taken for comparison, with an average running time of 0.3s. This running time is larger than Δt and grows sharply when the number of vehicles increases from 5 to 6. Even with computation time for coalitions, the proposed method is still more computationally efficient than the benchmark method. Meanwhile, as shown in Ta-

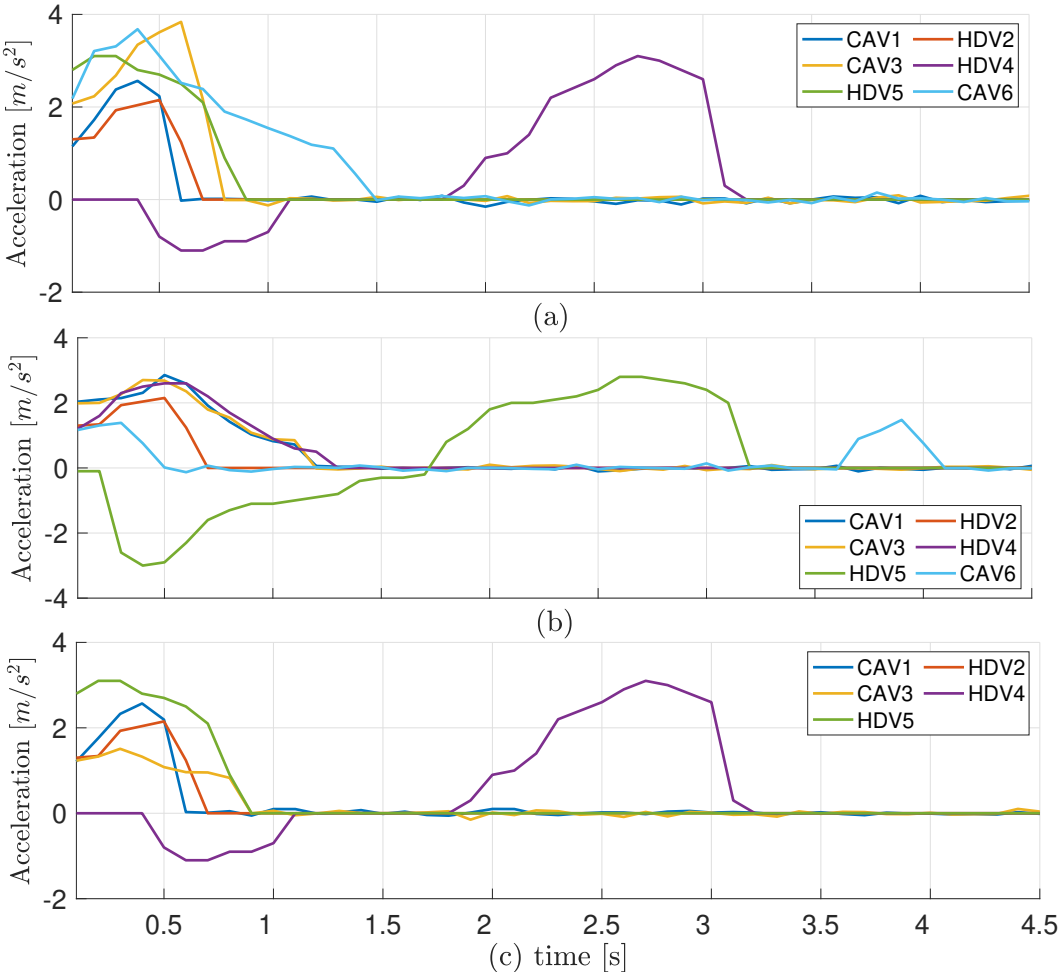

Figure 6.10: Acceleration of each vehicle in two case studies when HDVs are conservative. (a) is the result in Case 1.1, (b) is the result in Case 1.2, and (c) is the result in the Case 2

ble 6.3, the average distance to finish lane-changing of the two methods is similar, indicating our proposed method achieves a comparable good performance.

Table 6.2: Average running time for each step of two methods

	Proposed Method	Benchmark Method
Case 1.1	61.23 ms	472.4 ms
Case 1.2	62.18 ms	463.6 ms
Case 2	60.72 ms	302.1 ms

6.4.3 HIL simulation

In this section, to better emulate human drivers' behaviors and show the real-time performance of our proposed method, two HIL experiments are conducted based on

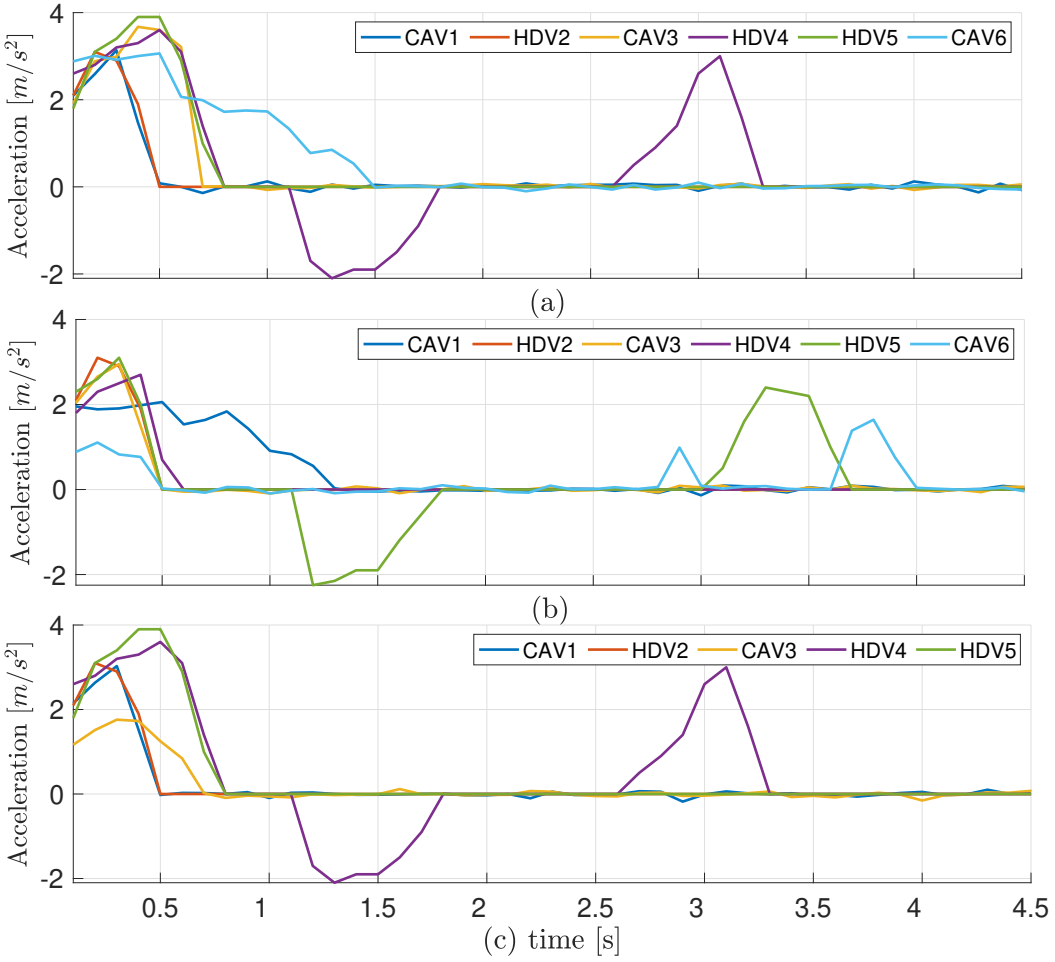

Figure 6.11: Acceleration of each vehicle in two case studies when HDVs are aggressive. (a) is the result in Case 1.1, (b) is the result in Case 1.2, and (c) is the result in the Case 2

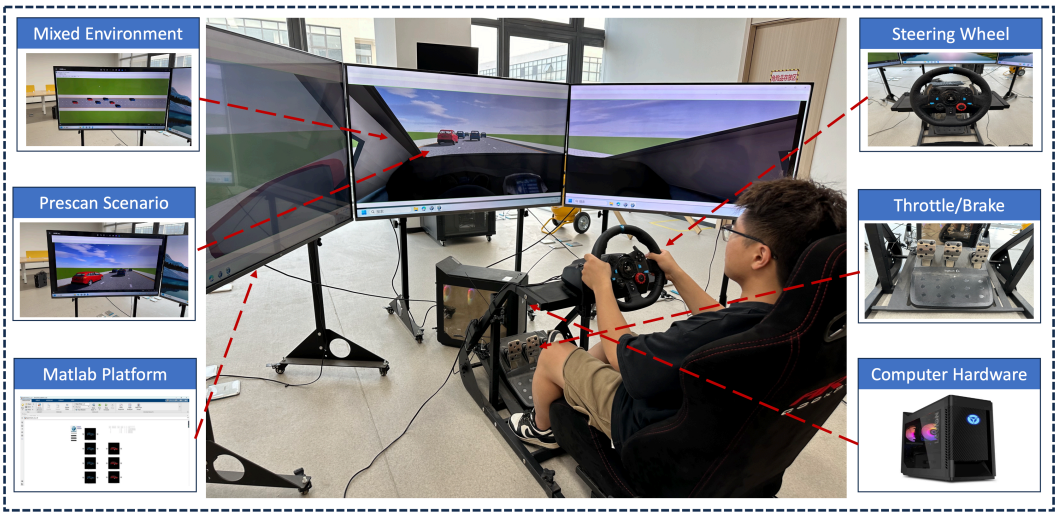

Figure 6.12: Human in the loop driving simulator.

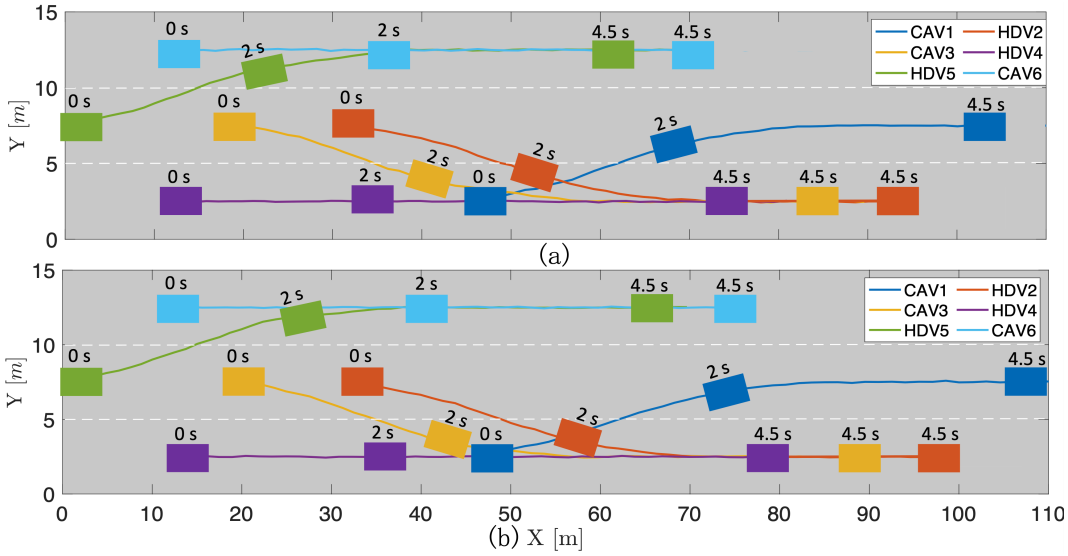

Figure 6.13: HIL trajectory of each vehicle in Case 1.1. (a) is the result when HDVs are conservative, (b) is the result when HDV are aggressive

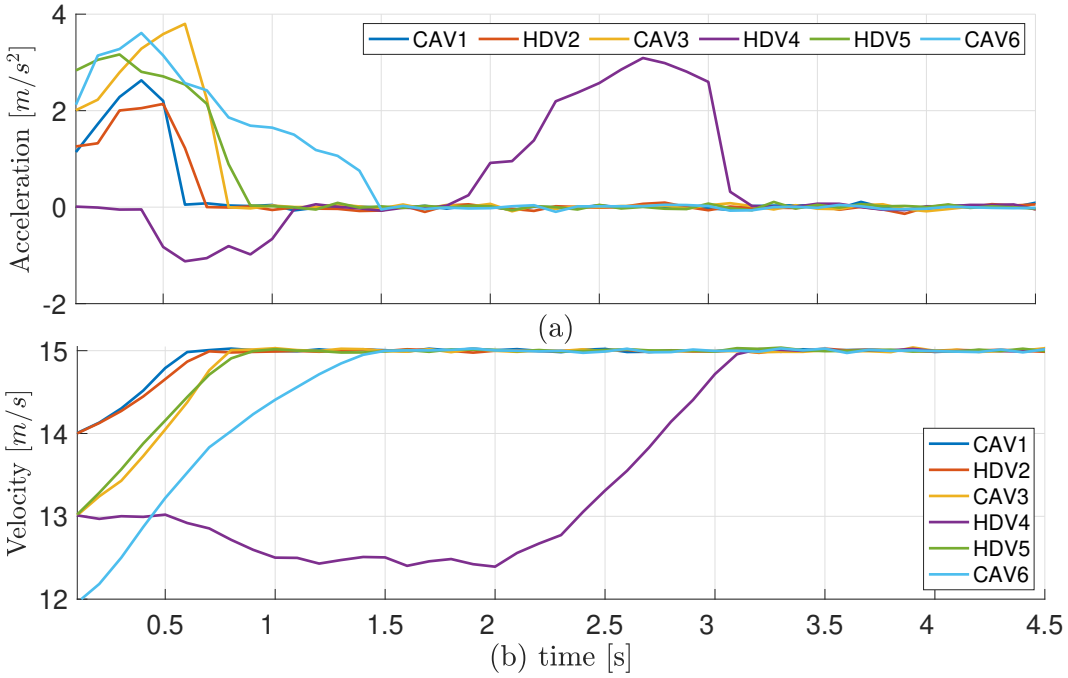

Figure 6.14: HIL trajectory of each vehicle in Case 1.1 when HDVs are conservative. (a) is the acceleration, (b) is the velocity

Table 6.3: Average distance to finish lane-changing of two methods

	Proposed Method	Benchmark Method
Case 1.1	58.24 m	57.96 m
Case 1.2	57.65 m	56.88 m
Case 2	56.83 m	56.31 m

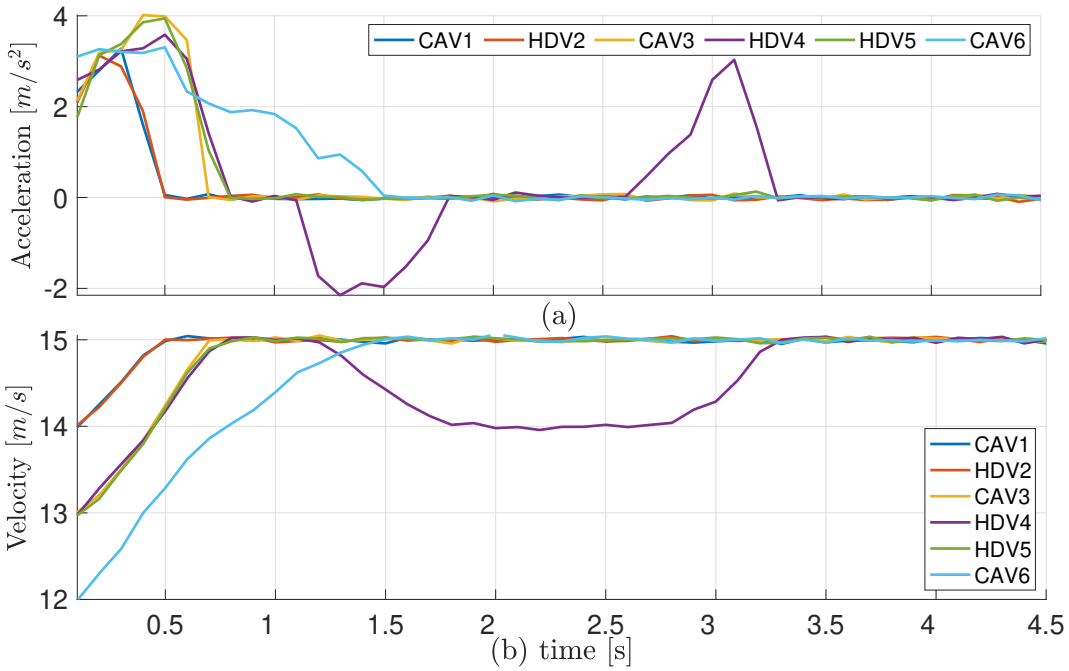

Figure 6.15: HIL trajectory of each vehicle in Case 1.1 when HDVs are aggressive. (a) is the acceleration, (b) is the velocity

Case 1.1. For simulating the three HDVs in the HIL experiment, three experienced human drivers simultaneously controlled three driver simulators (see Fig. 6.12), each performing real-time operations to mimic realistic driving behavior. In each experiment, drivers were instructed to accelerate to the desired velocity $v_{\max}$ and to reach the destination lanes, in accordance with the game cost function (6.27). To examine different driving behaviors, all drivers were asked to adopt conservative behaviors in one experiment and aggressive behaviors in the other. Conservative driving is characterized by gradual acceleration changes, whereas aggressive driving involves sharper variations in acceleration.

Each driving simulator includes three 65-inch displays, a Logitech G29 steering wheel, a throttle/brake pedal, and other components. The computer is equipped

with an Inter Core i5-10500 CPU, featuring 6 cores and 12 threads. This hardware configuration efficiently handled real-time vehicle control and interactions. The virtual scenarios are built in PreScan GUI, and all the construction of vehicle models and algorithms is completed on the Simulink platform. The parameter setup is the same as the parameters in Section 6.4.1.

As shown in Figs. 6.13 – 6.15, our proposed method is feasible and real-time applicable. Moreover, the performance of HIL experiments shown in Fig. 6.13 and Fig. 6.14 is not as smooth as the results shown in Fig. 6.8 to Fig. 6.11 (i.e. speed and acceleration). This is due to disturbances and lags involved in the sensors and experimental equipment used in the HIL setup, and the potential nonsmooth behavior introduced by the human pilots.

6.5 CONCLUSIONS

This chapter introduces a two-layer hierarchical control architecture for multi-vehicle lane-changing in mixed autonomy, which expands the single vehicle lane-changing control in Chapter 5 and completes the overall control framework proposed in this thesis. In the upper layer, vehicles are divided into different coalitions by the intersection controller based on vehicle states and lane-changing intentions, which could facilitate lane-changing while reducing the computation burden of global coordination. In the lower layer, the Stackelberg game is utilized to model the interactions between CAVs and HDVs within each coalition in the lane-changing scenario. Considering the modeling uncertainty, CAVs are governed by data-enabled predictive control, bypassing the system identification of complex environmental uncertainties instead of game-based optimal strategies.

In simulations, two case studies that contain HDVs with different driving styles are comprehensively analyzed. The results show that all vehicles perform successful lane-changing without colliding with other vehicles in each scenario. Moreover, HIL experiments are also conducted to show the feasibility and real-time performance of our proposed method.

Chapter 7

Conclusions and Future Work

7.1 Conclusions

Urban traffic coordination is a complex challenge due to the large number of vehicles involved, and this challenge becomes even greater in mixed traffic environments where both HDVs and CAVs coexist. This thesis proposes the urban traffic coordination framework shown in Fig. 1.4 to deal with the mixed traffic problem. By dividing the roads into the car-following zone and the lane-changing zone, this framework can decouple the traffic coordination problem into sub-problems, which can be solved efficiently through two separate control modules. The signal-vehicle coupled control module and the lane-changing control module are developed respectively for the car-following zone and the lane-changing zone in Fig. 1.4, with scalability and environmental impact considerations.

The signal-vehicle coupled control module is introduced in Chapter 4, where a two-layer intersection signal-vehicle coupled coordination scheme for joint control of intersection SPAT and speed trajectory of CAV and HDV is proposed. The method is developed based on a CAV-led mixed platoon model, where the motion of the HDVs is governed by a linearized intelligent driver model. In addition to the SPAT, the target platoon velocity and the number of passing platoons are continuously updated in the upper layer to minimize the total waiting time. Subsequently, the intersection controller utilizes the SPAT information to conduct optimal control of the mixed platoon within the control zone by manipulating the speed of the

leading CAVs. In addition, the benefit of our newly developed method is shown by comparisons with various traditional strategies. Additionally, the impacts of intersection traffic density, flow distribution, and the penetration rates of CAV and EV are investigated by comprehensive simulation trials.

The lane-changing control module is introduced in Chapter 5 and Chapter 6. In particular, a simple mixed traffic lane-changing scenario that contains one CAV and one HDV is considered in Chapter 5. A game-based lane change framework is proposed for the CAV, where the Stackelberg game method is used to model the interaction between HDVs and CAVs. An optimal strategy is designed, which is further shown to provide the asymptotically stable equilibrium point. The condition under which the optimal strategy can render the collision avoidance set invariant is provided. Numerical results show that the CAV can conduct a successful and safe lane change without colliding with the HDV. To extend the work proposed in Chapter 5, Chapter 6 introduces a two-layer hierarchical control architecture for multi-vehicle lane-changing in mixed autonomy. In particular, a game-based coalition formation is proposed in the upper layer, which could facilitate lane-changing control in the lower layer, and can significantly improve computation efficiency compared with the benchmark method that optimizes the trajectories of all vehicles involved in lane-changing as a whole. In the lower layer, a Stackelberg game-based framework is utilized to model the interaction between CAVs and HDVs, where both types of vehicles can change lanes. To enhance robustness against modeling uncertainty, a data-enabled predictive control is applied to CAVs. Numerical simulations and HIL experiments are conducted based on data representing different driving behaviors, whose results demonstrate the effectiveness of our proposed framework in various lane-changing scenarios involving HDVs with different aggressiveness.

7.2 Future Work

In the near future, multimodal urban transport involving different modes of transportation (like pedestrians, bicycles, and trains) will be mainstream. Enhancing the overall efficiency and safety of such complex systems, involving large numbers of

participants, will require the collection and analysis of vast amounts of data. To make use of this data and be computationally efficient, the AI-based methods and edge-cloud distributed control architectures will be utilized. However, the resilience to Cyber-Physical threats and communication delays is a big concern. As connectivity increases, so do vulnerabilities. Future studies should address cybersecurity risks and develop methods to remain robust against communication loss. The explainable AI should be pursued as a future research direction for AI-based traffic coordination. Further investigation should focus on developing interpretable AI models for CAVs' decisions, which is crucial for regulatory compliance and public trust, particularly in case scenarios (e.g., unpredictable pedestrians).

Large-scale traffic optimization in mixed urban traffic environments is needed. A feasible method is to decouple the network-level optimization into a series of sub-optimization problems, which greatly reduces the computational burden, but losing guarantees of global optimality. Thus, balancing the optimality and the computational efficiency in network-level traffic control is one of our future research directions. Another way is to develop a hierarchical control framework, which may contain the path planning layer, decision-making layer, SPAT optimization layer, etc. How to ensure reliability across different layers is a common issue. The theoretical analysis of these methods is worth further investigation. Moreover, traffic control at different levels is another important future research direction. For example, the SPAT control at the network level and the mixed-platoon formation at the arterial level are interdependent. Traffic control at different levels can jointly influence the operation of overall traffic networks. Future research may integrate different levels of traffic control to improve overall traffic efficiency by building a multi-level model. This multi-level model, combining macroscopic, mesoscopic, and microscopic control with consideration of various road users, should be developed to address different optimization objectives.

In addition, human uncertainties should also be considered more comprehensively in future research. The uncertainty of HDVs should be included in the theoretical analysis. For example, distributionally robust chance constraints can be used

to model human uncertainty and perform robustness analysis. The estimation of HDVs' aggressiveness should also be included to make the analysis more realistic. The rationality of humans is another concern. For example, in many game-based methods, humans are always assumed to be fully rational (i.e., human drivers activate turn signals before lane-changing), which is not always the case. The bounded rationality or irrationality of humans should be considered in future research. Finally, real vehicle testing is crucial to validate the robustness against human uncertainty. Restricted by experimental sites and equipment, few such tests have been conducted. Thus, large-scale mixed autonomy on-road simulation should be further conducted to validate the robustness under complex environments.

Bibliography

[1] J. Rios-Torres and A. A. Malikopoulos. A survey on the coordination of connected and automated vehicles at intersections and merging at highway on-ramps. *IEEE Transactions on Intelligent Transportation Systems*, 18:1066–1077, 5 2017.

[2] Jacopo Guanetti, Yeojun Kim, and Francesco Borrelli. Control of connected and automated vehicles: State of the art and future challenges. *Annual reviews in control*, 45:18–40, 2018.

[3] Statistics on vehicles in use. *https://www.oica.net/statistics/* [Online], 2024. International Organization of Motor Vehicle Manufacturers.

[4] Global statistical data regarding on-road vehicles. *https://www.oyez.org/cases/* [Online], 2024. World motor vehicle data from Motor Vehicle Manufacturers Association of the United States.

[5] Jinjue Li, Chunhui Yu, Zilin Shen, Zicheng Su, and Wanjing Ma. A survey on urban traffic control under mixed traffic environment with connected automated vehicles. *Transportation Research Part C: Emerging Technologies*, 154:104258, 09 2023.

[6] H. Jiang, J. Hu, S. An, M. Wang, and B. B. Park. Eco approaching at an isolated signalized intersection under partially connected and automated vehicles environment. *Transportation Research Part C: Emerging Technologies*, 79:290–307, 06 2017.

[7] Xiao Pan, Boli Chen, Stelios Timotheou, and Simos Evangelou. A convex optimal control framework for autonomous vehicle intersection crossing. *IEEE Transactions on Intelligent Transportation Systems*, 24:163–177, 01 2022.

[8] Markus Koschi and Matthias Althoff. Set-based prediction of traffic participants considering occlusions and traffic rules. *IEEE Transactions on Intelligent Vehicles*, 6:249–265, 06 2021.

[9] IEEE. Ethically aligned design. *https://standards.ieee.org/news/eadv2*, IEEE Press.

[10] From principles to practice ethically aligned design conceptual framework. *https://ethicsinaction.ieee.org/wp-content/uploads/ead1e principles to practice.pdf/*, IEEE.

[11] D. Rotman. The relentless pace of automation. *Technology Review*, 120:92–95, 03 2017.

[12] Steven E Shladover, Charles A Desoer, J Karl Hedrick, Masayoshi Tomizuka, Jean Walrand, W-B Zhang, Donn H McMahon, Huei Peng, Shahab Sheikholeslam, and Nick McKeown. Automated vehicle control developments in the path program. *IEEE Transactions on vehicular technology*, 40:114–130, 1991.

[13] Jeffrey D Rupp and Anthony G King. Autonomous driving-a practical roadmap. *SAE International*, 2010.

[14] Fabian Kröger. *From Automated to Autonomous Driving: A Transnational Research History on Pioneers, Artifacts and Technological Change (1950-2000)*, volume 70. Springer Nature, 2024.

[15] Siyu Teng, Xuemin Hu, Peng Deng, Bai Li, Yuchen Li, Yunfeng Ai, Dongsheng Yang, Lingxi Li, Zhe Xuanyuan, Fenghua Zhu, and Long Chen. Mo-

tion planning for autonomous driving: The state of the art and future perspectives. *IEEE Transactions on Intelligent Vehicles*, 8:3692–3711, 2023.

[16] Decarbonising uk transport: technology roadmaps. *https://www.gov.uk/government/publications/decarbonising-uk-transport-technology-roadmaps* [Online], 2021. GOV.UK.

[17] Electric vehicles: What's next vii: Confronting greenflation. *https://www.goldmansachs.com/intelligence/pages/electric-vehicles-whats-next-vii-confronting-greenflation.html* [Online], 2022. GOLDMAN SACHS RESEARCH.

[18] Keqiang Li, Jiawei Wang, and Yang Zheng. Cooperative formation of autonomous vehicles in mixed traffic flow: Beyond platooning. *IEEE Transactions on Intelligent Transportation Systems*, 23:15951–15966, 09 2022.

[19] Tobias Kessler, Klemens Esterle, and Alois Knoll. Mixed-integer motion planning on german roads within the apollo driving stack. *IEEE Transactions on Intelligent Vehicles*, 8:851–867, 01 2023.

[20] Xiancai Jiang and Qingpeng Shang. A dynamic (CAV)-dedicated lane allocation method with the joint optimization of signal timing parameters and smooth trajectory in a mixed traffic environment. *IEEE Transactions on Intelligent Transportation Systems*, 24:6436–6449, 06 2023.

[21] Xin Huang, Peiqun Lin, Mingyang Pei, Bin Ran, and Man-Chun Tan. Reservation-based cooperative eco-driving model for mixed autonomous and manual vehicles at intersections. *IEEE Transactions on Intelligent Transportation Systems*, 24:9501–9517, 09 2023.

[22] Mehrdad Tajali and Ali Hajbabaie. Traffic signal timing and trajectory optimization in a mixed autonomy traffic stream. *IEEE Transactions on Intelligent Transportation Systems*, 23:6525–6538, 07 2022.

[23] Yu Du, Wei Shangguan, and Linguo Chai. A coupled vehicle-signal control method at signalized intersections in mixed traffic environment. *IEEE Transactions on Vehicular Technology*, 70:2089–2100, 03 2021.

[24] Pengyuan Sun, Daisik Nam, R. Jayakrishnan, and Wenlong Jin. An eco-driving algorithm based on vehicle to infrastructure (v2i) communications for signalized intersections. *Transportation Research Part C: Emerging Technologies*, 144:103876, 2022.

[25] Xiao (Joyce) Liang, S. Ilgin Guler, and Vikash V. Gayah. Joint optimization of signal phasing and timing and vehicle speed guidance in a connected and autonomous vehicle environment. *Transportation Research Record*, 2673:70–83, 04 2019.

[26] Ramin Niroumand, Mehrdad Tajali, Leila Hajibabai, and Ali Hajbabaie. Joint optimization of vehicle-group trajectory and signal timing: Introducing the white phase for mixed-autonomy traffic stream. *Transportation Research Part C: Emerging Technologies*, 116:102659, 2020.

[27] Ramin Niroumand, Leila Hajibabai, Ali Hajbabaie, and Mehrdad Tajali. Effects of autonomous driving behavior on intersection performance and safety in the presence of white phase for mixed-autonomy traffic stream. *Transportation Research Record: Journal of the Transportation Research Board*, 2676(8):112–130, 2022.

[28] Mahmoud Pourmehrab, Lily Elefteriadou, Sanjay Ranka, and Marilo Martin-Gasulla. Optimizing signalized intersections performance under conventional and automated vehicles traffic. *IEEE Transactions on Intelligent Transportation Systems*, 21:2864–2873, 07 2020.

[29] Zhihong Yao, Zhao Bin, Yuan Tengfei, Haoran Jiang, and Yangsheng Jiang. Reducing gasoline consumption in mixed connected automated vehicles environment: A joint optimization framework for traffic signals and vehicle trajectory. *Journal of Cleaner Production*, 265:121836, 2020.

[30] Yang, Kaidi, Guler, S., Ilgin, Menendez, and Monica. Isolated intersection control for various levels of vehicle technology: Conventional, connected, and automated vehicles. *Transportation research, Part C: Emerging technologies*, 72:109–129, 2016.

[31] Hao Liu, Xiaoyun Lu, and Steven Shladover. Traffic signal control by leveraging cooperative adaptive cruise control (CACC) vehicle platooning capabilities. *Transportation Research Part C: Emerging Technologies*, 104:390–407, 07 2019.

[32] Kuoran Zhang, Jinxiang Wang, Nan Chen, and Guodong Yin. A non-cooperative vehicle-to-vehicle trajectory-planning algorithm with consideration of driver's characteristics. *Proceedings of the Institution of Mechanical Engineers, Part D: Journal of Automobile Engineering*, 233:095440701878339, 07 2018.

[33] Jinxiang Wang, Mengmeng Dai, Guodong Yin, and Nan Chen. Output-feedback robust control for vehicle path tracking considering different human drivers' characteristics. *Mechatronics*, 50, 05 2017.

[34] Peng Hang, Chen Lv, Yang Xing, Chao Huang, and Zhongxu Hu. Human-like decision making for autonomous driving: A noncooperative game theoretic approach. *IEEE Transactions on Intelligent Transportation Systems*, 22(4):2076–2087, 2021.

[35] Peng Hang, Chao Huang, Zhongxu Hu, Yang Xing, and Chen Lv. Decision making of connected automated vehicles at an unsignalized roundabout considering personalized driving behaviours. *IEEE Transactions on Vehicular Technology*, 70(5):4051–4064, 2021.

[36] Haitao Xia, Kanok Boriboonsomsin, and Matthew Barth. Dynamic eco-driving for signalized arterial corridors and its indirect network-wide energy/emissions benefits. *Journal of Intelligent Transportation Systems*, 17:31–41, 01 2013.

[37] Xiangmo Zhao, Xia Wu, Qi Xin, Kang Sun, and Shaowei Yu. Dynamic eco-driving on signalized arterial corridors during the green phase for the connected vehicles. *Journal of Advanced Transportation*, 2020:1–11, 01 2020.

[38] Ziran Wang, Guoyuan Wu, and Matthew Barth. Cooperative eco-driving at signalized intersections in a partially connected and automated vehicle environment. *IEEE Transactions on Intelligent Transportation Systems*, 21:2029–2038, 05 2020.

[39] Khan Muhammad, Amin Ullah, Jaime Lloret, Javier Del Ser, and V.H.C. Albuquerque. Deep learning for safe autonomous driving: Current challenges and future directions. *IEEE Transactions on Intelligent Transportation Systems*, 22:4316–4336, 07 2021.

[40] Bo Hu, Sunan Zhang, and Bocheng Liu. A hybrid algorithm combining data-driven and simulation-based reinforcement learning approaches to energy management of hybrid electric vehicles. *IEEE Transactions on Transportation Electrification*, 10:1257 – 1273, 03 2024.

[41] Sampo Kuutti, Richard Bowden, Yaochu Jin, Phil Barber, and Saber Fallah. A survey of deep learning applications to autonomous vehicle control. *IEEE Transactions on Intelligent Transportation Systems*, 22(2):712–733, 2021.

[42] Mengcheng Tang, Weichao Zhuang, Bingbing Li, Haoji Liu, Ziyou Song, and Guodong Yin. Energy-optimal routing for electric vehicles using deep reinforcement learning with transformer. *Applied Energy*, 350:121711, 2023.

[43] L. Hewing, K.P. Wabersich, M. Menner, and M.N. Zeilinger. Learning-based model predictive control: Toward safe learning in control. *Annual Review of Control, Robotics, and Autonomous Systems*, 3:269–296, 10 2020.

[44] Jeremy Coulson, John Lygeros, and Florian Dörfler. Data-enabled predictive control: In the shallows of the deepc. In *2019 18th European Control Conference (ECC)*, pages 307–312, 2019.

[45] Chaoyi Chen, Mengchi Cai, Jiawei Wang, Kai Li, Qing Xu, Jianqiang Wang, and Keqiang Li. Cooperation method of connected and automated vehicles at unsignalized intersections: Lane changing and arrival scheduling. *IEEE Transactions on Vehicular Technology*, 71(11):11351–11366, 2022.

[46] Adam Danczyk, Xuan Di, and Henry Liu. A probabilistic optimization model for allocating freeway sensors. *Transportation Research Part C: Emerging Technologies*, 67:378–398, 06 2016.

[47] Chunhui Yu, Wanjing Ma, and Xiaoguang Yang. A time-slot based signal scheme model for fixed-time control at isolated intersections. *Transportation Research Part B Methodological*, 140:176–192, 10 2020.

[48] F.V. Webster. Traffic signal settings. *Road Research Technical Paper*, Her Majesty's Stationery Office, London, UK, 1958.

[49] C Wong and Yi Liu. Lane-based optimization for signalized network configuration designs. *MATEC Web of Conferences*, 272:01048, 01 2019.

[50] Yiheng Feng, Larry Head, Shayan Khoshmagham, and Mehdi Zamanipour. A real-time adaptive signal control in a connected vehicle environment. *Transportation Research Part C: Emerging Technologies*, 55:460–473, 06 2015.

[51] Wanjing Ma, Lijuan Wan, Chunhui Yu, Li Zou, and Jianfeng Zheng. Multi-objective optimization of traffic signals based on vehicle trajectory data at isolated intersections. *Transportation Research Part C Emerging Technologies*, 120:102821, 11 2020.

[52] X. Tang, Guichuan Zhong, Shen Li, Kai Yang, Keqi Shu, Dongpu Cao, and Xianke Lin. Uncertainty-aware decision-making for autonomous driving at uncontrolled intersections. *IEEE Transactions on Intelligent Transportation Systems*, 24(9):9725–9735, 2023.

[53] Xiao Pan, Boli Chen, Li Dai, Stelios Timotheou, and Simos A. Evangelou. A hierarchical robust control strategy for decentralized signal-free intersection management. *IEEE Transactions on Control Systems Technology*, 31(5):2011–2026, 2023.

[54] J. Alonso, V. Milanes, J. Perez, E. Onieva, C. Gonzalez, and T. de Pedro. Autonomous vehicle control systems for safe crossroads. *Transportation Research Part C Emerging Technologies*, 19 (6):11095–1110, 6 2011.

[55] Farzaneh Azadi, Nikola Mitrovic, and Aleksandar Stevanovic. Combined flexible lane assignment and reservation-based intersection control in field-like traffic conditions. *Transportmetrica A: Transport Science*, 20:1–36, 09 2022.

[56] Wenqin Zhong, Keqiang Li, Jia Shi, Jie Yu, and Yugong Luo. Reservation-prioritization-based mixed-traffic cooperative control at unsignalized intersections. *IEEE Transactions on Intelligent Vehicles*, 9:4917–4930, 05 2024.

[57] Andreas Malikopoulos, C.G. Cassandras, and Yue Zhang. A decentralized energy-optimal control framework for connected automated vehicles at signal-free intersections. *Automatica*, 93:244–256, 07 2018.

[58] Taylor Li and Xuesong Simon Zhou. Recasting and optimizing intersection automation as a connected-and-automated-vehicle (CAV) scheduling problem: A sequential branch-and-bound search approach in phase-time-traffic hypernetwork. *Transportation Research Part B Methodological*, 105:479–506, 11 2017.

[59] Yue Zhang and C.G. Cassandras. A decentralized optimal control framework for connected automated vehicles at urban intersections with dynamic resequencing. *2018 IEEE Conference on Decision and Control (CDC)*, pages 217–222, 09 2018.

[60] Yue Zhang and C.G. Cassandras. An impact study of integrating connected automated vehicles with conventional traffic. *Annual Reviews in Control*, 48:347–356, 04 2019.

[61] Ruochen Hao, Yuxiao Zhang, Wanjing Ma, Chunhui Yu, Tuo Sun, and B. Arem. Managing connected and automated vehicles with flexible routing at "lane-allocation-free" intersections. *Transportation Research Part C Emerging Technologies*, 152:104152, 07 2023.

[62] Zhenning Li, Qiong Wu, Hao Yu, Cong Chen, Guohui Zhang, zong tian, and P. D. Prevedouros. Temporal-spatial dimension extension-based intersection control formulation for connected and autonomous vehicle systems. *Transportation Research Part C Emerging Technologies*, 104:234–248, 07 2019.

[63] Chunhui Yu, Yiheng Feng, Henry Liu, Wanjing Ma, and Xiaoguang Yang. Corridor level cooperative trajectory optimization with connected and automated vehicles. *Transportation Research Part C Emerging Technologies*, 105:405–421, 08 2019.

[64] Hao Yang, Hesham Rakha, and Mani Venkat Ala. Eco-cooperative adaptive cruise control at signalized intersections considering queue effects. *IEEE Transactions on Intelligent Transportation Systems*, 18(6):1575–1585, 2017.

[65] Zijia Zhong, Mark Nejad, and Earl E Lee. Autonomous and semiautonomous intersection management: A survey. *IEEE Intelligent Transportation Systems Magazine*, 13(2):53–70, 2021.

[66] G.F. Newell. Nonlinear effects in the dynamics of car following. *Oper. Res.*, 9 (2):209–229, 1961.

[67] P.G. Gipps. A behavioral car-following model for computer simulation. *Transp. Res. B Methodol.*, 15 (2):105–111, 1981.

[68] Martin Treiber, Ansgar Hennecke, and Dirk Helbing. Congested traffic states in empirical observations and microscopic simulations. *Physical Review E*, 62:1805–1824, 2000.

[69] Wonteak Lim, Seongjin Lee, Myoungho Sunwoo, and Kichun Jo. Hybrid trajectory planning for autonomous driving in on-road dynamic scenarios. *IEEE Transactions on Intelligent Transportation Systems*, 22:341–355, 01 2021.

[70] David Q Mayne, James B Rawlings, Christopher V Rao, and Pierre OM Scokaert. Constrained model predictive control: Stability and optimality. *Automatica*, 36(6):789–814, 2000.

[71] David Q Mayne, Saša V Raković, Rolf Findeisen, and Frank Allgöwer. Robust output feedback model predictive control of constrained linear systems. *Automatica*, 42(7):1217–1222, 2006.

[72] David Q Mayne, María M Seron, and Saša V Raković. Robust model predictive control of constrained linear systems with bounded disturbances. *Automatica*, 41(2):219–224, 2005.

[73] Hao Yang and Wen-Long Jin. A control theoretic formulation of green driving strategies based on inter-vehicle communications. *Transportation Research Part C: Emerging Technologies*, 41:48–60, 04 2014.

[74] Nicholas Kohut, Professor Hedrick, and Professor Borrelli. Integrating traffic data and model predictive control to improve fuel economy. *IFAC Proceedings Volumes*, 42:155–160, 12 2009.

[75] Simon Stebbins, Mark Hickman, Jiwon Kim, and Hai Vu. Characterising green light optimal speed advisory trajectories for platoon-based optimisation. *Transportation Research Part C: Emerging Technologies*, 82:43–62, 09 2017.

[76] Anye Zhou, Srinivas Peeta, and Jian Wang. Cooperative control of a platoon of connected autonomous vehicles and unconnected human-driven vehicles. *Computer-Aided Civil and Infrastructure Engineering*, 38, 03 2023.

[77] S.C. Dafermos. The traffic assignment problem for multiclass-user transportation networks. *Transp. Sci.*, 6 (1):73–87, 1972.

[78] Daniel Lazar, Erdem Bıyık, Dorsa Sadigh, and Ramtin Pedarsani. Learning how to dynamically route autonomous vehicles on shared roads. *Transportation Research Part C: Emerging Technologies*, 130:103258, 09 2021.

[79] Yi Guo and Jiaqi Ma. Drl-tp3: A learning and control framework for signalized intersections with mixed connected automated traffic. *Transportation Research Part C: Emerging Technologies*, 132:103416, 11 2021.

[80] Zhibin Chen, Fang He, Yafeng Yin, and Yuchuan Du. Optimal design of autonomous vehicle zones in transportation networks. *Transportation Research Part B Methodological*, 99:44–61, 12 2016.

[81] W. Krichene, Jack Reilly, S. Amin, and A.M. Bayen. Stackelberg routing on parallel transportation networks. *Handbook of Dynamic Game Theory*, pages 1107–1141, 08 2018.

[82] Chunhui Yu, Yiheng Feng, Henry Liu, Wanjing Ma, and Xiaoguang Yang. Integrated optimization of traffic signals and vehicle trajectories at isolated urban intersections. *Transportation Research Part B Methodological*, 112:89–112, 06 2018.

[83] Yiheng Feng, Chunhui Yu, and Henry Liu. Spatiotemporal intersection control in a connected and automated vehicle environment. *Transportation Research Part C: Emerging Technologies*, 89:364 – 383, 04 2018.

[84] Biao Xu, Xuegang Jeff Ban, Yougang Bian, Wan Li, Jianqiang Wang, Shengbo Eben Li, and Keqiang Li. Cooperative method of traffic signal optimization and speed control of connected vehicles at isolated intersections.

IEEE Transactions on Intelligent Transportation Systems, 20(4):1390–1403, 2019.

[85] Zhuofei Li, Lily Elefteriadou, and Sanjay Ranka. Signal control optimization for automated vehicles at isolated signalized intersections. *Transportation Research Part C: Emerging Technologies*, 49:1–18, 12 2014.

[86] Joyoung Lee, B. Park, Kristin Malakorn, and Jaehyun So. Sustainability assessments of cooperative vehicle intersection control at an urban corridor. *Transportation Research Part C: Emerging Technologies*, 32:193–206, 06 2013.

[87] Joyoung Lee, B. Park, and Ilsoo Yun. Cumulative travel-time responsive real-time intersection control algorithm in the connected vehicle environment. *Journal of Transportation Engineering*, 139:1020–1029, 10 2013.

[88] C.K. Wong and Su Wong. Lane-based optimization of signal timings for isolated junctions. *Transportation Research Part B: Methodological*, 37:63–84, 02 2003.

[89] C. Wong, S. Wong, and C. Tong. Lane-based optimization method for multi-period analysis of isolated signal control junctions. *Transportmetrica*, 2:53–85, 01 2006.

[90] C. Wong and Yehwen Lee. Convergence study of minimizing the nonconvex total delay using the lane-based optimization method for signal-controlled junctions. *Discrete Dynamics in Nature and Society*, 2012, 06 2012.

[91] Weili Sun, Yunpeng Wang, Guizhen Yu, and Henry Liu. Quasi-optimal feedback control for an isolated intersection under oversaturation. *Transportation Research Part C: Emerging Technologies*, 67:109–130, 06 2016.

[92] Mengyu Guo, Pin Wang, Ching-Yao Chan, and Sid Askary. A reinforcement learning approach for intelligent traffic signal control at urban inter-

sections. *IEEE Intelligent Transportation Systems Conference (ITSC). IEEE, Auckland, New Zealand*, 10 2019.

[93] Junchen Jin and Xiaoliang Ma. Adaptive group-based signal control by reinforcement learning. *Transportation Research Procedia*, 10:207–216, 07 2015.

[94] Duowei Li, Jianping Wu, Ming Xu, Ziheng Wang, and Kezhen Hu. Adaptive traffic signal control model on intersections based on deep reinforcement learning. *Journal of Advanced Transportation*, 2020:1–14, 08 2020.

[95] Duowei Li, Jianping Wu, Feng Zhu, Tianyi Chen, and Yiik Wong. Modeling adaptive platoon and reservation-based intersection control for connected and autonomous vehicles employing deep reinforcement learning. *Computer-Aided Civil and Infrastructure Engineering*, 38, 12 2022.

[96] Duowei Li, Feng Zhu, Jianping Wu, Yiik Wong, and Tianyi Chen. Managing mixed traffic at signalized intersections: An adaptive signal control and CAV coordination system based on deep reinforcement learning. *Expert Systems with Applications*, 238:121959, 10 2023.

[97] Li Song and Wei Fan. Traffic signal control under mixed traffic with connected and automated vehicles: A transfer-based deep reinforcement learning approach. *IEEE Access*, 9:145228–145237, 10 2021.

[98] B Ravi Kiran, Ibrahim Sobh, Victor Talpaert, Patrick Mannion, Ahmad A. Al Sallab, Senthil Yogamani, and Patrick Pérez. Deep reinforcement learning for autonomous driving: A survey. *IEEE Transactions on Intelligent Transportation Systems*, 23:4909–4926, 06 2022.

[99] Tian Tan, Feng Bao, Yue Deng, Alex Jin, Qionghai Dai, and Jie Wang. Cooperative deep reinforcement learning for large-scale traffic grid signal control. *IEEE Transactions on cybernetics*, 50(6):2687–2700, 2020.

[100] Yiheng Feng, Jianfeng Zheng, and Henry Liu. Real-time detector-free adaptive signal control with low penetration of connected vehicles. *Transportation Research Record: Journal of the Transportation Research Board*, 2672:036119811879086, 08 2018.

[101] Xiao Liang, S. Ilgin Guler, and Vikash Gayah. An equitable traffic signal control scheme at isolated signalized intersections using connected vehicle technology. *Transportation Research Part C: Emerging Technologies*, 110:81–97, 01 2020.

[102] Chengyuan Ma, Chunhui Yu, Cheng Zhang, and Xiaoguang Yang. Signal timing at an isolated intersection under mixed traffic environment with self-organizing connected and automated vehicles. *Computer-Aided Civil and Infrastructure Engineering*, 12 2022.

[103] Wanjing Ma, Li Jinjue, and Chunhui Yu. Shared-phase-dedicated-lane based intersection control with mixed traffic of human-driven vehicles and connected and automated vehicles. *Transportation Research Part C Emerging Technologies*, 135:103509, 02 2022.

[104] M.A.S. Kamal, Masakazu Mukai, Junichi Murata, and Taketoshi Kawabe. Model predictive control of vehicles on urban roads for improved fuel economy. *Control Systems Technology, IEEE Transactions on*, 21:831–841, 05 2013.

[105] Miao Yu and Jiancheng Long. An eco-driving strategy for partially connected automated vehicles at a signalized intersection. *IEEE Transactions on Intelligent Transportation Systems*, 23:1–14, 09 2022.

[106] Tinu Vellamattathil Baby, Viranjan Bhattacharyya, Pouria Karimi Shahri, Amirhossein Ghasemi, and Baisravan Homchaudhuri. A suggestion-based fuel efficient control framework for connected and automated vehciles in heterogeneous urban traffic. *Transportation Research Part C: Emerging Technologies*, 134:103476, 01 2022.

[107] Handong Yao and Xiaopeng Li. Decentralized control of connected automated vehicle trajectories in mixed traffic at an isolated signalized intersection. *Transportation Research Part C: Emerging Technologies*, 121:102846, 12 2020.

[108] Chengyuan Ma, Chunhui Yu, and XiaoguangYang. Trajectory planning for connected and automated vehicles at isolated signalized intersections under mixed traffic environment. *Transportation Research Part C Emerging Technologies*, 130:103309, 09 2021.

[109] Keqiang Li, Jiawei Wang, and Yang Zheng. Cooperative formation of autonomous vehicles in mixed traffic flow: Beyond platooning. *IEEE Transactions on Intelligent Transportation Systems*, 23:1–16, 09 2022.

[110] Xiao Xiao, Yunlong Zhang, Xiubin Wang, Shu Yang, and Tianyi Chen. Hierarchical longitudinal control for connected and automated vehicles in mixed traffic on a signalized arterial. *Sustainability*, 13:8852, 08 2021.

[111] Yanqiu Cheng, Xianbiao Hu, Qing Tang, Hongsheng Qi, and Hong Yang. A monte carlo tree search-based mixed traffic flow control algorithm for arterial intersection. *Transportation Research Record Journal of the Transportation Research Board*, 2674, 03 2020.

[112] Shupei Wang, Ziyang Wang, Rui Jiang, Ruidong Yan, and Lei Du. Trajectory jerking suppression for mixed traffic flow at a signalized intersection: A trajectory prediction based deep reinforcement learning method. *IEEE Transactions on Intelligent Transportation Systems*, 23:18989–19000, 10 2022.

[113] Pin-Chun Chen, Xiangguo Liu, Chung-Wei Lin, Chao Huang, and Qi Zhu. Mixed-traffic intersection management utilizing connected and autonomous vehicles as traffic regulators. *28th Asia and South Pacific Design Automation Conference. Association for Computing Machinery, Tokyo, Japan*, pages 52–57, 01 2023.

[114] C. Chen, J. Wang, Q. Xu, J. Wang, and K. Li. Mixed platoon control of automated and human-driven vehicles at a signalized intersection: Dynamical analysis and optimal control. *Transportation Research Part C: Emerging Technologies*, 127:103138, 2021.

[115] Peiqun Lin, Jiahui Liu, Peter Jin, and Bin Ran. Autonomous vehicle-intersection coordination method in a connected vehicle environment. *IEEE Intelligent Transportation Systems Magazine*, 9:37–47, 01 2017.

[116] David Rey and Michael Levin. Blue phase: Optimal network traffic control for legacy and autonomous vehicles. *Transportation Research Part B Methodological*, 130:105–129, 11 2019.

[117] Rongjian Dai, Chuan Ding, Xinkai Wu, Bin Yu, and Guangquan Lu. Coupling control of traffic signal and entry lane at isolated intersections under the mixed-autonomy traffic environment. *IEEE Transactions on Intelligent Transportation Systems*, 24:10628–10642, 10 2023.

[118] B. Li, Weichao Zhuang, Hao Zhang, Hao Sun, Haoji Liu, Jianrun Zhang, Guodong Yin, and Boli Chen. Traffic-aware ecological cruising control for connected electric vehicle. *IEEE Transactions on Transportation Electrification*, 10:5225 – 5240, 09 2024.

[119] B. Li, Weichao Zhuang, Hao Zhang, Ruixuan Zhao, Haoji Liu, Linghu Qu, Jianrun Zhang, and Boli Chen. A comparative study of energy-oriented driving strategy for connected electric vehicles on freeways with varying slopes. *Energy*, 289:129916, 02 2024.

[120] Xiao Liang, S. Ilgin Guler, and Vikash Gayah. Signal timing optimization with connected vehicle technology: Platooning to improve computational efficiency. *Transportation Research Record: Journal of the Transportation Research Board*, 2672:036119811878684, 07 2018.

[121] Zhen Yang, Yiheng Feng, and Henry Liu. A cooperative driving framework for urban arterials in mixed traffic conditions. *Transportation Research Part C: Emerging Technologies*, 124:102918, 03 2021.

[122] Tarek Ghoul and Tarek Sayed. Real-time signal-vehicle coupled control: An application of connected vehicle data to improve intersection safety. *Accident; Analysis and Prevention*, 162:106389, 11 2021.

[123] Zixin Wang, Hanyu Zhu, Yong Zhou, and Xiliang Luo. Joint traffic signal and connected vehicle control in iov via deep reinforcement learning. *IEEE Wireless Communications and Networking Conference (WCNC)*, pages 1–6, 03 2021.

[124] S. Gong and L. Du. Cooperative platoon control for a mixed traffic flow including human drive vehicles and connected and autonomous vehicles. *Transp. Res. B Methodol.*, 116:25–61, 10 2018.

[125] Yang Xing, Chen Lv, Dongpu Cao, and Chao Lu. Energy oriented driving behavior analysis and personalized prediction of vehicle states with joint time series modeling. *Applied Energy*, 261, 01 2020.

[126] Xuan Di, Xu Chen, and Eric Talley. Liability design for autonomous vehicles and human-driven vehicles: A hierarchical game-theoretic approach. *Transportation Research Part C: Emerging Technologies*, 118:102710, 09 2020.

[127] Wilko Schwarting, Javier Alonso-Mora, and Daniela Rus. Planning and decision-making for autonomous vehicles. *Annual Review of Control, Robotics, and Autonomous Systems*, 1:187–210, 05 2018.

[128] Jinxiang Wang, Junmin Wang, Rongrong Wang, and Chuan Hu. A framework of vehicle trajectory replanning in lane exchanging with considerations of driver characteristics. *IEEE Transactions on Vehicular Technology*, 66:3583–3596, 05 2017.

[129] Xuewu Ji, Liu Yulong, Xiangkun He, Kaiming Yang, Xiaoxiang Na, Chen Lv, and Yahui Liu. Interactive control paradigm-based robust lateral stability controller design for autonomous automobile path tracking with uncertain disturbance: A dynamic game approach. *IEEE Transactions on Vehicular Technology*, 67:6906–6920, 08 2018.

[130] Chuan Hu, Zhenfeng Wang, Hamid Taghavifar, Yechen Qin, Jinghua Guo, and Chongfeng Wei. Mme-ekf-based path-tracking control of autonomous vehicles considering input saturation. *IEEE Transactions on Vehicular Technology*, 68:5246–5259, 06 2019.

[131] Zhang Xizheng and Xiaolin Zhu. Autonomous path tracking control of intelligent electric vehicles based on lane detection and optimal preview method. *Expert Systems with Applications*, 121:38–48, 12 2018.

[132] Hao Sun, Bingbing Li, Hao Zhang, Li Dai, Giuseppe Fedele, Weichao Zhuang, and Boli Chen. Ecological electric vehicle platooning: An adaptive tube-based distributed model predictive control approach. *IEEE Transactions on Transportation Electrification*, PP:1–1, 05 2024.

[133] Joshué Pérez, Vicente Milanes, Enrique Onieva, Jorge Godoy, and Javier Alonso. Longitudinal fuzzy control for autonomous overtaking. *2011 IEEE International Conference on Mechatronics, ICM 2011*, pages 188–193, 04 2011.

[134] Chao Huang, Chen Lv, Peng Hang, and Yang Xing. Toward safe and personalized autonomous driving: Decision-making and motion control with DPF and CDT techniques. *IEEE/ASME Transactions on Mechatronics*, 26(2):611–620, 2021.

[135] Shaobing Xu, Robert Zidek, Zhong Cao, Pingping Lu, Xinpeng Wang, Boqi Li, and Huei Peng. System and experiments of model-driven motion planning and control for autonomous vehicles. *IEEE Transactions on Systems, Man, and Cybernetics: Systems*, 52:5975 – 5988, 09 2022.

[136] Liangzhi Li, Kaoru Ota, and Mianxiong Dong. Humanlike driving: Empirical decision-making system for autonomous vehicles. *IEEE Transactions on Vehicular Technology*, 67(8):6814–6823, 2018.

[137] Hongyan Guo, Dongpu Cao, Hong Chen, Zhenping Sun, and Yunfeng Hu. Model predictive path following control for autonomous cars considering a measurable disturbance: Implementation, testing, and verification. *Mechanical Systems and Signal Processing*, 118:41–60, 03 2019.

[138] Zhihong Yao, Haowei Deng, Yunxia Wu, Zhao Bin, Gen Li, and Yangsheng Jiang. Optimal lane-changing trajectory planning for autonomous vehicles considering energy consumption. *Expert Systems with Applications*, 225:120133, 04 2023.

[139] Zhiqiang Zhang, Lei Zhang, Junjun Deng, Wang Mingqing, Zhenpo Wang, and Dongpu Cao. An enabling trajectory planning scheme for lane change collision avoidance on highways. *IEEE Transactions on Intelligent Vehicles*, 8:147–158, 01 2023.

[140] Riccardo Marino, Stefano Scalzi, and Mariana Netto. Nested pid steering control for lane keeping in autonomous vehicles. *Control Engineering Practice - CONTROL ENG PRACTICE*, 19:1459–1467, 12 2011.

[141] Rui Xiong, Lijing Li, Chunxi Zhang, Kun Ma, Xiaosu Yi, and Huasong Zeng. Path tracking of a four-wheel independently driven skid steer robotic vehicle through a cascaded ntsm-pid control method. *IEEE Transactions on Instrumentation and Measurement*, 71:1–11, 03 2022.

[142] Changzhu Zhang, Jinfei Hu, Jianbin Qiu, Weilin Yang, Hong Sun, and Qijun Chen. A novel fuzzy observer-based steering control approach for path tracking in autonomous vehicles. *IEEE Transactions on Fuzzy Systems*, 27:278 – 290, 02 2019.

[143] Xinyu Wang, Mengyin Fu, Hongbin Ma, and Yi Yang. Lateral control of autonomous vehicles based on fuzzy logic. *Control Engineering Practice*, 34:1–17, 05 2013.

[144] Mohamed Elbanhawi, Milan Simic, and Reza Jazar. Receding horizon lateral vehicle control for pure pursuit path tracking. *Journal of Vibration and Control*, 24, 05 2016.

[145] Hongbo Gao, Zhen Kan, and Keqiang Li. Robust lateral trajectory following control of unmanned vehicle based on model predictive control. *IEEE/ASME Transactions on Mechatronics*, 27:1278 – 1287, 06 2022.

[146] Shuo Cheng, Liang Li, Xiang Chen, Jian Wu, and Hong Wang. Model-predictive-control-based path tracking controller of autonomous vehicle considering parametric uncertainties and velocity-varying. *IEEE Transactions on Industrial Electronics*, 68:8698 – 8707, 07 2020.

[147] Xiaolin Tang, Kai Yang, Hong Wang, Jiahang Wu, Yechen Qin, Wenhao Yu, and Dongpu Cao. Prediction-uncertainty-aware decision-making for autonomous vehicles. *IEEE Transactions on Intelligent Vehicles*, 7:849–862, 12 2022.

[148] Luca Crosato, Hubert Shum, Edmond Ho, and Chongfeng Wei. Interaction-aware decision-making for automated vehicles using social value orientation. *IEEE Transactions on Intelligent Vehicles*, pages 1339–1349, 02 2023.

[149] Clara Marina Martinez, Mira Heuke, Bo Gao, and Dongpu Cao. Driving style recognition for intelligent vehicle control and advance driver assistance: A survey. *IEEE Transactions on Intelligent Transportation Systems*, 19:666–676, 03 2018.

[150] Sheng Yu, Boli Chen, Imad M. Jaimoukha, and Simos A. Evangelou. Game-theoretic model predictive control for safety-assured autonomous vehicle overtaking in mixed-autonomy environment. In *2024 European Control Conference (ECC)*, pages 3728–3733, 2024.

[151] David Fridovich-Keil, Ellis Ratner, Lasse Peters, Anca D. Dragan, and Claire J. Tomlin. Efficient iterative linear-quadratic approximations for nonlinear multi-player general-sum differential games. *IEEE international conference on robotics and automation (ICRA)*, pages 1475–1481, 2020.

[152] Jun Moon and Tamer Başar. Linear quadratic mean field stackelberg differential games. *Automatica*, 97:200–213, 11 2018.

[153] Yaning Lin, Xiushan Jiang, and Weihai Zhang. An open-loop stackelberg strategy for the linear quadratic mean-field stochastic differential game. *IEEE Transactions on Automatic Control*, 64(1):97–110, 2019.

[154] Hamed Kebriaei and Luigi Iannelli. Discrete-time robust hierarchical linear-quadratic dynamic games. *IEEE Transactions on Automatic Control*, 63(3):902–909, 2018.

[155] Jiangfeng Nan, Weiwen Deng, and Bowen Zheng. Intention prediction and mixed strategy nash equilibrium-based decision-making framework for autonomous driving in uncontrolled intersection. *IEEE Transactions on Vehicular Technology*, 71(10):10316–10326, 2022.

[156] Xiaoxiang Na and David Cole. Game-theoretic modeling of the steering interaction between a human driver and a vehicle collision avoidance controller. *IEEE Transactions on Human-Machine Systems*, 45:25–38, 02 2015.

[157] Xiaoxiang Na and David Cole. Application of open-loop stackelberg equilibrium to modeling a driver's interaction with vehicle active steering control in obstacle avoidance. *IEEE Transactions on Human-Machine Systems*, 47:673–685, 10 2017.

[158] Qingyu Zhang, Reza Langari, H. Eric Tseng, Dimitar Filev, Steven Szwabowski, and Serdar Coskun. A game theoretic model predictive controller with aggressiveness estimation for mandatory lane change. *IEEE Transactions on Intelligent Vehicles*, 5:75–89, 03 2020.

[159] Chao Wei, Yuanhao He, Hanqing Tian, and Yanzhi Lv. Game theoretic merging behavior control for autonomous vehicle at highway on-ramp. *IEEE Transactions on Intelligent Transportation Systems*, 23(11):21127–21136, 2022.

[160] Robbin van Hoek, Jeroen Ploeg, and Henk Nijmeijer. Cooperative driving of automated vehicles using b-splines for trajectory planning. *IEEE Transactions on Intelligent Vehicles*, 6:594–604, 09 2021.

[161] Yasir Ali, Zuduo Zheng, Shimul Md. Mazharul Haque, and Meng Wang. A game theory-based approach for modelling mandatory lane-changing behaviour in a connected environment. *Transportation Research Part C Emerging Technologies*, 106:220–242, 07 2019.

[162] Yongjun Yan, Jinxiang Wang, Yan Wang, Chuan Hu, Hanwen Huang, and Guodong Yin. A cooperative trajectory planning system based on the passengers' individual preferences of aggressiveness. *IEEE Transactions on Vehicular Technology*, 72:395–406, 01 2023.

[163] Shoucai Jing, Fei Hui, Xiangmo Zhao, Jackeline Rios-Torres, and Asad Khattak. Cooperative game approach to optimal merging sequence and on-ramp merging control of connected and automated vehicles. *IEEE Transactions on Intelligent Transportation Systems*, 20:4234–4244, 11 2019.

[164] Nikita Smirnov, Yuzhou Liu, Aso Validi, Walter Morales-Alvarez, and Cristina Olaverri Monreal. A game theory-based approach for modeling autonomous vehicle behavior in congested, urban lane-changing scenarios. *Sensors*, 21:1523, 02 2021.

[165] Victor Mejia, Frank Lewis, Mushuang Liu, Yan Wan, Subramanya Nageshrao, and Dimitar Filev. Game-theoretic lane-changing decision making and payoff learning for autonomous vehicles. *IEEE Transactions on Vehicular Technology*, 71:3609–3620, 04 2022.

[166] Julian Bernhard and Alois Knoll. Risk-constrained interactive safety under behavior uncertainty for autonomous driving. *IEEE Intell. Veh. Symp*, pages 63–70, 07 2021.

[167] Sunan Zhang, Weichao Zhuang, Bingbing Li, Ke Li, Tianyu Xia, and Bo Hu. Integration of planning and deep reinforcement learning in speed and lane change decision-making for highway autonomous driving. *IEEE Transactions on Transportation Electrification*, PP:1–1, 04 2024.

[168] Bo Hu, Bocheng Liu, and Sunan Zhang. A data-driven reinforcement learning based energy management strategy via bridging offline initialization and online fine-tuning for a hybrid electric vehicle. *IEEE Transactions on Industrial Electronics*, 71:12869 – 12878, 10 2024.

[169] Can Xu, Wanzhong Zhao, Chunyan Wang, Taowen Cui, and Chen Lv. Driving behavior modeling and characteristic learning for human-like decision-making in highway. *IEEE Transactions on Intelligent Vehicles*, 8:1994 – 2005, 02 2023.

[170] Qingyu Meng, Hongyan Guo, Yanran Liu, Hong Chen, and Dongpu Cao. Trajectory prediction for automated vehicles on roads with lanes partially covered by ice or snow. *IEEE Transactions on Vehicular Technology*, 72:6972 – 6986, 06 2023.

[171] Abdoulaye Ly and Moulay Akhloufi. Learning to drive by imitation: An overview of deep behavior cloning methods. *IEEE Transactions on Intelligent Vehicles*, 6:195 – 209, 06 2020.

[172] Yunxiao Shan, boli zheng, Chen Longsheng, Long Chen, and de chen. A reinforcement learning-based adaptive path tracking approach for autonomous driving. *IEEE Transactions on Vehicular Technology*, 69:10581 – 10595, 08 2020.

[173] Meng Liu, Fei Zhao, Jialun Yin, Jianwei Niu, and Yu Liu. Reinforcement-tracking: An effective trajectory tracking and navigation method for au-

tonomous urban driving. *IEEE Transactions on Intelligent Transportation Systems*, 23:6991–7007, 07 2022.

[174] Bo Hu, Lei Jiang, Sunan Zhang, and Qiang Wang. An explainable and robust motion planning and control approach for autonomous vehicle on-ramping merging task using deep reinforcement learning. *IEEE Transactions on Transportation Electrification*, 10:6488–6496, 03 2024.

[175] Changxi You, Jianbo Lu, Dimitar Filev, and Panagiotis Tsiotras. Highway traffic modeling and decision making for autonomous vehicle using reinforcement learning. *IEEE Intell. Vehicles Symp. (IV), Changshu, China*, 06 2018.

[176] Jianglin Lan, Dezong Zhao, and Daxin Tian. Data-driven robust predictive control for mixed vehicle platoons using noisy measurement. *IEEE Transactions on Intelligent Transportation Systems*, 24(6):6586–6596, 2023.

[177] Jan C. Willems, Paolo Rapisarda, Ivan Markovsky, and Bart L.M. De Moor. A note on persistency of excitation. *Systems and Control Letters*, 54(4):325–329, 2005.

[178] Felix Fiedler and Sergio Lucia. On the relationship between data-enabled predictive control and subspace predictive control. In *2021 European Control Conference (ECC)*, pages 222–229, 2021.

[179] Florian Dörfler, Jeremy Coulson, and Ivan Markovsky. Bridging direct and indirect data-driven control formulations via regularizations and relaxations. *IEEE Transactions on Automatic Control*, 68(2):883–897, 2023.

[180] Jiawei Wang, Yang Zheng, Chaoyi Chen, Qing Xu, and Keqiang Li. Leading cruise control in mixed traffic flow: System modeling, controllability, and string stability. *IEEE Transactions on Intelligent Transportation Systems*, 23:12861 – 12876, 08 2022.

[181] Zhiwen Qiang, Li Dai, Boli Chen, and Yuanqing Xia. Distributed model predictive control for heterogeneous vehicle platoon with inter-vehicular spacing constraints. *IEEE Transactions on Intelligent Transportation Systems*, 24(3):3339–3351, 2023.

[182] Yongjun Yan, Lin Peng, Tong Shen, Jinxiang Wang, Dawei Pi, Dongpu Cao, and Guodong Yin. A multi-vehicle game-theoretic framework for decision making and planning of autonomous vehicles in mixed traffic. *IEEE Transactions on Intelligent Vehicles*, 8(11):4572–4587, 2023.

[183] Shukai Chen and Daniel Jian Sun. An improved adaptive signal control method for isolated signalized intersection based on dynamic programming. *IEEE Intelligent Transportation Systems Magazine*, 8:4–14, 04 2016.

[184] Wan Li and Xuegang Ban. Connected vehicles based traffic signal timing optimization. *IEEE Transactions on Intelligent Transportation Systems*, 20:4354–4366, 12 2019.

[185] Chaoyi Chen, Mengchi Cai, Jiawei Wang, Kai Li, Qing Xu, Jianqiang Wang, and Keqiang Li. Cooperation method of connected and automated vehicles at unsignalized intersections: Lane changing and arrival scheduling. *IEEE Transactions on Vehicular Technology*, 71:11351–11366, 11 2022.

[186] W. Zhao, D. Ngoduy, S. Shepherd, R. Liu, and M. Papageorgiou. A platoon based cooperative eco-driving model for mixed automated and human-driven vehicles at a signalised intersection. *Transportation Research Part C: Emerging Technologies*, 95:802–821, 2018.

[187] Mladen Čičić, Xi Xiong, Li Jin, and Karl Henrik Johansson. Coordinating vehicle platoons for highway bottleneck decongestion and throughput improvement. *IEEE Transactions on Intelligent Transportation Systems*, 23(7):8959–8971, 2022.

[188] Yi Guo, Jiaqi Ma, Chenfeng Xiong, Xiaopeng Li, Fang Zhou, and Wei Hao. Joint optimization of vehicle trajectories and intersection controllers with

connected automated vehicles: Combined dynamic programming and shooting heuristic approach. *Transportation Research Part C: Emerging Technologies*, 98:54–72, 01 2019.

[189] J. Hu, P. Bhowmick, F. Arvin, A. Lanzon, and B. Lennox. Cooperative control of heterogeneous connected vehicle platoons: An adaptive leader-following approach. *IEEE Robotics and Automation Letters*, 5:977–984, 02 2020.

[190] Ksander de Winkel, Tugrul Irmak, Riender Happee, and Barys Shyrokau. Standards for passenger comfort in automated vehicles: Acceleration and jerk. *Applied Ergonomics*, 106:103881, 2023.

[191] Mas Kamal, M. Mukai, J. Murata, and T. Kawabe. Ecological vehicle control on roads with up-down slopes. *IEEE Transactions on Intelligent Transportation Systems*, 12:783–794, 03 2011.

[192] Xiao Pan, Boli Chen, Stelios Timotheou, and Simos A. Evangelou. A convex optimal control framework for autonomous vehicle intersection crossing. *IEEE Transactions on Intelligent Transportation Systems*, 24(1):163–177, 2023.

[193] Edward L. Zhu and Francesco Borrelli. A sequential quadratic programming approach to the solution of open-loop generalized nash equilibria. *2023 IEEE International Conference on Robotics and Automation (ICRA)*, pages 3211–3217, 2023.

[194] Haimin Hu and Jaime F. Fisac. Active uncertainty reduction for human-robot interaction: An implicit dual control approach. *International Workshop on the Algorithmic Foundations of Robotics*, 2023.

[195] Mingyang Chen, Jingjing Jiang, and Boli Chen. A game-based optimal and safe lane change control of autonomous vehicles in mixed traffic scenario. *2024 IEEE Conference on Control Technology and Applications (CCTA)*, pages 52–57, 2024.

[196] Sheng Yu, Boli Chen, Imad M. Jaimoukha, and Simos A. Evangelou. Game-theoretic model predictive control for safety-assured autonomous vehicle overtaking in mixed-autonomy environment. *2024 European Control Conference (ECC)*, pages 3728–3733, 2024.

[197] Xiaojing Zhang, Alexander Liniger, and Francesco Borrelli. Optimization-based collision avoidance. *IEEE Transactions on Control Systems Technology*, 29(3):972–983, 2021.

[198] Aaron D. Ames, Xiangru Xu, Jessy W. Grizzle, and Paulo Tabuada. Control barrier function based quadratic programs for safety critical systems. *IEEE Transactions on Automatic Control*, 62:3861–3876, 08 2017.

[199] Filiberto Fele, Ezequiel Debada, José María Maestre, and Eduardo F. Camacho. Coalitional control for self-organizing agents. *IEEE Transactions on Automatic Control*, 63:2883–2897, 09 2018.

[200] Jiawei Wang, Yang Zheng, Keqiang Li, and Qing Xu. Deep-lcc: Data-enabled predictive leading cruise control in mixed traffic flow. *IEEE Transactions on Control Systems Technology*, 31:2760–2776, 06 2023.